Elisabete Priscila Pinto Ferreira

IDENTIFICATION AND CHARACTERIZATION OF SMALL MOLECULE INTERACTIONS WITH TRANSTHYRETIN AMYLOID FIBERS

Mestrado em Química Medicinal

Departamento de Química

FCTUC

Setembro 2015

· U C ·

UNIVERSIDADE DE COIMBRA

Elisabete Priscila Pinto Ferreira

IDENTIFICATION AND CHARACTERIZATION OF SMALL MOLECULE INTERACTIONS WITH TRANSTHYRETIN AMYLOID FIBERS

Dissertação apresentada para provas de Mestrado em Química Medicinal

Orientador: Prof. Dr. Rui M. M. Brito

Setembro 2015

UNIVERSIDADE DE COIMBRA

Acknowledgments

I would like to acknowledge Prof. Rui Brito for the scientific guidance, freedom to pursue new hypothesis and the possibility to perform the presented work.

To Zaida Lourenço de Almeida for all her generosity in sharing her knowledge and all the help in the laboratory and Tiago Faria for the initial support, patience and all the knowledge transmitted.

To Pedro Cruz for making the NMR experiences possible and overall availability to help and to Marta Silva e Sousa for the protein expression and for being always ready to give her advice.

To Cândida Silva for the availability to share her knowledge and the elements of the Protein Biophysical Chemistry Group for the good atmosphere and the spirit of mutual help.

To my classmate Pedro Fernandes for the good humour and support, everyone in this group would be glad to visit OAZ (Oliveira de Azeméis).

I want to thank all my friends for never forgetting me, even with my typical hermit behaviour, and for the interest demonstrated in my work.

I want to specially thank to my family: my parents, Armanda and António, and my grandparents, Raquelina and Olímpio for making me what I am today and for all the trust, confidence and investment in me, and also to Jorge Barbosa for all the "peace, love and understanding".

Table of contents

Table of figures

Index of tables

Abbreviations

ACF	Autocorrelation function
AFM	Atomic force microscopy
ASO	Antisense oligonucleotide
CCD	Charge-coupled device
CD	Circular dichroism
CNSA	Central nervous system selective amyloidosis
CSF	Cerebrospinal fluid
DLS	Dynamic light scattering
EGCG	Epigallocatechin-3-gallate
FAC	Familial amyloid cardiomyopathy
FAP	Familial amyloid polyneuropathy
IDOX	4'-iodo-4'-deoxydoxorubicin
ITC	Isothermal titration calorimetry
OA	Oculoleptomeningeal amyloidosis
PAD	Pulse amplifier and discriminator
PBS	Phosphate buffered saline
PI	Polydispersity index
PMT	Photomultiplier tube
RBP	Retinol binding protein
SDP	Size distribution processor
siRNA	Small interfering ribonucleic acid
SSA	Senile systemic amyloidosis
STD NMR	Saturation transfer difference nuclear magnetic resonance
T3	3,5,3'-triiodo-L-thyronine
T4	3,5,3',5'-tetraiodo-L-thyronine or thyroxine
TEM	Transmission electron microscopy
ThT	Thioflavin-T
TTR	Transthyretin
TUDCA	Tauroursodeoxycholic acid
WT-TTR	Wild-type transthyretin

Resumo

A transtirretina (TTR) é uma das várias proteínas conhecidas por sofrerem alterações conformacionais e formarem agregados e fibras amiloides insolúveis e altamente estáveis que se acumulam nos tecidos extracelulares causando doenças. A amiloidose senil sistémica, a polineuropatia amiloidótica familiar, a cardiomiopatia amiloidótica familiar e a rara amiloidose seletiva do sistema nervoso central são as principais patologias em que a TTR está implicada.

Embora o transplante de fígado e o medicamento Tafamidis sejam usados como abordagens terapêuticas, atualmente não há cura ou tratamento totalmente eficaz para as amiloidoses da TTR e várias estratégias terapêuticas têm vindo a ser desenvolvidas visando as diferentes etapas do processo de formação de fibras. A desagregação de oligómeros e fibras amiloides é uma dessas estratégias. Para selecionar eficientemente compostos com esse efeito é necessário desenvolver um protocolo específico de *screening* que consiga identificar e caracterizar a interação desses compostos com as fibras.

Com este objetivo três protocolos diferentes de formação de fibras de TTR tipo selvagem foram estudadas para selecionar e caracterizar o protocolo de formação de fibras mais relevante e apropriado. Adicionalmente a técnica STD NMR (diferença de transferência de saturação por ressonância magnética nuclear) foi selecionada e usada para estudar a interação da doxiciclina, composto conhecido por desagregar fibras amiloides de TTR mutante, com fibras de TTR tipo selvagem, e um ensaio de dispersão dinâmica de luz foi desenvolvido e utilizado para caraterizar o efeito deste composto na desagregação de fibras.

Os resultados demonstraram que o protocolo de formação de fibras induzidas pelo calor possui algumas vantagens sobre os outros protocolos mas requer uma melhor caracterização. A STD NMR foi aplicada com sucesso na caracterização da interação da doxiciclina com as fibras de TTR tipo selvagem, indicando os resultados que a doxiciclina interage de modo diverso com amiloide de TTR tipo selvagem formado em diferentes condições experimentais. O ensaio de dispersão dinâmica de luz permitiu a caracterização do efeito da doxiciclina nas fibras ao longo do tempo e demonstrou que a doxiciclina desagrega fibras amiloides pré-formadas de TTR tipo selvagem.

Palavras-chave: Amiloide, transtirretina, doxiciclina, desagregação de fibras

Abstract

Transthyretin (TTR) is one of several proteins that are known to undergo conformational changes and form aggregates and insoluble highly stable amyloid fibrils, which accumulate in extracellular tissues, causing diseases. Senile systemic amyloidosis (SSA), familial amyloid polyneuropathy (FAP), familial amyloid cardiomyopathy (FAC), and the rare central nervous system selective amyloidosis (CNSA) are the main pathologies in which TTR is implicated.

Although liver transplant and more recently the medicine Tafamidis are in use as therapeutic approaches, currently there is no cure or completely effective treatment for TTR amyloidosis and several therapeutic strategies targeting different steps of the fibril formation pathway are under development. The disruption of amyloid aggregates and fibrils is one of those strategies. To properly select compounds for that purpose a specific screening protocol that can identify and characterize the interaction of the compounds with the fibrils must be developed.

With this purpose three wild type-TTR (WT-TTR) fibril formation protocols were studied to select and characterize the most relevant and appropriate fibril formation protocol. Additionally saturation transfer difference nuclear magnetic resonance (STD NMR) was selected and used to study the interaction of doxycycline, a known TTR fibril disrupter, with WT-TTR fibrils, and a dynamic light scattering (DLS) assay was developed and performed to characterize the effect of this compound on fibril disruption.

The results show that the heat-induced fibril formation protocol have some advantages over the other fibril formation protocols but requires further characterization. ^{1}H STD NMR was successfully applied in probing the interaction of doxycycline with WT-TTR fibrils, with the results indicating that doxycycline interacts diversely with WT-TTR amyloid fibrils formed in different experimental conditions. The DLS assay allowed the characterization of the effect of doxycycline on WT-TTR fibrils over time and demonstrated that doxycycline disassembles pre-formed WT-TTR fibrils.

Keywords: Amyloid, transthyretin, doxycycline, fibril disruption

Chapter 1: Introduction

1.1-Amyloid

1.1.1 - The multiplicity of protein states

From a chemical point of view proteins are the most structurally complex and functionally sophisticated group of biomacromolecules. They participate in the majority of biological processes partaking in a great diversity of vital functions. Following their synthesis, in order to perform their biological function, the majority of the proteins need to acquire a specific three-dimensional structure, the native structure, in a process called folding. In addition to the native structure proteins can also populate various other states (Figure 1) including disorder and partially ordered conformations and different aggregated assemblies.

The populations of the different states and their interconversion are determined by different factors such as their different thermodynamic stabilities, free energy barriers associated with the corresponding transitions and also the rates of synthesis and degradation, the propensity to interact with chaperones and to undergo post-translational and other chemical modifications[1].

Despite the quality control mechanisms present in the cell, such as chaperones and the proteasome[2], proteins are sometimes irreversibly trapped as misfolded conformations. Misfolded proteins cannot correctly accomplish their biological activity. Additionally they often aggregate and/or interact inappropriately with other cellular components leading to impairment of cell viability and eventually to cell death[3]. Many diseases known as misfolding or conformational diseases result from their presence in a living system.

Currently considerable attention is given to a group of protein folding diseases known as amyloidosis. In these diseases specific peptides or proteins fail to fold or to remain correctly folded and then aggregate (often with other components) so as to give rise to "amyloid" deposits in tissues and organs.

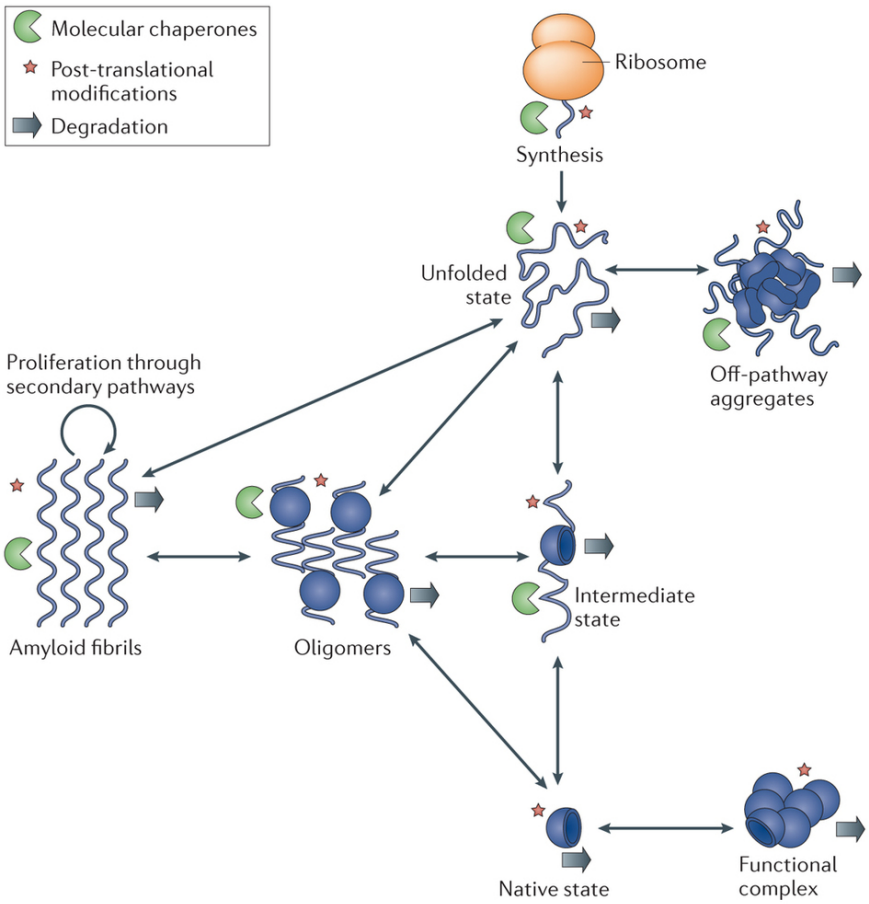

Figure 1: Possible protein conformational states and assemblies[1]. Schematic representation of some of the states accessible to a polypeptide chain following its synthesis in a ribosome. The amyloid state of a protein is a highly ordered form of aggregate in which the polypeptide chains adopt a fibrillar structure.

1.1.2 - The amyloid state of proteins and disease

1.1.2.1- Properties of Amyloid

Amyloid structures have a series of specific tinctorial and biophysical characteristics, namely a very high level of kinetic and thermodynamic stability, that reflect a common core structure based on the presence of highly organised β-sheets. According to the modern biophysical definition amyloid is an unbranched protein fiber whose repeating substructure consists of β-strands that run perpendicular to the fiber axis, forming a cross-β sheet of indefinite length[4].

Amyloid fibrils from different proteins are very similar at the nanometre length scale[5,6]. Electron microscopy and atomic force microscopy (AFM) studies showed that they appear as unbranched filamentous structures only a few nanometres in diameter (6-12 nm) but often micrometres in length[1,7]. It was also observed that they consist of multiple protofilaments that twist around each other to form mature fibrils[8].

X-ray diffraction studies identified X-ray fiber diffraction patterns with a meridional reflection at 4.7 Å corresponding to the inter-β strand spacing and an equatorial reflection at 6–11 Å corresponding to the distance between stacked β-sheets[5] (Figure 2).

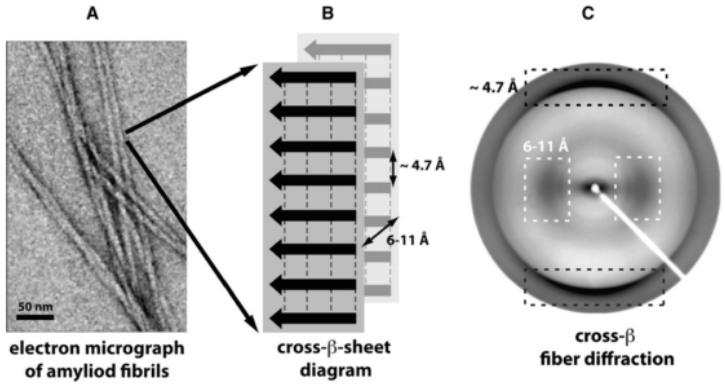

Figure 2: Structure of Amyloids. (A) Amyloid fibrils are composed of long filaments that are visible in negatively stained transmission electron micrographs. (B Schematic diagram of the cross-β sheet structure in a fibril, with the backbone hydrogen bonds represented by dashed lines, indicating the repetitive spacings that give rise to (C) the typical fibre diffraction pattern with a meridional reflection at 4.7 Å (black dashed box) and an equatorial reflection at 6–11 Å (white dashed box)[4].

Recent developments in cryo-electron microscopy, solid-state NMR spectroscopy and X-ray diffraction studies of peptide microcrystals confirmed previous observations and allowed to obtain amyloid structures at atomic resolution[9,10].

The internal order of amyloid structures gives them specific tinctorial properties. These properties are very important in the clinic as well as in the laboratory. Congo red is typically used in histological staining of amyloid, where it shows a typical red-green birefringence under polarized light when bound to amyloid[11]. Thioflavin T is used in pre-clinical research as *in vitro* staining and detection method, it exhibits a fluorescence spectral red-shift when bound to amyloid[12].

1.2.2- Amyloidosis

Many human diseases are associated with protein aggregation. To date there are approximately 50 disorders which are associated with the formation of extracellular amyloid fibrils or intracellular inclusions with amyloid-like characteristics[6]. These disorders can be broadly grouped into three categories: neurodegenerative conditions, in which aggregation occurs in the brain; non-neuropathic localized amyloidosis, in which aggregation occurs in a single type of tissue other than the brain; and non-neuropathic systemic amyloidosis, in which aggregation occurs in multiple tissues[6]. In table 1 some examples of diseases belonging to each category can be observed.

Table 1: Examples of human diseases associated with amyloid.

Disease	Aggregating protein or peptide
Neurodegenerative diseases	
Alzheimer's disease	Amyloid- β peptide
Spongiform encephalopathies	Prion protein or its fragments
Parkinson's disease	α-synuclein
Amyotrophic lateral sclerosis	Superoxide dismutase 1
Huntington's disease	Huntingtin fragments
Familial amyloidotic polyneuropathy	Transthyretin mutants
Non-neuropathic localized amyloidosis	
Amyloid light chain amyloidosis	Immunoglobulin light chains or its fragments
Amyloid A amyloidosis	Serum amyloid A1 protein fragments
Senile systemic amyloidosis	Wild-type transthyretin
Haemodialysis-related amyloidosis	β2-microglobulin
Lysozyme amyloidosis	Lysozyme mutants
Non-neuropathic systemic amyloidosis	
Apolipoprotein A1 amyloidosis	Apo A-1 fragments
Type II diabetes	Amylin
Injection-localized amyloidosis	Insulin

In several forms of amyloidosis the bulk of the deposited protein is enough to disrupt normal organ or tissue function. However in some cases precursors to amyloid fibrils, such as low molecular weight oligomers and/or structured protofibrils, rather than the mature fibrils into which they convert are the likely origins of pathological behaviour[13,14].

1.2 - Transthyretin

The protein currently known as transthyretin (TTR) was first discovered in 1942 in human plasma and in the cerebrospinal fluid (CSF)[15,16] receiving the name prealbumin because of its electrophoretic migration pattern compared to albumin. Afterwards, to better describe its main physiological roles that are the transport of thyroid hormones[17] and retinol trough binding to retinol binding protein[18], the name was changed to transthyretin. TTR belongs to the group of amyloidogenic proteins being involved in several amyloidosis.

1.2.1- Genetic aspects

The human TTR gene is found on chromosome 18q11.2-q12.1[19]. To date over 100 mutations have been identified[20]. The vast majority is disease causing and related to amyloid deposition affecting predominantly peripheral nerve and/or the heart[21]. Only a small portion of TTR mutations is seemingly non-amyloidogenic[21].

1.2.2- Structure

Human TTR is a homotetrameric protein with a total molecular mass of 55 kDa. Each monomeric subunit has 127 aminoacids and consists of eight β-strands and a short α-helix (Figure 3A). Each monomer has a β-sandwich fold composed of two four-stranded β-sheets labelled DAGH and CBEF (Figure 3B). The dimer is formed mainly through antiparallel β-strand interactions between the H-strands, resulting in a continuous eight stranded β-sheet comprising strands DAGH and H'G'A'D'. The F strands also participate in the dimerization through interactions between side chains and interconnecting water molecules (Figure 3C)[22].

To form the functional and soluble tetramer, two dimers interact through hydrophobic contacts and hydrogen bounds between the AB and GH loops as well as strand H (Figure 3D)[23].

1.2.3- Synthesis and catabolism

In humans transthyretin is mostly biosynthesized in the liver[24] but also in the choroid plexuses of the brain[25], retinal pigment epithelial cells of the eye[26] and α-cells of pancreatic islets[27]. It is predominantly found in the plasma (0.2 mg/ml=3.63 μM in the tetrameric form) and represents a high proportion of the total protein in the cerebrospinal fluid[28].

TTR has a biological half-life of approximately 2.5 days and it is catabolized primarily by the liver and by excretory loss via the kidneys and gastrointestinal tract[29].

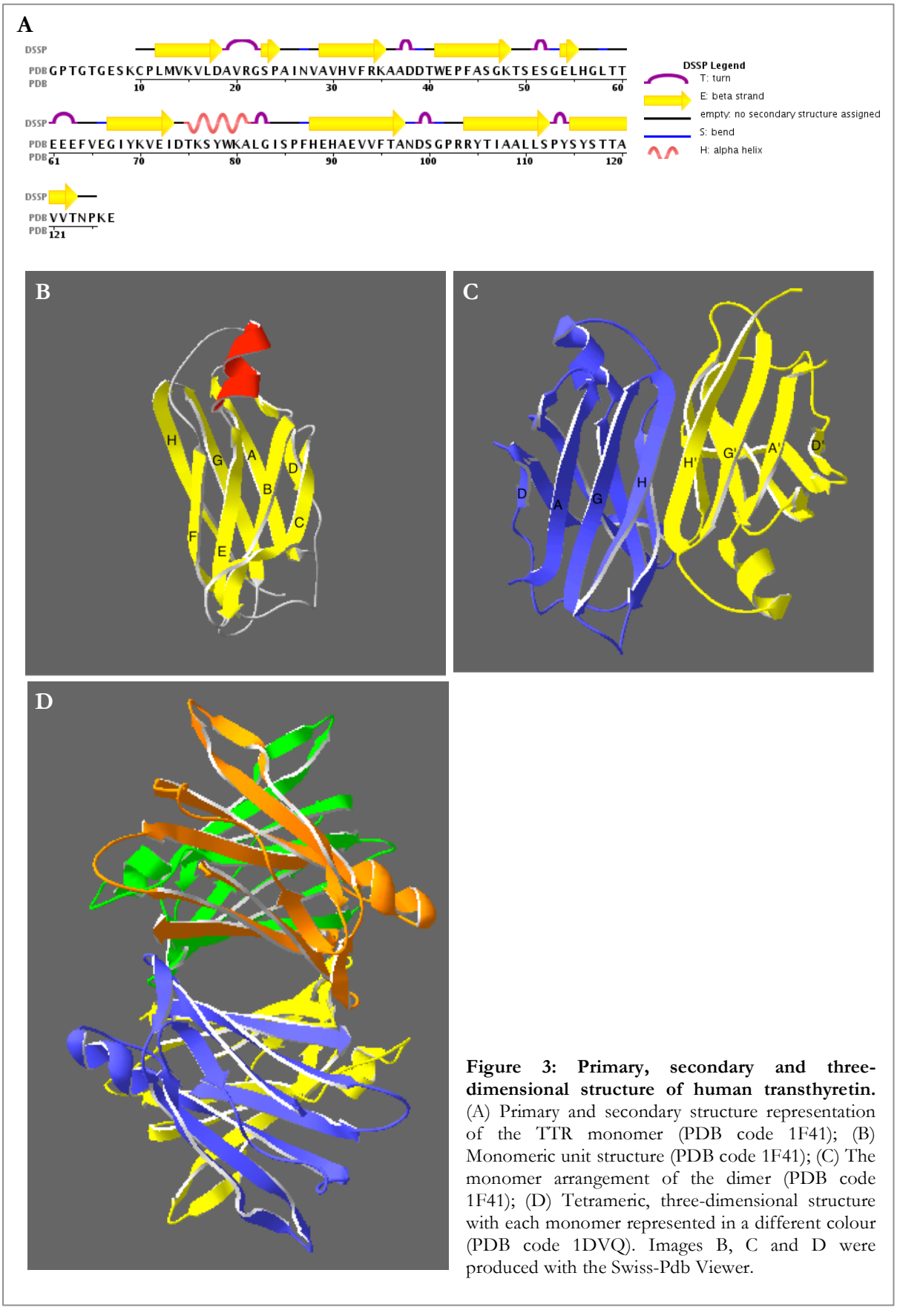

Figure 3: Primary, secondary and three-dimensional structure of human transthyretin. (A) Primary and secondary structure representation of the TTR monomer (PDB code 1F41); (B) Monomeric unit structure (PDB code 1F41); (C) The monomer arrangement of the dimer (PDB code 1F41); (D) Tetrameric, three-dimensional structure with each monomer represented in a different colour (PDB code 1DVQ). Images B, C and D were produced with the Swiss-Pdb Viewer.

1.2.4- Function

TTR transports the thyroid hormones T4 (3,5,3',5'-tetraiodo-L-thyronine or thyroxine) and T3 (3,5,3'-triiodo-L-thyronine) (Figure 4) having two sites for hormone binding (Figure 5). TTR binds approximately 15-20% of the circulating thyroid hormones, thyroxine binding globulin has the highest affinity for this hormones and binds approximately 75% while albumin, having the lowest affinity, binds 5%[30]. In the central nervous system TTR is the only identified thyroid hormone carrier.

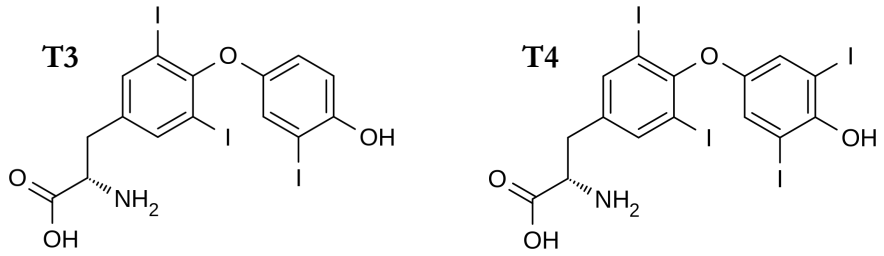

Figure 4: Chemical structure of 3,5,3'-triiodo-L-thyronine (T3) and 3,5,3',5'-tetraiodo-L-thyronine or thyroxine (T4).

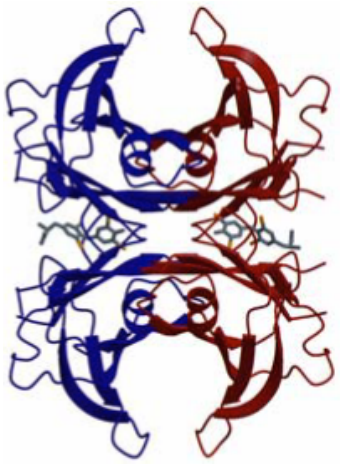

Figure 5: Three-dimensional structure of transthyretin in complex with two molecules of T4 (represented in grey)[31].

Retinol (Figure 6) is secreted from the liver bound to the retinol binding protein (RBP). RBP binds to TTR preventing extensive loss of the low molecular weight RBP through glomerular filtration[18]. Both the apo and holo form of RBP has the ability to bind to TTR, but affinity is significantly higher for the holo form[32]. The RBP-TTR complex (Figure 7) transports 90-95% of retinol.

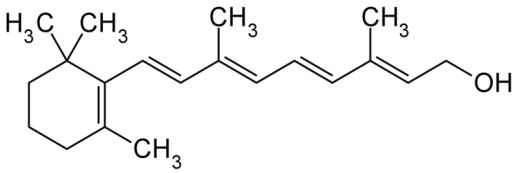

Figure 6: Chemical structure of retinol.

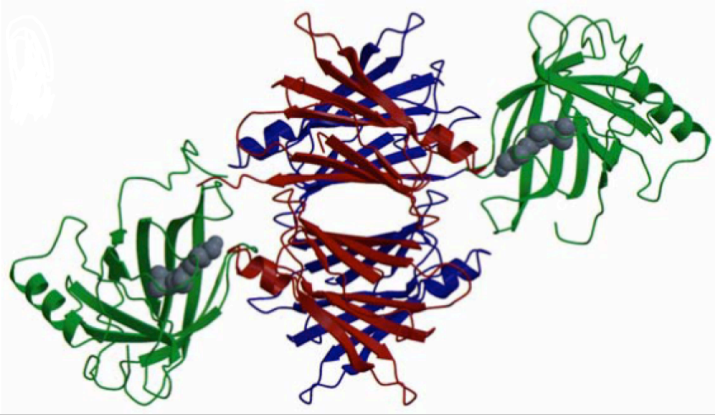

Figure 7: Three-dimensional structure of transthyretin in complex with RBP (represented in green) and retinol (represented in grey)[33].

Besides this well studied carrier functions, it has been suggested over the years that TTR may also participate in the maintenance and function of the central nervous system. TTR has been shown to play an important role in behaviour, cognition, amidated neuropeptide processing and nerve regeneration[34]. It has also been suggested that TTR has a neuroprotective action in Alzheimer's disease and cerebral ischemia[34].

Recently it has also been found that TTR can function as a protease and seems able to proteolytically process apolipoprotein AI, cleaving it at residue Phe225 positioned in the C-terminus[35].

1.2.5 - Transthyretin amyloidosis

Fibrillar structures formed by TTR are implicated in several amyloidosis (Table 2). TTR amyloidosis can be divided in two types: age-related or senile amyloidosis and familial or hereditary amyloidosis (Table 2). In the age-related amyloidosis fibrils are derived from wild-type TTR (WT-TTR) and in hereditary amyloidosis TTR variants are implicated.

1.2.5.1- Age-related/senile amyloidosis

Senile Systemic Amyloidosis (SSA) is strongly correlated with ageing, typically presenting itself after age 60 and affecting 25% of the population over the age of 80[36]. SSA is an idiopathic disease characterized by the deposition of WT-TTR fibrils[37] in many organs. It is often asymptomatic however in some individuals, predominantly men, it can give rise to heavy deposit formation in the heart resulting in congestive heart failure[38].

1.2.5.2- Familial/hereditary amyloidosis

Familial Amyloid Polyneuropathy (FAP), Familial Amyloid Cardiomyopathy (FAC) and the rare Central Nervous System selective Amyloidosis (CNSA) are pathologies caused by the more than 100 different TTR variants known[39].

Familial Amyloid Polyneuropathy

FAP was first discovered and described by the portuguese physician Prof. Corino de Andrade as a peculiar form of peripheral neuropathy[40]. After been reported in Portugal in 1952 was subsequently described in Japan[41] and Sweden[42] and it is now believed to occur worldwide. TTR was identified in the amyloid deposits in 1978[43].

In this autosomal dominant disorder mutant forms of TTR aggregate to form amyloid fibrils that deposit in tissues, especially the peripheral nervous system. The most common mutation is by far the Val30Met[44], typically found in Portugal, Sweden and Japan but also worldwide[39].

The clinical onset of this lethal pathology is characterized by sensory peripheral neuropathy of the lower limbs, primarily affecting pain and temperature sensation. These symptoms are later followed by motor impairments and autonomic dysfunction with the cardiocirculatory, gastrointestinal and genito-urinary systems affected[45].

The disease onset, typically in the third or fourth decade of life, and disease progression depend on the existing mutation. However multigenic and environmental modulating factors may contribute to the course of the disease[46].

Familial Amyloid Cardiomyopathy

In FAC TTR amyloid can infiltrate any or all of the cardiovascular structures, including the conduction system, the atrial and ventricular myocardium, valvular tissue, and the coronary and large arteries[47] which may lead to restrictive cardiomyopathy and heart failure. The most common TTR mutation associated with FAC is the Val122Ile and is found in 3-4% of the African-American population in the USA[48].

Central Nervous System selective Amyloidosis

CNSA or oculoleptomeningeal amyloidosis (OA) is a more uncommon disease where the site of amyloid deposition is the central nervous system (CNS), predominantly leptomeninges and subarachnoid vessels[49]. Approximately 13 different mutations, such as Asp18Gly and Ala25Thr, have been associated with the development of CNSA in humans[49]. These mutations are generally the most destabilizing and amyloidogenic.

Table 2: Human Transthyretin-Associated Amyloidosis[50]

Amyloidosis	Clinical classification	Amyloid constituting	Affected population
Senile Systemic Amyloidosis	Cardiomyopathy	WT-TTR	25% over 80 years of age worldwide
Familial Amyloid Cardiomyopathy	Cardiomyopathy	Mutant TTR (e.g. Val122Ile)	3-4% of the African American population in the USA
Familial Amyloid Polyneuropathy	Peripheral neuropathy +/- cardiomyopathy	Val30Met	European (Portugal, Sweden) and Japanese
		Mutant TTR	Worldwide
Central Nervous System Selective Amyloidosis	CNS amyloidosis	Highly destabilized mutants of TTR (e.g. Ala25Thr, Asp18Gly)	Rare

1.2.6 - Transthyretin amyloid formation

Over the years the molecular mechanisms and kinetics involved in amyloid formation have been subject of considerable scientific interest[51]. As previously described, amyloid TTR is involved in several diseases. Understanding the molecular mechanism of aggregation is very useful to prevent or control amyloid formation and has already contributed to the design of small molecules that can inhibit certain steps of the aggregation process[52].

The aggregation process starts with the dissociation of the native tetramer into monomers followed by partial unfolding of the monomeric units that become prone to aggregation[53–55](Figure 8).

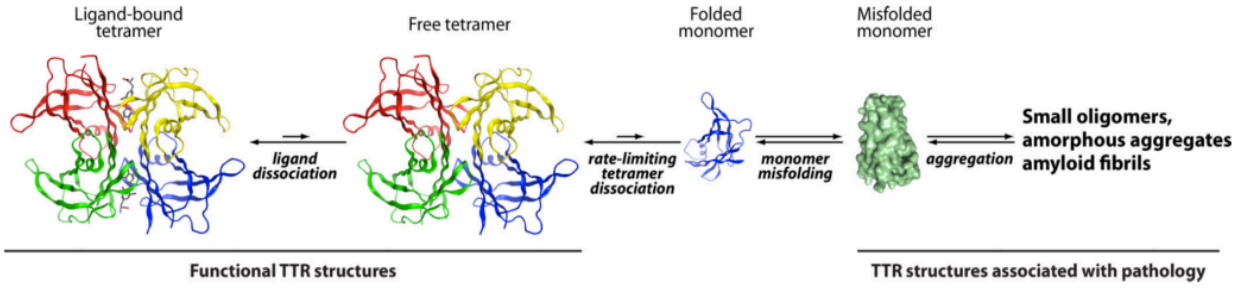

Figure 8: TTR amyloid cascade[56].

Until recently the details of TTR fibril formation from the monomeric amyloidogenic intermediate to mature fibrils were not well understood and the characteristics of the intermediate assembly states remained elusive. AFM and dynamic light scattering were used to describe the morphological features of transthyretin protofibrillar amyloid intermediates[57]. In this study annular oligomers composed by 8–16 monomers were the first morphologically distinct intermediates observed in acid-induced WT-TTR aggregation.

A novel kinetic model was presented this year to describe the aggregation of WT-TTR triggered by the addition of salt to acid-unfolded TTR monomers[58]. This model proposes a two-step kinetic mechanism to analyse the aggregation reaction kinetics. According to this model the initial step is faster and leads to the formation of globular oligomers with 6 to 10 monomers, the second step is slower leading to the formation of fibrils.

1.2.7 - Transthyretin Amyloid structure and toxicity

As previously described amyloid fibrils have common structural morphologies being composed of multiple protofilaments that twist around each other to form mature fibrils. Early studies of Val30Met TTR amyloid fibrils using image reconstruction from electron micrographs showed that the diameter of the fibrils was about 130 Å and in cross-section they exhibited 4-fold symmetry with four proto-filaments, each measuring 40 to 50 Å across, arranged around a central hollow core[59]. Subsequently the structure of these fibrils was investigated by fibre diffraction methods using synchrotron radiation and it was discovered a novel molecular structure consisting of β-sheets extended in regular helical twists along the length of the fibre. This 115.5 Å repeat along the fibre axis was interpreted as a 24 β - stranded unit, with its constituent β strands arranged perpendicular to the fibre axis, forming a complete helical turn around an axis parallel to the fibre axis[60].

Posterior X-ray diffraction studies hypothesized that axially arrayed TTR monomers constitute the protofilament[61], this was corroborated by the size of the repeating pattern, 29 Å which is similar to the size of the monomer[61].

Efforts have been made to determine the three-dimensional arrangement of the TTR subunits in the amyloid fibrils using site-directed spin labelling EPR studies[62] and H/D exchange NMR[63]. In agreement with the previous experimental data a structural model of an amyloid protofilament was constructed using molecular modelling methods[64]. This model is formed by two extended continuous β-sheets with the β-strands perpendicular to the main axis of the protofilament and a helical twist with a period of 48 β-strands (Figure 9). More recently amyloid fibbers of WT-TTR were studied using protease digestion, mass spectrometry and solid-state NMR[65]. This study proposed a different structure and arrangement of the monomeric subunits with a particularly different configuration of the β-sheets (Figure 10).

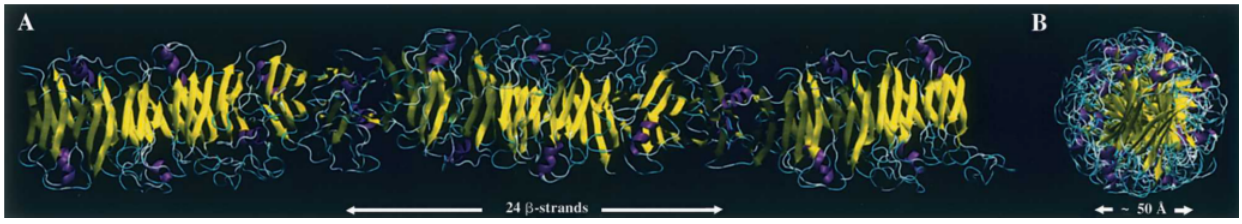

Figure 9: (A) Schematic representation of the TTR protofilament model obtained, showing the size of half of the repeating unit. (B) Protofilament cross-section dimension including only the core β -strands[64].

Studying the TTR amyloid structure and the arrangement of the subunits is of particular importance in the development of therapies that may prevent the association of the amyloidogenic species or induce disaggregation of the amyloid fibrils.

Regarding TTR amyloid toxicity it has been demonstrated that amyloid fibrils are not the most toxic species in the aggregation pathway. *In vitro* studies on human neuroblastoma cell lines have shown that monomeric and small oligomeric species are very cytotoxic and mature TTR fibrils do not induce considerable toxicity[14,66,67]. Furthermore Sousa and colleagues verified that small nonfibrillar deposits of TTR are linked with nerve degeneration in FAP patients and demonstrated the cytotoxicity of the prefibrillar structures in cell culture assays[68].

Ultrastructural analysis of amyloid-laden cardiomyocytes from autopsied patients with FAP revealed intracellular structural changes that correlated with the degree of amyloid deposition. This cells were physically limited by amyloid fibrils with loss of cross-talk with surrounding cells and tissues[69]. It was hypothesized that this may lead to metabolic disturbances, cell degeneration, and ultimately cell loss[69]. The other histopathologic and cell culture studies presented in this work showed that TTR amyloid fibrils and prefibrillar aggregates had no acute cytotoxic effects.

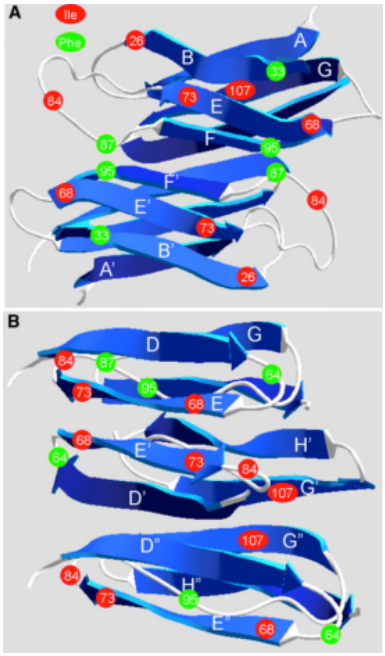

Figure 10: Plausible models for the TTR amyloid[65]. (A) Representation of the previously suggested TTR amyloid model with strands B, E, and F (front) comprising one sheet and strands A, G, and H (back) comprising the other sheet of the amyloid core[62]. The C and D strands have been excluded for clarity. (B) New TTR amyloid model based on protease digestion and solid-state NMR spectroscopy results. The N-terminal region up to residue 50 was excluded for clarity. The D strand and part of the D loop interact with the E strand, while the former F strand and helix becomes the linker to the sheet composed of the interacting G and H strands. Isoleucine residues (red) and phenylalanine residues (green) are labeled[65].

1.2.8 - Therapeutic Strategies for Transthyretin Amyloidosis

To date there is no cure or completely effective treatment for TTR amyloidosis. Considering the current knowledge about TTR and TTR amyloid formation, various strategies targeting different steps of the pathway are under development (Figure 11)[70,71].

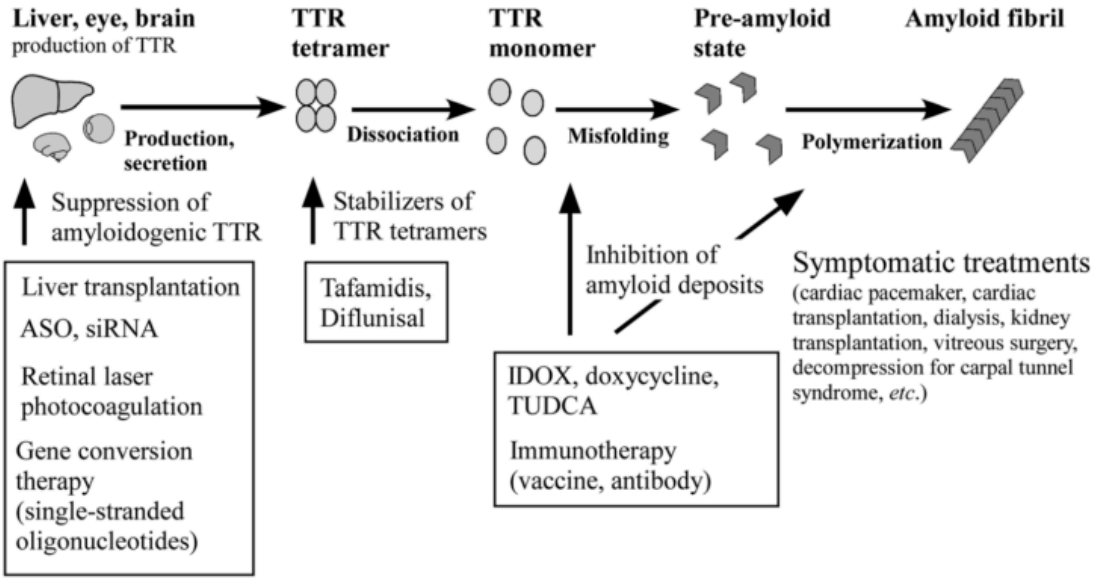

Figure 11: TTR amyloid formation and therapies[71]

1.2.8.1 - Strategy 1: Inhibition of TTR synthesis

Currently the most successful treatment for hereditary systemic TTR amyloidosis is orthotopic liver transplantation (OLT). The rationale behind the method is that since TTR is produced mainly by the liver, the synthesis of mutant TTR is abolished.

Regarding the treatment of FAP, OLP has reportedly halted the progression of clinical manifestations[72]. The first OLT for a FAP patient was performed in 1990 and currently approximately 120 OLTs are performed worldwide each year[73]. OLT reportedly prolonged the survival of FAP Val30Met patients but was less effective with non-Val30Met FAP patients who have cardiomyopathy or leptomeningeal dominant symptoms[74]. OLT is also a very invasive procedure, with high healthcare costs and limited to the availability of healthy livers.

Gene therapy for TTR amyloidosis is currently under development. Small interfering RNAs (siRNAs) and antisense oligonucleotides (ASO) are effective gene-silencing tools and have been effective in

inhibiting the production of various TTR mutants and WT-TTR both *in vitro* and *in vivo*[75,76]. A phase 3 clinical trial using an ASO and a phase 2 clinical trial using a siRNA targeting TTR are ongoing[77].

The occurrence of ocular complications in FAP patients increases with time[78] even after OLP because retinal pigment epithelial cells of the eye continued to synthesize mutant TTR. Retinal laser photocoagulation may be used to mitigate ocular manifestations in FAP patients. This technique, commonly used to treat many retinal diseases, damages the retinal pigment epithelium and has already prevented progression of amyloid deposition in the vitreous and on the retinal surface in certain FAP patients without causing any adverse effects[79].

1.2.8.2 - Strategy 2: Prevent the Formation of the Amyloidogenic Intermediate

TTR tetramer dissociation leads to formation of amyloidogenic intermediate species. Therefore, stabilizing tetrameric TTR is a promising method to prevent amyloid formation. Presently two drugs with this mechanism of action, tafamidis and diflunisal are in development.

Tafamidis, or 2-(3,5-dichloro-phenyl)-benzoxazole-6-carboxylic acid, has been approved in Europe (2011) and Japan (2013) for treatment of adult FAP patients with early symptomatic polyneuropathy to delay neurological impairment. In the clinical trials this small molecule has delayed peripheral neurologic impairment in 60% of the patients in early stages of the disease[80,81].

Diflunisal, a nonsteroidal anti-inflammatory drug developed in 1971, is also in clinical trials for its repurposing as a FAP medication. It has already demonstrated the reduction of rate progression of neurological impairment and preservation of quality of life[82].

Long-term therapeutic effects of those TTR stabilizers are not yet known, they are far of being regarded as a curative treatment. Currently a great number of structurally diverse small molecules are being investigated to act as tetramer stabilizers. One of the major difficulties in the selection of these compounds is the non-specific binding to other plasma proteins compromising their efficacy.

1.2.8.3 - Strategy 3/4: Prevent the Association of the Amyloidogenic Species and Disaggregation of the Amyloid Fibrils

Blocking the association of the amyloidogenic units into aggregates and fibrils may be regarded as a promising therapeutic strategy. This approach has some drawbacks because the structure of this intermediary amyloidogenic unit is not yet completely known may be highly heterogeneous. Fibril disruption is also a possible therapeutic strategy that has been under study in the last years.

Immunotherapies are one of the candidates for TTR amyloidosis treatment using these strategies. Several antigenic mapping methods have been used to study whether major antigenic sites differed for

WT-TTR, mutant TTR and *in situ* amyloid fibrils[83]. A TTR mutant, Y78F, designed to destabilize the native structure has been shown to expose a cryptic epitope recognized by a monoclonal antibody that reacts only with highly amyloidogenic mutants presenting the amyloid fold or with amyloid fibrils[84]. Immunization of transgenic mice carrying the most common FAP-associated TTR mutant (Val30Met) with TTR Y78F showed a significant reduction in TTR deposition suggesting that Y78F induced production of an antibody that reacts specifically with deposits and leads to an immune response effective in removing/preventing TTR deposition[85].

Epigallocatechin-3-gallate (EGCG), 4′-iodo-4′-deoxydoxorubicin (IDOX), tauroursodeoxycholic acid (TUDCA) and doxycycline are regarded as possible therapeutic compounds. EGCG, a natural polyphenol from green tea, was demonstrated to act as a tetramer stabilizer of TTR Val30Met[86] and also as an amyloid fibril disruptor *in vitro*[87]. *In vivo* studies with FAP mice models confirmed this results[88]. A single-center observational trial showed that patients suffering from cardiomyopathy derived from mutant TTR, treated with green tea or green tea extracts presented improvements in their condition, namely a decrease of cardiac wall thickness and mass, suggesting that EGCG halted TTR deposition and increase TTR amyloid deposits clearance[89].

IDOX, a tetracycline antibiotic, was shown to interact with five types of amyloid fibrils, including TTR amyloid, inhibiting fibril growth[90]. *In vitro* studies with Leu55Pro-TTR and IDOX demonstrated that this compound disrupts preformed amyloid fibrils without producing toxic species[91].

TUDCA, a natural compound with potent anti-apoptotic and anti-oxidant actions that reduces cytotoxicity in several neurodegenerative diseases[92], was tested in transgenic mice for human Val30Met-TTR mutation leading to a decrease in TTR deposition[93]. The mechanism for this result remains to be elucidated, however, the effect as a TTR stabilizer and inhibitor of fibril formation was discarded[93].

Doxycycline (Figure 12) is a synthetic tetracycline derivative with similar antimicrobial activity. Doxycycline has demonstrated anti-amyloidogenic activity *in vitro*[94], acts as Leu55Pro-TTR amyloid fibril disrupter *in vitro*[91] and disaggregates amyloid deposits in Val30Met TTR transgenic mice with concomitant decrease of various tissue markers[95,96].

This compound also has been administrated in combination with TUDCA in the TTR Val30Met transgenic mouse model[97]. This approach resulted in a significant reduction in TTR deposition and associated tissue markers. Currently a phase-II clinical trial using this combination is in progression displaying promising results[98]. In this clinical study no severe adverse effects were reported, no clinical progression of cardiac involvement was observed and the neuropathy remained substantially stable over one year[98].

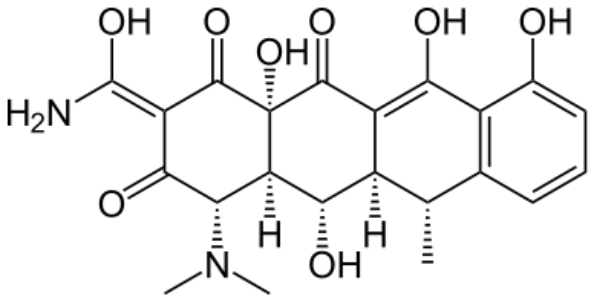

Figure 12: Structure of doxycycline.

Aims

The overall objective of this work is the development of an experimental protocol to screen for WT-TTR fibril disrupters.

More specifically the aims are:

- ✓ Select and characterize the most relevant and appropriate fibril formation protocol;
- ✓ Choose appropriate experimental methods that can provide relevant information about the effect of the candidate compounds on fibril interaction and/or disruption;
- ✓ Define the most effective order of assays to be performed that can save time and resources without compromising the screening process;
- ✓ Validate the protocol using compounds that already have been established as TTR fibril disrupters, for example doxycycline.

Chapter 2: Experimental section

2.1 – Materials

Recombinant human WT-TTR was produced in an *Escherichia coli* expression system and purified according to a previously described protocol[58].

Doxycycline was purchased from AK Scientific (Union City, USA). Hydrochloric acid was obtained from Merck (Frankfurt, Germany).

Sodium azide, thioflavin-T, deuterium oxide, dimethyl sulfoxide-d_6 and all the other reagents used for buffer and sample preparation were purchased from Sigma-Aldrich (St. Louis, USA), and obtained with the highest purity available.

2.2 – Methods

2.2.1 - Dynamic Light Scattering

Dynamic Light Scattering (DLS), also known as Photon Correlation Spectroscopy or Quasi-Elastic Light Scattering, is a well-established technique for measuring the size and size distribution of molecules and particles in solution typically in the submicron region[99]. This technique can be used to measure samples consisting of particles suspended in a liquid (e.g. proteins, polymers, micelles, nanoparticles, colloidal dispersions and emulsions). This method has several key advantages: it is non-invasive and non-destructive, allowing complete sample recovery, small quantity of sample is required and allows fast analysis and high throughput [99].

2.2.1.1 - Principles

DLS measures Brownian motion relating this to the size of the particles. Colloidal sized particles in a liquid undergo random motion due to multiple collisions with the thermally driven molecules of the liquid (Brownian motion). The larger the particle, the slower the Brownian motion will be.

When a solution with particles in Brownian motion is irradiated with a monochromatic light beam, typically a laser light, the intensity of the scattered light fluctuates over very short timescales at a rate that is dependent upon the size of the particles. Analysis of these intensity fluctuations yields the Brownian motion velocity. The Brownian motion velocity is determined by a property called translational diffusion coefficient (D).

For a solution of given viscosity, at constant temperature, the rate of diffusion or diffusion coefficient is inversely related to the particle size according to the Stokes-Einstein equation (Equation 1):

$$d(H) = \frac{\kappa \mathrm{T}}{3\pi\eta D} \qquad \text{(Equation 1)}$$

Where d(H) is the hydrodynamic diameter, D is the translational diffusion coefficient, κ is the Boltzmann's constant, T is the absolute temperature and η is the viscosity of the solvent.

The diameter measured in DLS is called hydrodynamic diameter referring to how a particle diffuses within a fluid, it is the diameter of a sphere that has the same translational diffusion coefficient as the particle. This value will depend not only on the size of the particle "core", but also on any surface structure, as well as the concentration and type of ions in the medium.

2.2.1.2 - Instrumentation

The DLS set up for the Beckman Coulter N5 Submicron Particle Size Analyser, used in this work, is illustrated in figure 13. In a DLS experiment the laser passes through the focusing lens and then hits the optical cell with the solution containing the particles being analysed. The light is scattered and the six fiber-optic receptors, stepper motor and photomultiplier (PMT) tube define the angle of scattered light detection. The PMT produces a current pulse for every photon of scattered light detected, transforming a variation of intensity in a variation of voltage. This burst of current passes to the pulse amplifier and discriminator (PAD) and the PAD determines whether the pulse is larger than a certain threshold level in which case it is shaped and amplified so that it is easily detected by the digital autocorrelator[100].

The digital autocorrelator computes the autocorrelation function (ACF) of the current pulses. The ACF is the mathematical transformation of the signal into a function (Equation 2):

$$G(\tau) = < I(t) \times I(t+\tau) > \qquad \text{(Equation 2)}$$

Where: G(**τ**) = ACF; I(t) = intensity detected at time t; I(t+**τ**) = intensity detected at time t+**τ**; **τ** = delay time; <> = quantity enclosed is a time average. By computing the ACF for a large range of **τ**s, a quantitative measure of the light fluctuations (or the changes in the pattern of particles) is found. This quantitative measure of the time scale of fluctuations (called the decay time) is directly related to particle size[100].

The microprocessor receives the information of the digital autocorrelator and takes the commands trough the software translating them into the appropriate form to drive the digital autocorrelator, set the temperature or select an angle for measurement[100].

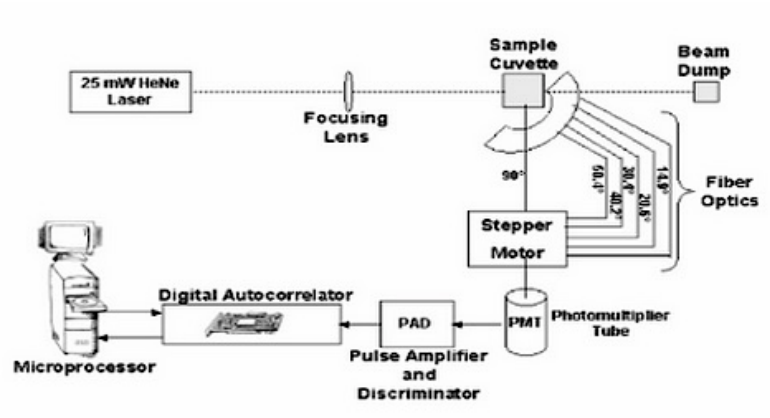

Figure 13: Functional block diagram of the Beckman Coulter N5 Submicron Particle Size Analyser[100].

2.2.1.2 – Result analysis

The Beckman Coulter N5 Submicron Particle Size Analyser controlled by the PCS software can provide two forms of data analysis: unimodal and size distribution processor (SDP). Both analyses can provide results in terms of particle size and/or molecular weight.

Unimodal analysis is a faster method, but it only determines the mean-scattering-intensity-weighted particle size (particle mean size) with the standard deviation of the size distribution and the polydispersity index (PI) of the particle size distribution. The limitation of the unimodal analysis is that it is less accurate for complex distributions. Although unimodal results are more accurate for size distributions that are not extremely polydisperse, the mean size provided is still a reliable measure of the sample's mean size even if the true distribution is complex. PI values below 0.1 indicate that the sample is monomodal (narrow distribution), values over 0.3 indicate that the sample is considered polydisperse.

SDP analysis determines the particle size distribution without assuming a unimodal distribution. Since the N5 equipment does not count individual particles the different decay times (due to the different sized particles) are mixed together in a composite ACF that characterizes all the particles simultaneously. The software mathematically separates the decay times using an algorithm based on a FORTRAN program called CONTIN. SDP analyses provide histograms of particle size distributions that can be displayed in three different formats: intensity, volume (weight) or number. In intensity histograms the magnitude of each peak is proportional to the percent (% amt) of the total scattered intensity due to particles of each size. The intensity distribution can be converted to a volume distribution if the complex refractive index of the particles is known. Number distributions are determined by dividing the volume results by the cubed diameter of the particles in the distribution.

2.2.2 - Saturation Transfer Difference Nuclear Magnetic Resonance

Saturation transfer difference nuclear magnetic resonance (STD NMR) is one of the ligand-based nuclear magnetic resonance techniques most widely used for the study of protein-ligand interactions[101]. Nowadays this technique is an important tool in drug discovery. STD NMR can be used as a screening technique for the identification of lead compounds and in the identification of ligand moieties important for binding[102].

STD NMR has several key advantages in comparison with other NMR based screening methods such as reduced protein (or receptor) requirements, no in depth NMR information about the target is needed because the focus is on the ligand signals, it is applicable to large molecular weight proteins and it is relatively easy to applicate[103].

However, this technique also suffers from some drawbacks. This method can only be used to probe low affinity interactions (dissociation constant, K_D, ranging from 10^{-8} M to 10^{-3} M)[104] , it does not detect high-affinity ligands that undergo slow chemical exchange on the NMR time scale or ligands with very low affinity.

The acronym STD describes the bases of the method that involves saturation and difference. Basically an STD experiment involves subtracting a spectrum in which the protein was selectively saturated (on-resonance spectrum) from one recorded without protein saturation (off-resonance spectrum) (Figure 14). The on-resonance spectrum is obtained by irradiation on the protein signals at a frequency range where no ligand protons resonate. Selective saturation of a single protein resonance will result in a rapid spread of the magnetization over the entire protein (spin diffusion)[105]. If the ligand binds to the receptor protein the saturation also transfers to the ligand[105]. The off-resonance spectrum is taken without protein irradiation. In the difference spectrum only the signals of the ligand that received saturation transfer from the protein via spin diffusion, through the nuclear Overhauser effect (NOE), will remain.

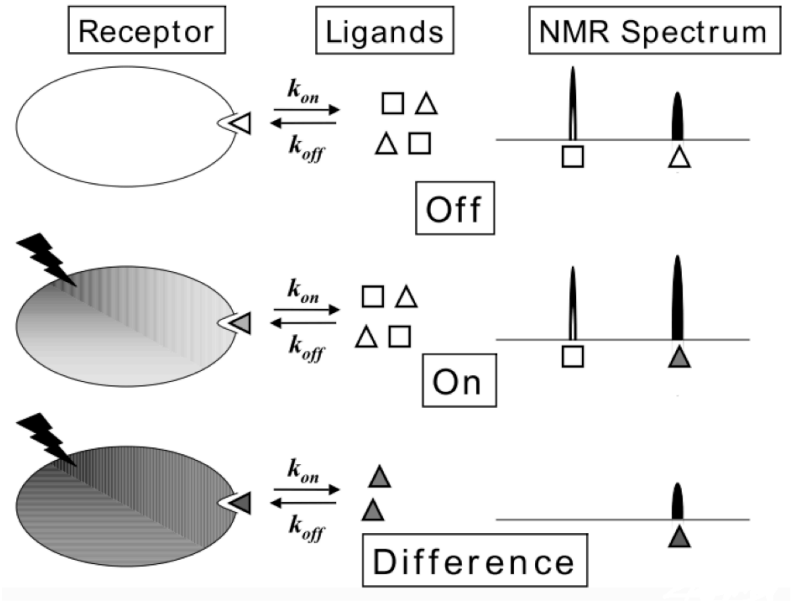

Figure 14: Scheme of the STD NMR experiment[103]**.**

2.2.3 - Circular Dichroism

Circular dichroism (CD) is defined as the unequal absorption of left-handed and right handed circularly polarized light (Equation 3) occurring when a molecule contains one or more chiral chromophores. CD spectroscopy measures the CD of molecules over a range of wavelengths.

$$\Delta A(\lambda) = A(\lambda)_{LCPL} - A(\lambda)_{RCPL} \qquad \text{(Equation 3)}$$

A chiral chromophore is optically active yielding a CD signal for one of the following reasons: (a) it is intrinsically chiral because of its structure, (b) it is covalently linked to a chiral centre in the molecule or (c) it is placed in an asymmetric environment by virtue of the three-dimensional structure adopted by the molecule[106].

CD is an important technique in the study of large biological molecules namely proteins and especially for secondary structure determination[107]. In proteins, the chromophores of interest include the peptide bond (absorption below 240 nm), aromatic amino acid side chains (absorption in the range 260 to 320 nm) and disulphide bonds (weak broad absorption bands centred around 260 nm)[106].

Far-UV CD encompasses the spectral region between 180 and 250 nm and provides information about protein secondary structure. Absorption in this region is predominantly based on the excitation of electronic transitions in amide groups, there is a weak but broad n➔π* transition centred around 220 nm and a more intense π➔π* transition around 190 nm.

The peptide backbone forms characteristic secondary structures such as α-helices, β-sheets, turns, and disordered sections with specific Φ, Ψ dihedral angles and H-bond patterns affecting the CD spectrum. These different structural elements have characteristic CD spectra (Figure 15).

CD data is usually presented in terms of ellipticity (θ) (degrees) or differential absorbance (ΔA).

Differential absorbance can be converted in ellipticity using the following expression (Equation 4):

$$\theta\text{obs} = 32.98\,\Delta\text{A} \qquad \text{(Equation 4)}$$

For protein far-UV CD this units are usually converted in mean residue ellipticity using the following expression (Equation 5):

$$[\theta]\text{MRW} = \frac{\theta obs \times 100 \times MM}{c \times l \times nA} \qquad \text{(Equation 5)}$$

Where: $[\theta]_{MRW}$ = mean residue ellipticity (deg.cm^2.dmol^{-1}); θ_{obs} = observed ellipticity (degrees); MM= molecular mass (Da); c = concentration (g/ml); l = pathlength (cm); nA = number of aminoacids residues per protein or peptide.

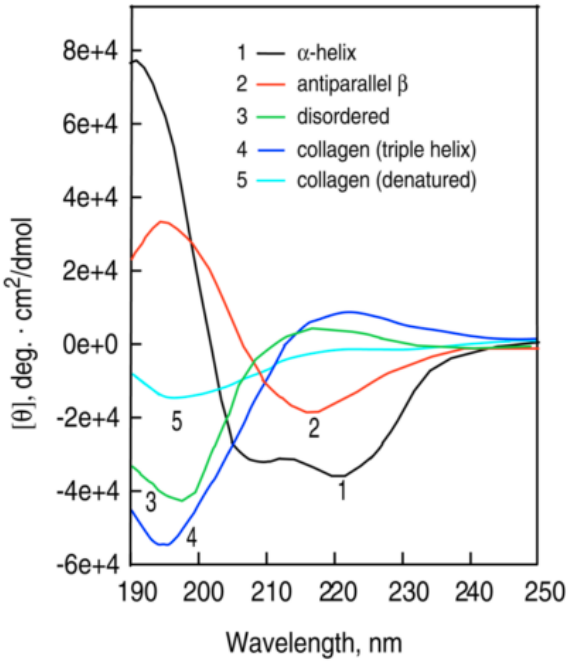

Figure 15: Circular dichroism spectra of polypeptides and proteins with representative secondary structures[107].

2.2.4 - Fluorescence Spectroscopy

Fluorescence spectroscopy, also known as fluorometry or spectrofluorometry, is a type of electronic spectroscopy. This technique involves using a beam of light (usually UV) to excite the electrons in certain chemical groups, named fluorophores, causing them to emit light of a lower energy, tipically but not necessarily visible light.

As represented in the Jablonski diagram (Figure 16) when the fluorophore absorbs energy it goes from the ground singlet electronic state (S0) to a higher energy excited singlet state (S1). A fluorophore is usually excited to some higher vibrational level of S1 but it rapidly relax to the lowest vibrational level of S1 in a process called internal conversion. Fluorescence emission occurs as the fluorophore decay from the singlet electronic excited states to an allowable vibrational level in the electronic ground state[108].

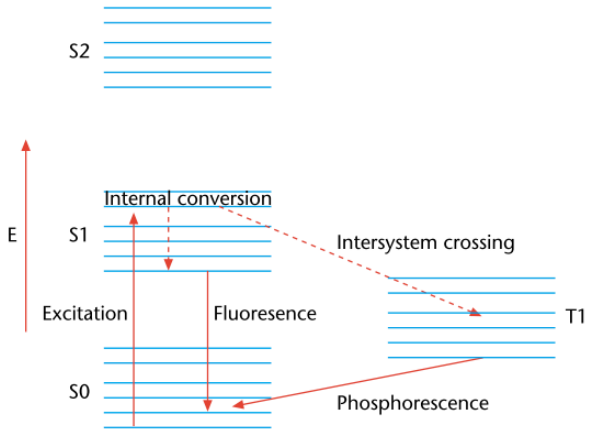

Figure 16: The Jablonski diagram of fluorophore excitation, radiative decay and nonradiative decay pathways. E represents the energy scale; S0 is the ground singlet electronic state; S1 and S2 are the successively higher energy excited singlet electronic states. T1 is the lowest energy triplet state[109].

Fluorescence spectroscopy is one of the most useful biophysical techniques available to study structure and function of biological molecules, particularly proteins, due to sensitivity, ease of use, and flexibility[110]. It has been used to study protein folding, dynamics, assembly, interactions, as well as membrane structure and also has been successfully applied to investigate protein aggregation, including amyloid fibril formation[58] and the interaction of amyloidogenic proteins with membranes, as well as their dynamic structures[111].

Tryptophan, tyrosine and phenylalanine residues are naturally occurring fluorophores in proteins. The intrinsic fluorescence of proteins has been extensively explored to study protein dynamics and conformational changes[110]. Extrinsic fluorescent dyes can also be used in various fields of protein analysis[112]. Recently, the use of extrinsic fluorescent dyes such as ANS, Bis-ANS, Nile Red, Thioflavin T

and others has increased, because of their versatility, sensitivity and suitability for high-throughput screening.

In this particular work the extrinsic fluorescent dye Thioflavin T is extensively used.

2.2.4.1 – Thioflavin T

In 1959, Vassar and Culling were the first to describe the use of Thioflavin T (ThT) (Fig.17) as a potent fluorescent marker of amyloid deposits in histology[12]. They noticed that ThT selectively localized amyloid deposits exhibiting a dramatic increase in fluorescent brightness[12].

Further studies expanded the range of applications of ThT from histology to *in vitro* characterization[113]. This benzathiole dye upon binding to amyloid fibrils displays a dramatic shift of the fluorescence excitation maximum (from 385 nm to 450 nm) and the emission maximum (from 445 nm to 482 nm) becoming highly fluorescent.

Despite its common use in the diagnosis of amyloid fibrils in *ex vivo*, *in vitro*, and animal model studies the molecular mechanism of ThT binding to amyloid fibrils is still being elucidated[114].

In the particular case of the interaction between ThT and TTR amyloid fibrils it has been shown that ThT dramatically increases its fluorescence quantum yield when bound to mature amyloid fibrils. However, this does not occur in the presence of the native tetramer or the unfolded monomer and only a minor increase is observed in the presence of early oligomers and protofibrils[115].

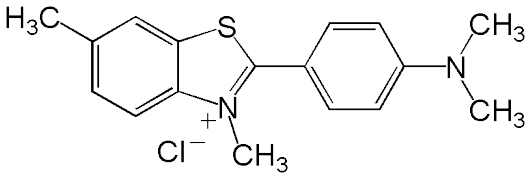

Figure 17: Thioflavin T structure.

2.2.5 - Turbidity assays

The turbidity assays used to probe protein aggregation and for high-throughput screening of *in vitro* amyloid fibrillogenesis inhibitors[116] are based on monitoring the absorbance of the sample over time. The increase in turbidity is due to protein precipitation under acidic conditions, with fibrils and/or amorphous aggregates being formed depending on the pH, temperature and time. These methods are sensitive to total insoluble protein since turbidity does not give information on the nature of the aggregate species[50].

2.2.6 – Transmission electron microscopy

Transmission electron microscopy (TEM) is a technique based on the interaction of an electron beam with a sample. In a transmission electron microscope a cathode ray source is used to emit and accelerate a high-voltage electron beam, which is focused by electrostatic and electromagnetic lenses. When the electrons pass through a thin specimen, an image carrying the information about the structure of the specimen is formed from the electrons transmitted through the specimen. This image is then magnified and focused by an objective lens and appears on an imaging screen that can be a fluorescent screen, photographic plate, or light sensitive sensor such as a CCD (charge-coupled device) camera.

Because biological macromolecules have low contrast when viewed by TEM, strategies such as negative staining are used. In this strategy the stain, typically uranyl acetate, circumscribes the macromolecule, the shape of which is deduced from distribution of the stain, which scatters most of the electrons.

TEM offers very powerful magnification and resolution (up to 0.2 nm) and has been used to study the morphology of protein aggregates and fibrils[117].

2.3 – Experimental protocol

2.3.1 – Sample preparation

After a careful review of the literature several experimental conditions were tested to produce amyloid fibrils of WT-TTR.

2.3.1.1 - WT-TTR fibrils assembly at pH 2 with 0.1 M NaCl

Samples of acid-unfolded TTR at pH 2 were prepared by dialysis against 10 mM HCl for 96 hours at 4°C in a Slide-A-Lyzer cassette with a molecular weight cut off membrane of 3500 Da. TTR aggregation was induced by addition of NaCl to a final concentration of 0.1 M[115]. Aggregation was carried out for at least a week at room temperature. The TTR concentration as tetramer used was approximately 80 μM. TTR concentration was determined by UV/visible spectroscopy in a UV500 Spectronic Unicam spectrometer by reading the absorption at 280 nm and using the TTR molar absorption coefficient (ε_{280}=7,76 x 10^4 $M^{-1}cm^{-1}$)[55].

2.3.1.2 - WT-TTR fibrils assembly at pH 2 with 0.1 M NaCl followed by pH change to 7.4

Mature TTR fibrils assembled at pH 2 with 0.1 M NaCl were diluted in phosphate buffered saline (PBS) pH 7.4 to the desired final concentration.

2.3.1.3 - WT-TTR fibrils assembly at pH 4.4

Aggregation was induced by addition of WT-TTR in 10 mM sodium phosphate, 100 mM KCl and 1 mM EDTA (pH 7.2) to an equivalent volume of 200 mM sodium acetate, 100 mM KCl and 1 mM EDTA (pH 4.32)[53]. The resulting solution with a pH of 4.4 was incubated for 72 hours at room temperature. The TTR concentration ranged between 7.2 and 40 μM.

2.3.1.4 - WT-TTR fibrils assembly at pH 4.4 followed by pH change to 7.4

Mature TTR fibrils assembled at pH 4.4 were diluted five times in Tris-HCl buffer at pH 8.7.

2.3.1.4 - WT-TTR fibrils induced by heating at pH 7.4

WT-TTR was dialyzed against 2 mM sodium phosphate and 20 mM NaCl at pH 7.4 over night at 4°C and diluted in the same buffer to a final concentration as tetramer of 3.6 μM. Fibrillar structures are obtained by heating the protein samples at 60°C for 6 days without stirring[118]. WT-TTR fibrils were then maintained at 37°C.

2.3.2 – Dynamic light scattering

To study the effect of doxycycline on WT-TTR fibril disruption, WT-TTR pre-formed fibrils (3.6 μM) were incubated with or without 50x molar excess of doxycycline and with 0,02% of sodium azide to prevent microorganism growth.

To study the effect of doxycycline on WT-TTR aggregation, doxycycline was added before the addition of 200 mM sodium acetate, 100 mM KCl and 1 mM EDTA (WT-TTR fibrils assembled at pH 4.4) and before the heating of protein samples at 60°C (WT-TTR fibrils induced by heating at pH 7.4). TTR, doxycycline and sodium azide concentrations were the same for the fibril disruption tests.

DLS measurements were carried out in 5 x 5 mm pathlength cuvettes and performed at 25°C or at 37°C, in the case of WT-TTR fibrils induced by heating at pH 7.4, in a N5 Submicron Particle Size Analyzer (Beckman Coulter, Miami, USA) controlled by the PCS software. Each sample was gently shaken and measured ten times with an equilibration time of 5 minutes and an acquisition time of 90 seconds. The sample volume used in these assays was 300 μl.

All the buffer solutions were previously filtered through 0.2 μm syringe filters (Whatman, England).

2.3.3 – STD NMR

All NMR spectroscopy experiments were performed at 25°C on a Bruker Avance III 400 MHz spectrometer equiped with a BBFO probe.

NMR samples, with a final volume of 350 μl, contained 20 μM of WT-TTR fibrils in the corresponding buffer, 10% of D2O and a 100x molar excess of doxycycline prepared in dimethyl sulfoxide-d6.

For STD NMR experiments, a pseudo-2D version of the STD NMR sequence was used for the interleaved acquisition of on- and off-resonance spectra. Selective saturation of the protein was achieved by a train of Gauss-shaped pulses of 50 ms length each, separated by a 1 ms delay.

The on-resonance irradiation of the protein was performed at a chemical shift of 0.75 ppm. Off-resonance irradiation was set at 50 ppm where no protein signals were present. Saturation time was 5 sec. The total scan number in STD experiments varied between 512 and 1536. Water suppression was performed by excitation sculpting.

2.3.4 – Circular dichroism spectroscopy

Far-UV CD data were acquired on an Olis DSM 20 circular dichroism spectropolarimeter continuously purged with nitrogen, equipped with a Quantum Northwest CD 150 Temperature-Controller system and controlled by the Globalworks software. Scans were collected between 195-260 nm at 1 nm intervals, three spectral scans with an integration time of 5 seconds per nm were averaged. The protein concentration used was 3.6 μM, the volume 50 μl and the cuvette pathlength was 0.2 mm. Baselines with buffer were also acquired and subtracted from the raw CD data.

2.3.5 – Thioflavin-T assay

ThT was used to probe amyloid formation. A freshly prepared stock solution of ThT (in 5 mM glycine–NaOH buffer, pH 9.0) was added to protein solutions (3.6 μM) in the absence or presence of 50x molar excess of doxycycline relative to protein. The samples final volume was 350 μl and the final concentration of ThT was 10 μM.

The stock solution was previously filtered through 0.2 μm syringe filters and the concentration determined by UV/visible spectroscopy in a UV500 Spectronic Unicam spectrometer by reading the absorption at 411 nm and using the thioflavin-T molar absorption coefficient ($2.2 \times 10^4\ M^{-1}cm^{-1}$).

Fluorescence experiments were preformed on a Varian Carey Eclipse spectrofluorometer equiped with a temperature controller system and controlled by the Varian Cary Eclipse software version 1.1.

ThT emission was monitored at 485 nm with the excitation wavelength set to 450 nm. Assays were carried out in 5 x 5 mm pathlength cuvettes with excitation and emission slits of 5 nm and continuous agitation with a magnetic stirrer. Spectra of ThT fluorescence were collected between 460 and 560 nm with an excitation wavelength of 450 nm. Baselines without protein were also acquired and subtracted from the corresponding raw data.

2.3.6 - Turbidity assays

Absorbance measurements were performed in a 96-well microplate at 450, 500, 550, 600 and 650 nm at 25°C or 37°C on a BioTek Eon microplate spectrophotometer controlled by the Gen 5 software version 2.01. The plates were shaken in an orbital way during 30 sec before the measurement.

Sample preparation was performed as described for the DLS assay but in this case the final volume in each well was 100 µl. The absorption values of the blanks were determined and subtracted from the corresponding raw data.

2.3.7 - Transmission electron microscopy

WT-TTR fibrils were analysed by TEM. The sample aliquots (5 µL) were adsorbed onto carbon coated collodium films supported on 400-mesh copper grids for 1 minute. The grids were negatively stained with 1% uranyl acetate and visualized using a FEI-Tecnai G2 Spirit Biotwin transmission electron microscope equipped with a MegaView III– SIS CCD camera.

Chapter 3: Results

In this work three WT-TTR fibril formation protocols were tested: pH 2 with 0.1 M NaCl, pH 4.4 and 60°C heating. These protocols and the alteration of sample pH were studied by DLS, turbidimetry, CD and TEM. ^{1}H STD NMR was used to study the interaction of doxycycline with WT-TTR fibrils and DLS and turbidimetry assays were performed to study the effect of doxycycline on the disruption of WT-TTR fibrils. In the DLS assays unimodal size analysis and SDP analysis were performed, despite the high polydispersity index of all the samples which was around 1, unimodal size analysis was performed to have a quicker and easier assessment of size alteration, however the sizes represented in the graphics cannot be considered a good estimation of the real size of fibrils.

3.1 - WT-TTR fibrils assembled at pH 2 with 0.1 M NaCl

3.1.1 - Study by ^{1}H STD NMR of the interaction of doxycycline with WT-TTR fibrils assembled at pH 2 with 0.1 M NaCl

To evaluate if doxycycline was able to bind to WT-TTR fibrils assembled at pH 2 with 0,1 M NaCl, ^{1}H STD NMR analysis was performed. The ^{1}H–NMR spectrum of the free ligand in the same buffer used to prepare WT-TTR fibrils, ^{1}H STD NMR spectrum of doxycycline (2 mM) in the presence of TTR fibrils (20 μM) and the off-resonance spectrum are represented in figure 18. The ^{1}H NMR STD spectrum of doxycycline in the presence of TTR fibrils (Figure 18B) indicates that doxycycline binds to WT-TTR fibrils. The signals present in the STD spectrum identified by their chemical shifts represent the doxycycline protons that are in direct contact with the fibrils. Signals from the aromatic protons H8, H7 and H9, the protons H5a and H6 and from the three methylic groups are observed. There are additional signals between 2,5 and 3 ppm that could not be unambiguously assigned due to the high density of resonances in this region. Additionally the resonances of the ligand broaden when in solution with the fibrils due to alteration of the relaxation time, which is further evidence of binding.

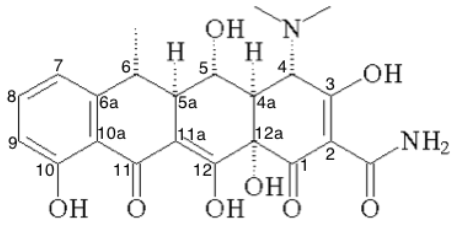

Doxycycline

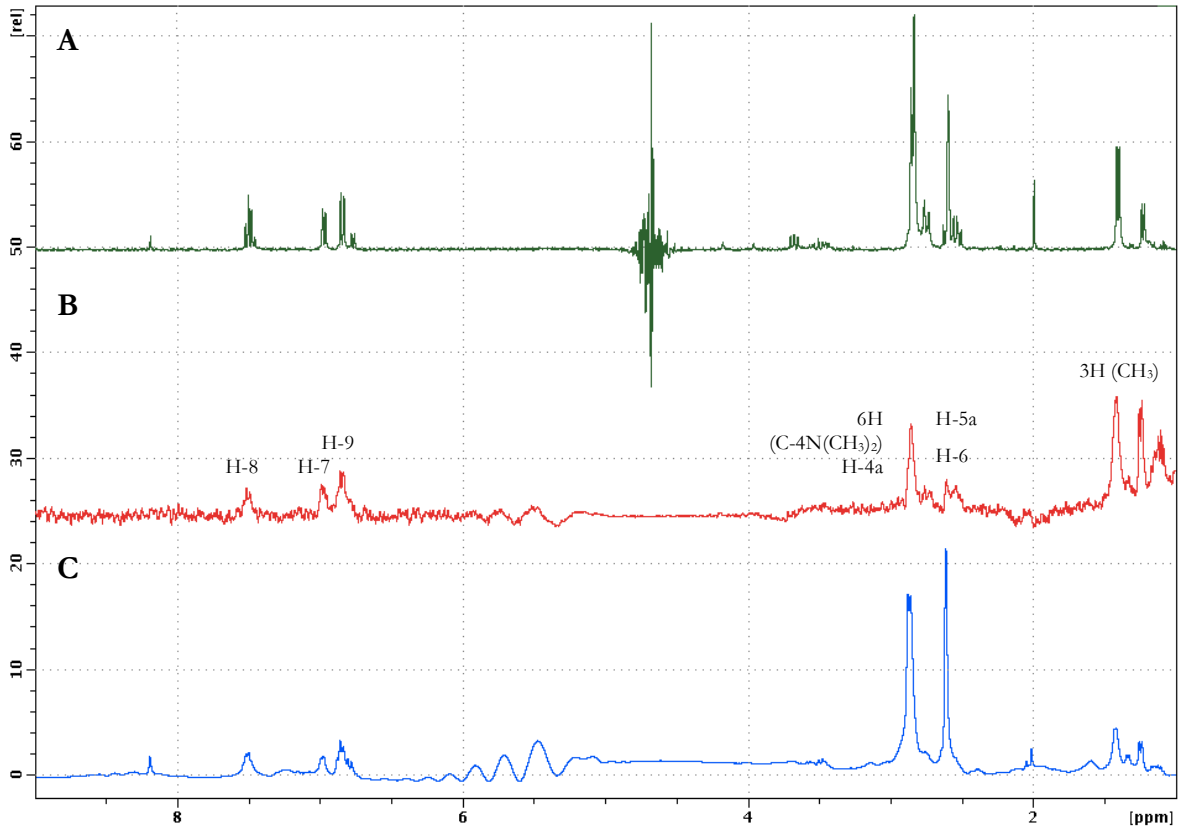

Figure 18: ^{1}H STD NMR of doxycycline (2 mM) in the presence of WT-TTR fibrils (20 µM) assembled at pH 2 and 0.1 M NaCl. A- Reference ^{1}H NMR spectrum of doxycycline at the corresponding pH; B- ^{1}H STD NMR spectrum with the doxycycline protons involved in the binding identified; C-Off resonance spectrum.

3.1.2 - Effect of doxycycline on the disruption of WT-TTR fibrils assembled at pH 2 with 0.1 M NaCl

The effect of doxycycline on WT-TTR fibrils assembled at pH 2 with 0,1 M NaCl was studied by DLS (Figure 19). WT-TTR pre-formed fibrils were incubated either in the absence or presence of a 50x molar excess of doxycycline and DLS measurements were carried out everyday until apparent size stabilization.

Right after the addition of doxycycline to the mature pre-formed fibrils (0 days) is observable a disruption of the fibrils is observed. The population of particles with a diameter between 100 and 1000 increases and the population of particles above 5000 nm decreases when compared to the control (Figure 19A, 0 days). However this immediate apparent effect was not maintained over time. In the following days the mean size increased and the populations of smaller particles decreased (Figure 19A, 7 days). In spite of this occurrence, when comparing the control with the doxycycline treated fibrils in the assay endpoint, 11 days, it is observed an increase in the polydispersity of the samples treated with doxycycline, with a larger population of small particles (between 100 and 1000 nm), which indicates fibril disruption.

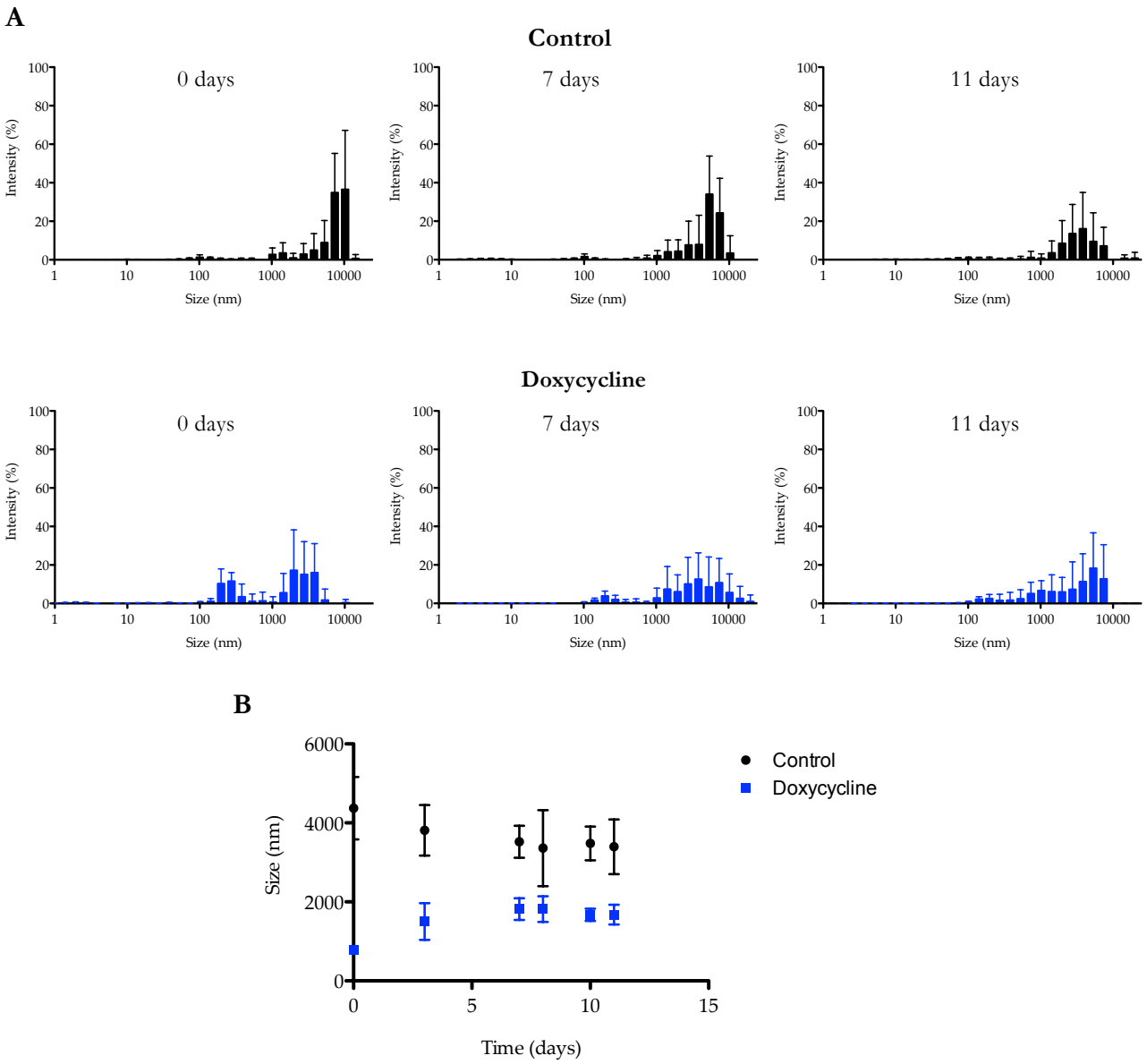

Figure 19: DLS analysis of the effect of doxycycline on WT-TTR pre-formed fibrils assembled at pH 2 with 0.1 M NaCl. WT-TTR fibrils (3.6 μM) were incubated either in the absence (Control) or presence of a 50x molar excess of doxycycline (Doxycycline) for the indicated period of time at room temperature. (A) SDP analysis represented as size distribution; (B) Unimodal size analysis.

3.2 - WT-TTR fibrils assembled at pH 2 with 0.1 M NaCl that undergo pH change to 7.4

3.2.1 - Effect of pH change to 7.4 in WT-TTR fibrils assembled at pH 2 with 0.1 M NaCl

In the case of WT-TTR the *in vitro* amyloid fibrillogenesis is often initiated by acidification of the medium, the low pH leading to the disassembly of TTR's quaternary structure followed by partial unfolding of the monomer that becomes prone to aggregation[119]. This process is also affected by other factors such as temperature, protein concentration, ionic strength and agitation.

Westermark and colleagues proposed the low pH environment, found in lysosomes, as a prerequisite for amyloid formation *in vivo*[119,120]. This proposal implies the formation of amyloid intermediates intracellularly, which is not consistent with the observation that TTR amyloid deposits are extracellular. Afterwards Quintas and colleagues demonstrated that the TTR tetramer dissociates to non-native monomeric species at pH 7 and nearly physiological ionic strengths, and that the monomeric species may self-assemble into high molecular mass aggregates, which contradicted that proposal[55].

The extracellular location of the WT-TTR amyloid deposits is widely demonstrated[23]. In this location, the pH is not acidic but around 7.4. Therefore, to develop a protocol to screen for WT-TTR fibril disrupters, mimicking the environment of the fibrils is very important. The pH may affect not only the overall structure of the fibrils but also the efficacy of the compound being tested. For this reason the pH of WT-TTR fibrils assembled at pH 2 with 0.1 M NaCl was changed to 7.4 diluting the very concentrated fibril stock in PBS.

The effect of pH change was studied by DLS, CD and TEM to observe if this pH alteration induces modifications in the size and structure of the WT-TTR fibrils. The DLS results (Figure 20) show that the alteration of pH from 2 to 7.4 lead to an immediate increase of particle populations above 10000 nm and a decrease in the particle populations between 1000 and 10000 nm (Figure 20B, 0 days) when compared to the control sample at pH 2 (Figure 20A, 0 days). Over time the larger particle populations decreased and the particle populations between 100 and 1000 nm increased. Size stabilization started around eight days after pH change. In the assay final day, day eleven, the sample at pH 7.4 had larger populations of smaller particles (between 100 and 1000 nm) and the populations of particles between 1000 and 10000 nm remained more similar to the particle populations at pH 2.

The unimodal size analysis is in accordance with the SDP analysis. We can clearly see an increase in the size of the fibrils at pH 7.4 in the first three days and a decrease in the overall size over time, in the last days of the assay the mean size of the fibrils at pH 7.4 is smaller than at pH 2.

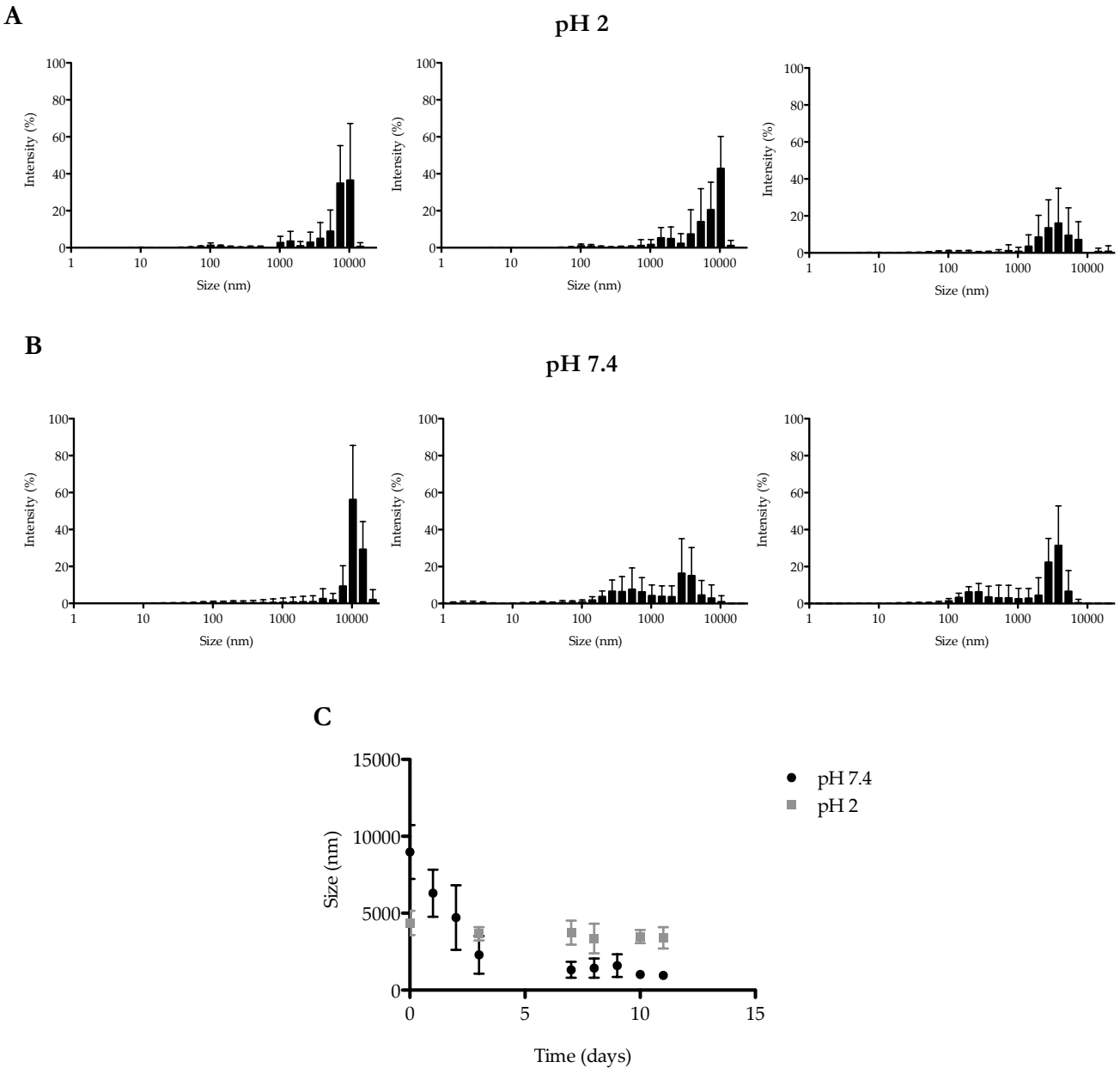

Figure 20: DLS analysis of the effect of pH change to 7.4 in WT-TTR fibrils assembled at pH 2 with 0.1 M NaCl. (A) SDP analysis represented as size distribution by intensity of WT-TTR fibrils (3.6 μM) assembled at pH 2 with 0.1 M NaCl at 0, 8 and 11 days; (B) SDP analysis represented as size distribution of WT-TTR fibrils assembled at pH 2 with 0.1 M NaCl that undergo pH change to 7.4 at 0, 8 and 11 days; (C) Unimodal size analysis over time of WT-TTR fibrils assembled at pH 2 with 0.1 M NaCl and that undergo pH change to 7.4.

The possible changes on the secondary structure of the WT-TTR fibrils were analysed by far-UV CD. WT-TTR fibrils have a characteristic far-UV CD spectrum with a minimum around 212 nm.

At pH 2 this typical CD spectrum is clearly observed (Figure 21) however at pH 7.4 the minimum at 212 nm is not as pronounced, indicating a loss in β-sheet secondary structure.

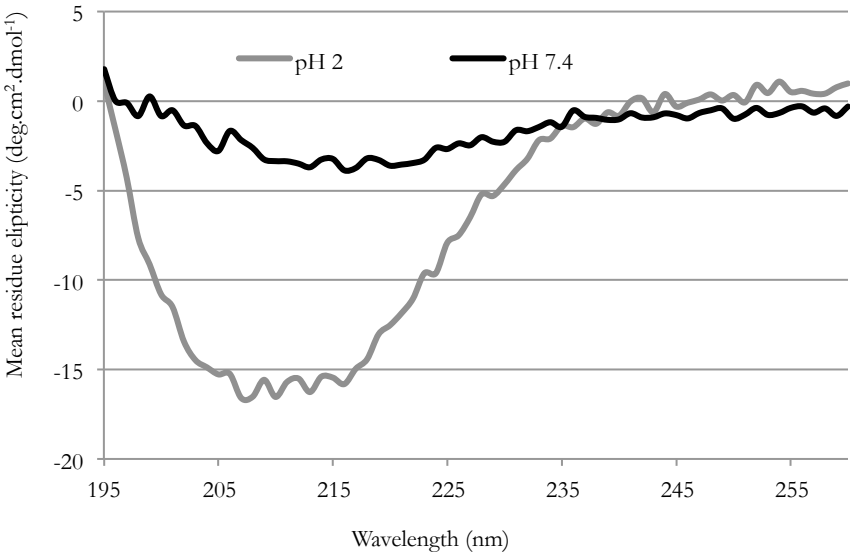

Figure 21: Far-UV CD spectra of WT-TTR fibrils assembled at pH 2 with 0.1 M NaCl (grey) and of WT-TTR fibrils assembled at pH 2 with 0.1 M NaCl that undergo pH change to 7.4 at 24 hours (black). Scans were collected between 195-260 nm at 1 nm intervals, three spectral scans with an integration time of 5 seconds per nm were averaged. The protein concentration used was 3.6 μM and the cuvette pathlength was 0.2 mm. Baselines with buffer were also acquired and subtracted from the raw CD data.

The TEM results (Figure 22) corroborated the observations made by DLS. The WT-TTR fibrils, which appear as white "lines" in the micrographs, at pH 2 seem to be very long unbranched structures (Figure 22A). At pH 7.4 they appear to be a bit shorter and are sometimes bundled together (Figure 22B).

As previously stated, the ThT assay is a feasible indication of the presence of amyloid structures. This fluorescence assay was also applied to the WT-TTR fibrils at pH 7.4 displaying positive results (Figure 23). In the fluorescence spectrum the emission maximum around 482 nm results from the binding of ThT to amyloid fibrils.

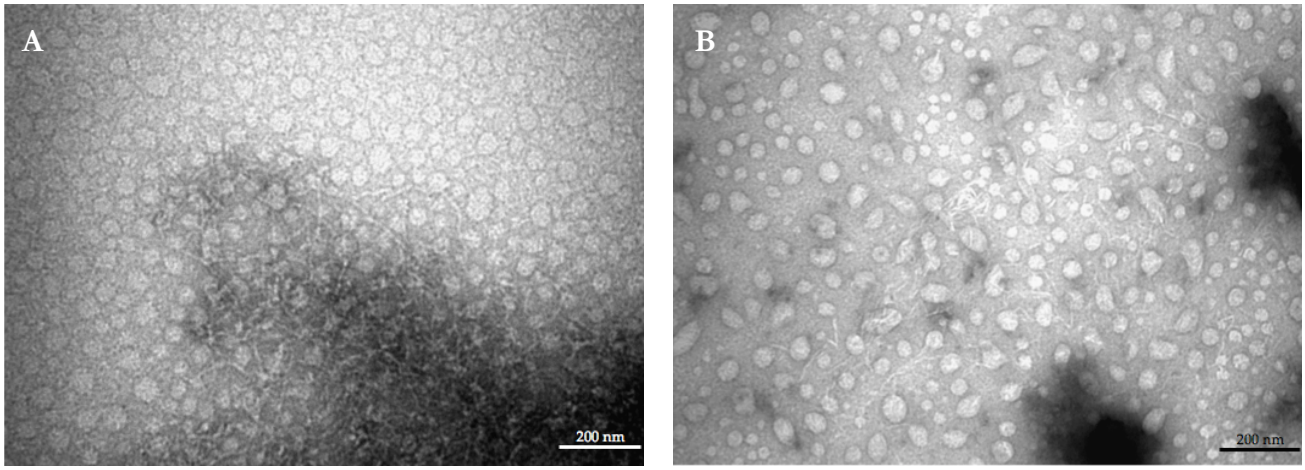

Figure 22: : TEM images of WT-TTR fibrils assembled at pH 2 with 0.1 M NaCl (A) and that undergo pH change to 7.4 (B). The images were taken approximately one month after pH change using a TTR concentration of 3.6 μM.

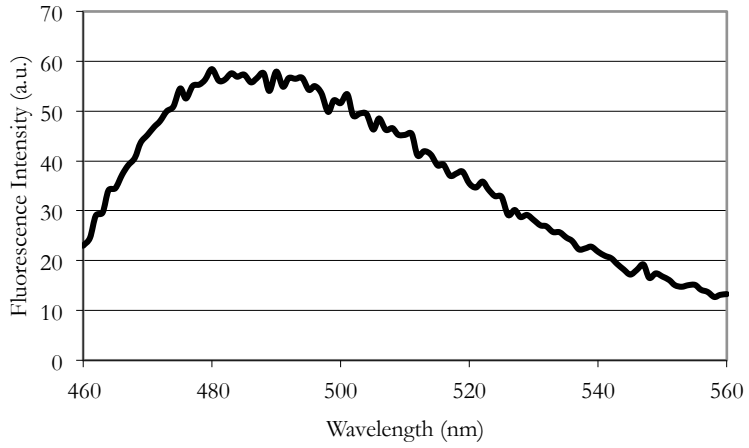

Figure 23: Thioflavin-T assay of WT-TTR fibrils assembled at pH 2 with 0.1 M NaCl that undergo pH change to 7.4. The spectrum of ThT fluorescence was collected between 460 and 560 nm with an excitation wavelength of 450 nm. The protein concentration used was 3.6 μM and the cuvette pathlength was 5 mm. A baseline spectrum with buffer and ThT was also acquired and subtracted from the raw fluorescence data.

3.2.2 - Study by ^{1}H STD NMR of the interaction of doxycycline with WT-TTR fibrils assembled at pH 2 with 0.1 M NaCl that undergo pH change to 7.4

To access if doxycycline was able to bind to WT-TTR fibrils assembled at pH 2 with 0,1 M NaCl after undergoing pH change to 7.4 ^{1}H STD NMR was performed. The ^{1}H NMR spectrum of the free ligand in the same buffer used to prepare WT-TTR fibrils, the ^{1}H NMR STD spectrum of doxycycline (2 mM) in the presence of TTR fibrils (20 µM) and the off-resonance spectrum are represented in figure 24. Similarly to what happens at pH 2 the ^{1}H NMR STD spectrum of doxycycline in the presence of TTR fibrils at pH 7.4 (Figure 24B) indicates that doxycycline binds to WT-TTR fibrils. However the protons implicated in the binding are not the same. In the STD spectrum only the protons H5a and H6 and from the three methylic groups are observed. Signals from the aromatic protons were not present. There are additional signals between 2,5 and 3 ppm that could not be unambiguously assigned due to the high density of resonances in this region.

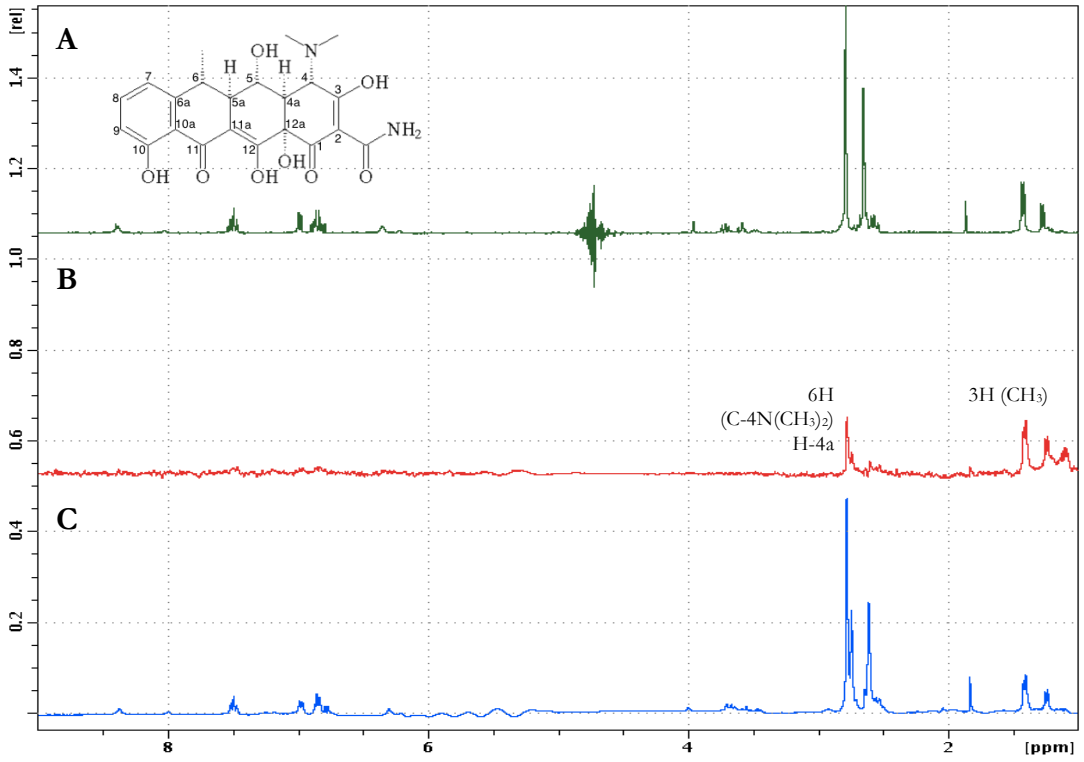

Figure 24: ^{1}H STD NMR of doxycycline (2 mM) in the presence of WT-TTR fibrils (20 µM) assembled at pH 2 and 100 mM NaCl that after undergoing pH change to 7.4. A- Reference ^{1}H NMR spectrum of doxycycline at the corresponding pH; B- ^{1}H STD NMR spectrum with the doxycycline protons involved in the binding identified; C-Off resonance spectrum.

3.2.3 - Effect of doxycycline on the disruption of WT-TTR fibrils assembled at pH 2 with 0.1 M NaCl that undergo pH change to 7.4

The effect of doxycycline on WT-TTR fibrils assembled at pH 2 with 0,1 M NaCl that undergo pH change to 7.4 was studied by DLS (Figure 25). After size stabilization, also followed by DLS (Figure 20), WT-TTR fibrils at pH 7.4 were incubated either in the absence or presence of a 50x molar excess of doxycycline and DLS measurements were carried out everyday until apparent size stabilization.

After doxycycline addition there were no immediate relevant effects in the fibril sizes (Figure 25A, 0 days). These observations were maintained for approximately ten days, after that period of time the particle populations with a size over 1000 nm started to decrease in the sample treated with doxycycline (Figure 25B, 10 days). In the assay endpoint, at seventeen days, the sample treated with doxycycline didn't have any significant population of particles equal or bigger to 1000 nm. This was not observed in the control sample that had particle populations between 1000 and 10000 nm (Figure 25A, 17 days). These observations indicate that doxycycline disrupts WT-TTR fibrils assembled at pH 2 with 0,1 M NaCl that undergo pH change to 7.4. The effect is not immediate but it is visible after seventeen days of incubation.

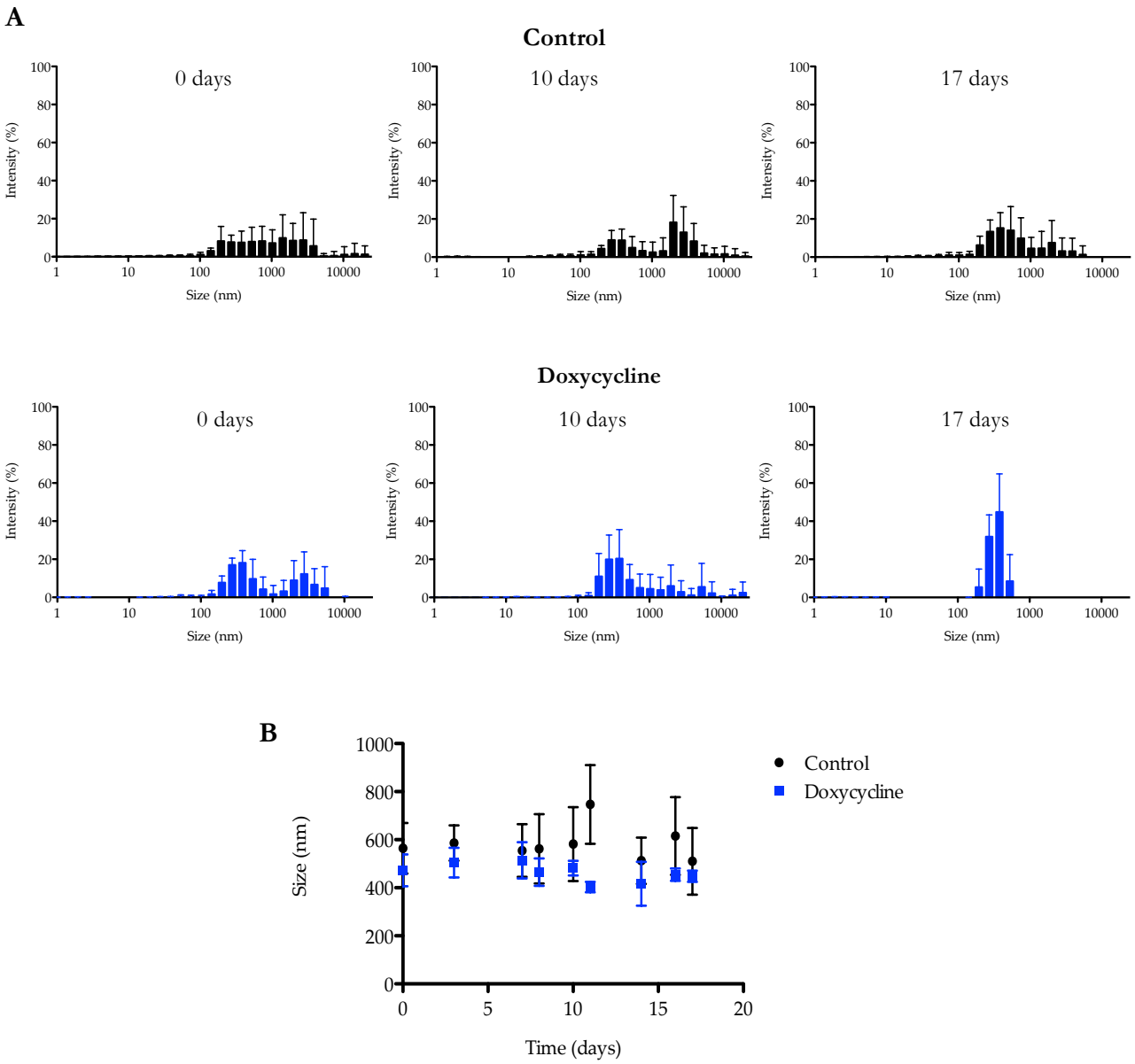

Figure 25: DLS analysis of the effect of doxycycline on WT-TTR pre-formed fibrils assembled at pH 2 with 0.1 M NaCl that undergo pH change to 7.4. WT-TTR fibrils (3.6 µM) were incubated either in the absence (Control) or presence of a 50x molar excess of doxycycline (Doxycycline) for the indicated period of time at room temperature. (A) SDP analysis represented as size distribution; (B) Unimodal size analysis.

3.3 - WT-TTR fibrils assembled at pH 4.4

3.3.1 - Effect of doxycycline on WT-TTR fibril assembly at pH 4.4

To investigate if doxycycline could prevent fibril assembly at pH 4.4 turbidimetry, DLS and fluorescence assays were performed. Doxycycline was added to WT-TTR in 10 mM sodium phosphate, 100 mM KCl and 1 mM EDTA before the addition of an equivalent volume of 200 mM sodium acetate, 100 mM KCl and 1 mM EDTA. The final concentration of WT-TTR was 3.6 μM and doxycycline concentration was 180 μM (50 x molar excess). A control was also performed without the addition of doxycycline. Turbidimetry and DLS measurements were performed every day for three days and in the sixth day.

Turbidimetry results (Figure 26) show that doxycycline does not arrest WT-TTR aggregation. In the first three days doxycycline seems to promote aggregation but in the sixth day the aggregation is lower in the doxycycline treated sample.

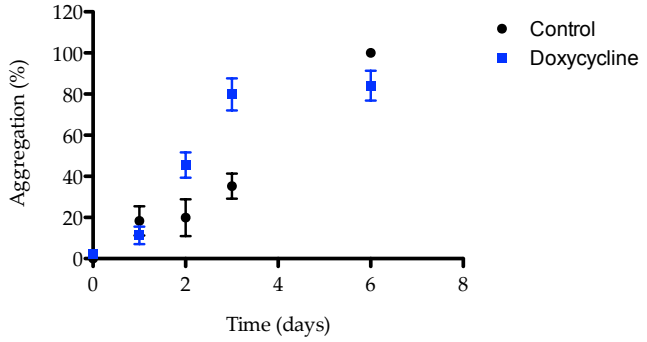

Figure 26: Effect of doxycycline on WT-TTR fibril assembly at pH 4.4 monitored by turbidimetry. Samples were incubated either in the absence (control) or presence of a 50 x molar excess of doxycycline for the indicated period of time at room temperature. Absorbance measurements were performed in a 96-well microplate at 450, 500, 550, 600 and 650 nm at 25°C. The percent aggregation was calculated for each wavelength using the following formula: Aggregation (%)= ((Abs$_{\lambda}$-Abs$_{min}$)/(Abs$_{max}$-Abs$_{min}$)) x100. The percentages of aggregation for each wavelength were then averaged and represented with the corresponding standard deviation. Baselines without protein were also acquired and subtracted from the corresponding raw data before the calculation.

The DLS assay also demonstrates that doxycycline doesn't arrest WT-TTR aggregation at pH 4.4 (Figure 27). The particle populations distribution of the control and doxycycline treated samples are similar in the first three days. Doxycycline marginally increases the size of bigger particle populations in the sixth day. Once again unimodal size analysis was performed to have a quicker and easier assessment of size alteration despite the high PI of the samples (Figure 27B).

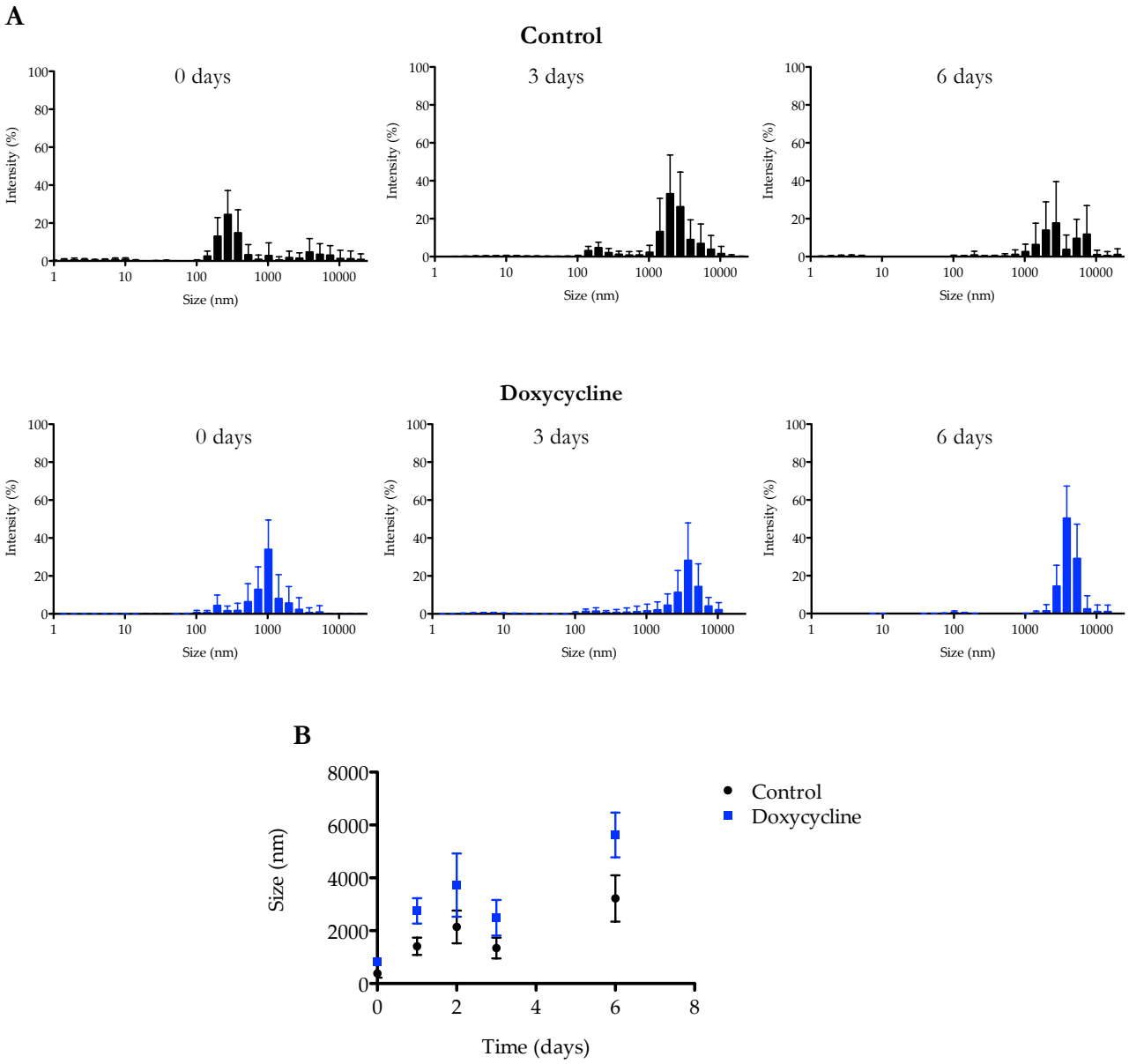

Figure 27: DLS analysis of the effect of doxycycline on WT-TTR fibril assembly at pH 4.4. WT-TTR fibrils (3.6 μM) were incubated either in the absence (Control) or presence of a 50x molar excess of doxycycline (Doxycycline) for the indicated period of time at room temperature. (A) SDP analysis represented as size distribution; (B) Unimodal size analysis.

The effect of doxycycline on the very first stages of WT-TTR amyloid formation at pH 4.4 was also studied. For that purpose a ThT fluorescence assay was performed. Doxycycline was added to WT-TTR in 10 mM sodium phosphate, 100 mM KCl and 1 mM EDTA before the addition of an equivalent volume of 200 mM sodium acetate, 100 mM KCl and 1 mM EDTA. The final concentration of WT-TTR was 3.6 μM and doxycycline concentration was 180 μM (50x molar excess). A control was also performed without the addition of doxycycline. After that, ThT (10 μM) was added and ThT emission was monitored at 485 nm with the excitation wavelength set to 450 nm for twelve hours. This assay

demonstrates that doxycycline does not affect the kinetic of WT-TTR amyloid formation at pH 4.4 in the first twelve hours of aggregation (Figure 28).

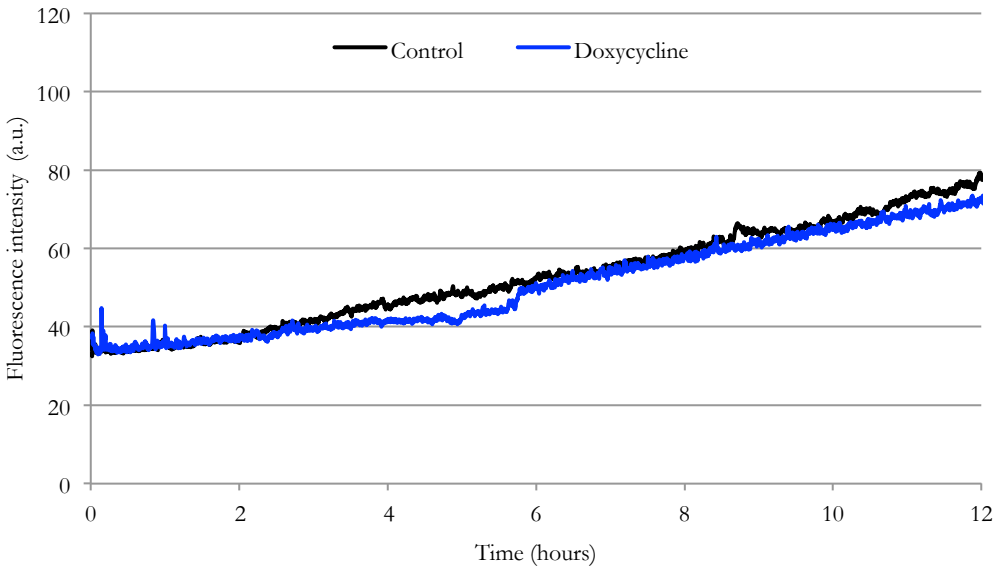

Figure 28: TTR aggregation kinetics monitored by ThT fluorescence. WT-TTR fibrils (3.6 μM) were incubated either in the absence (black) or presence of a 50x molar excess of doxycycline (blue) with ThT (10 μM) for twelve hours at 25°C. ThT emission was monitored at 485 nm with the excitation wavelength set to 450. Baselines without protein were also acquired and subtracted from the corresponding raw data.

3.3.2 - Study by ^{1}H STD NMR of the interaction of doxycycline with WT-TTR fibrils assembled at pH 4.4

To access if doxycycline was able to bind to WT-TTR fibrils assembled at pH 4.4 ^{1}H STD NMR analysis was performed. The ^{1}H NMR spectrum of the free ligand in the same buffer used to prepare WT-TTR fibrils, the ^{1}H NMR STD spectrum of doxycycline (2 mM) in the presence of TTR fibrils (20 µM) and the off-resonance spectrum are represented in figure 29. Doxycycline proton signals are absent in the ^{1}H NMR STD spectrum of doxycycline in the presence of TTR fibrils at pH 4.4 (Figure 29B). This may be due to the lack of binding or very weak binding between doxycycline and the fibrils, but could also be due to a very strong binding, outside the detection limits of the technique or even due to other technical reasons such as the physical state of the sample. Unlike what happens with the other fibril samples prepared at pH 2 with 0,1 M NaCl the sample with WT-TTR fibrils assembled at pH 4.4 is extremely turbid and the fibrils and aggregates seem to quickly precipitate in the NMR tube.

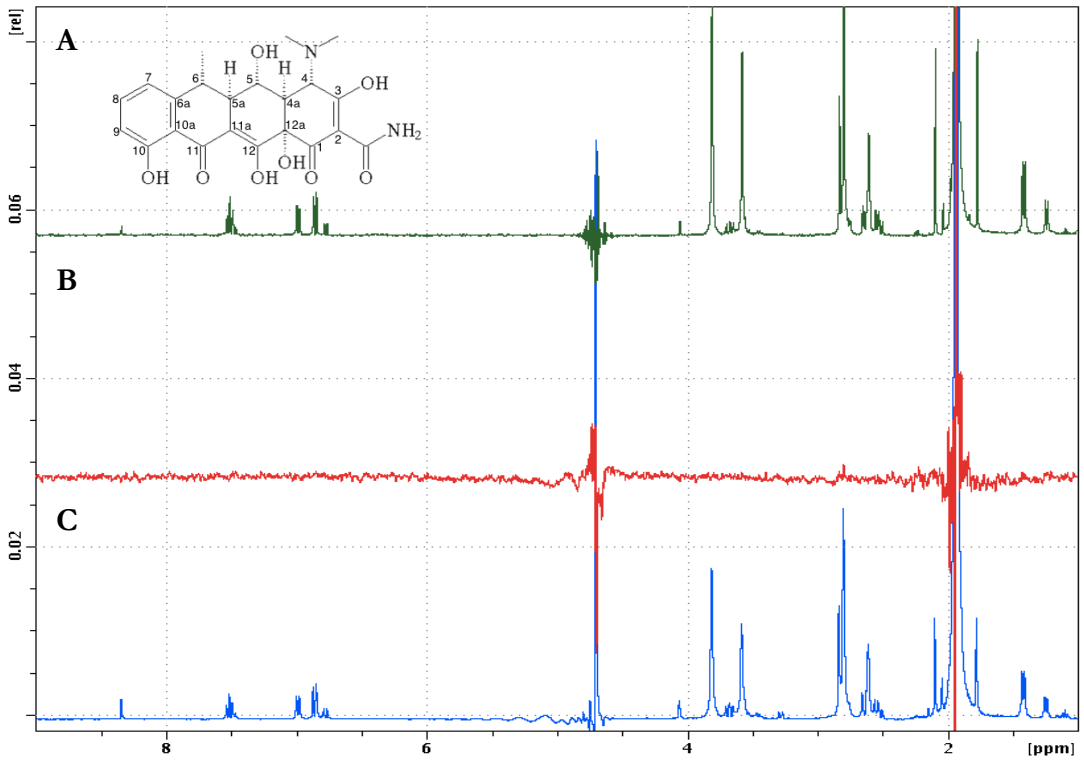

Figure 29: ^{1}H STD-NMR of doxycycline (2 mM) in the presence of WT-TTR fibrils (20 µM) assembled at pH 4.4. A- Reference ^{1}H NMR spectrum of doxycycline at the corresponding pH; B- ^{1}H STD-NMR spectrum; C- Off resonance spectrum.

3.3.3 - Effect of doxycycline on the disruption of WT-TTR fibrils assembled at pH 4.4

The effect of doxycycline on WT-TTR fibril disruption was studied by turbidimetry and DLS. In the turbidimetry assay doxycycline was added to WT-TTR in 10 mM sodium phosphate, 100 mM KCl and 1 mM EDTA before the addition of an equivalent volume of 200 mM sodium acetate, 100 mM KCl and 1 mM EDTA. The final concentration of WT-TTR was 3.6 μM and doxycycline concentration was 180 μM (50 x molar excess), a control was also performed without the addition of doxycycline. After that turbidimetry measurements were performed everyday until apparent stabilization. In this assay fibril disruption by doxycycline was observed (Figure 30). A clear decrease in the turbidimetry of doxycycline treated samples, observable around the fifteenth day of incubation, implies that the species in solution are smaller than in the previous days. This effect increases in the following days reaching a maximum in the twenty-first day of doxycycline treatment.

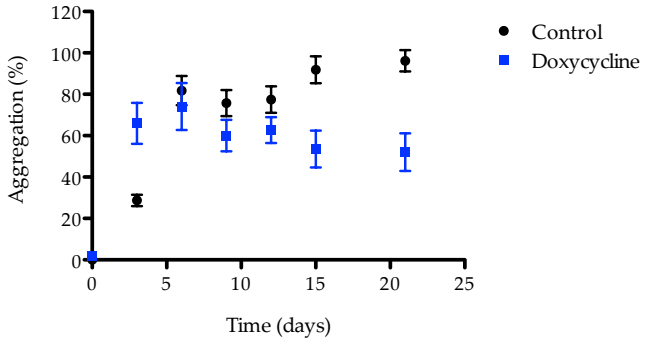

Figure 30: Effect of doxycycline on WT-TTR fibril disruption at pH 4.4 monitored by turbidimetry. Samples were incubated either in the absence (control) or presence of a 50 x molar excess of doxycycline for the indicated period of time at room temperature. Absorbance measurements were performed in a 96-well microplate at 450, 500, 550, 600 and 650 nm at 25°C. The percent aggregation was calculated for each wavelength using the following formula: Aggregation (%)= ((Absλ-Absmin)/(Absmax-Absmin)) x100. The percentages of aggregation for each wavelength were then averaged and represented with the corresponding standard deviation. Baselines without protein were also acquired and subtracted from the corresponding raw data before the calculation.

The conditions described for the turbidimetry assay were repeated in the DLS assay. An additional experiment was performed: doxycycline was added to WT-TTR fibrils assembled at pH 4.4 after fibril assembly and size stabilization, which occurred at day seven. Similarly to what was verified in the turbidimetry assay (Figure 30) the results show that doxycycline disrupts WT-TTR fibrils. This effect is not immediate but is noticeable after fifteen days of incubation (Figure 30B), reaching a maximum in the twenty-first day. At this point the major particle population in the control sample have sizes ranging between 1000 and 10000 nm, in the doxycycline treated sample the most abundant particle populations

have a size smaller than 1000 nm. This is not as noticeable in the doxycycline treated sample after fibril assembly but nevertheless is noticeable a decrease in the larger size particle populations and an increase in the smaller size populations.

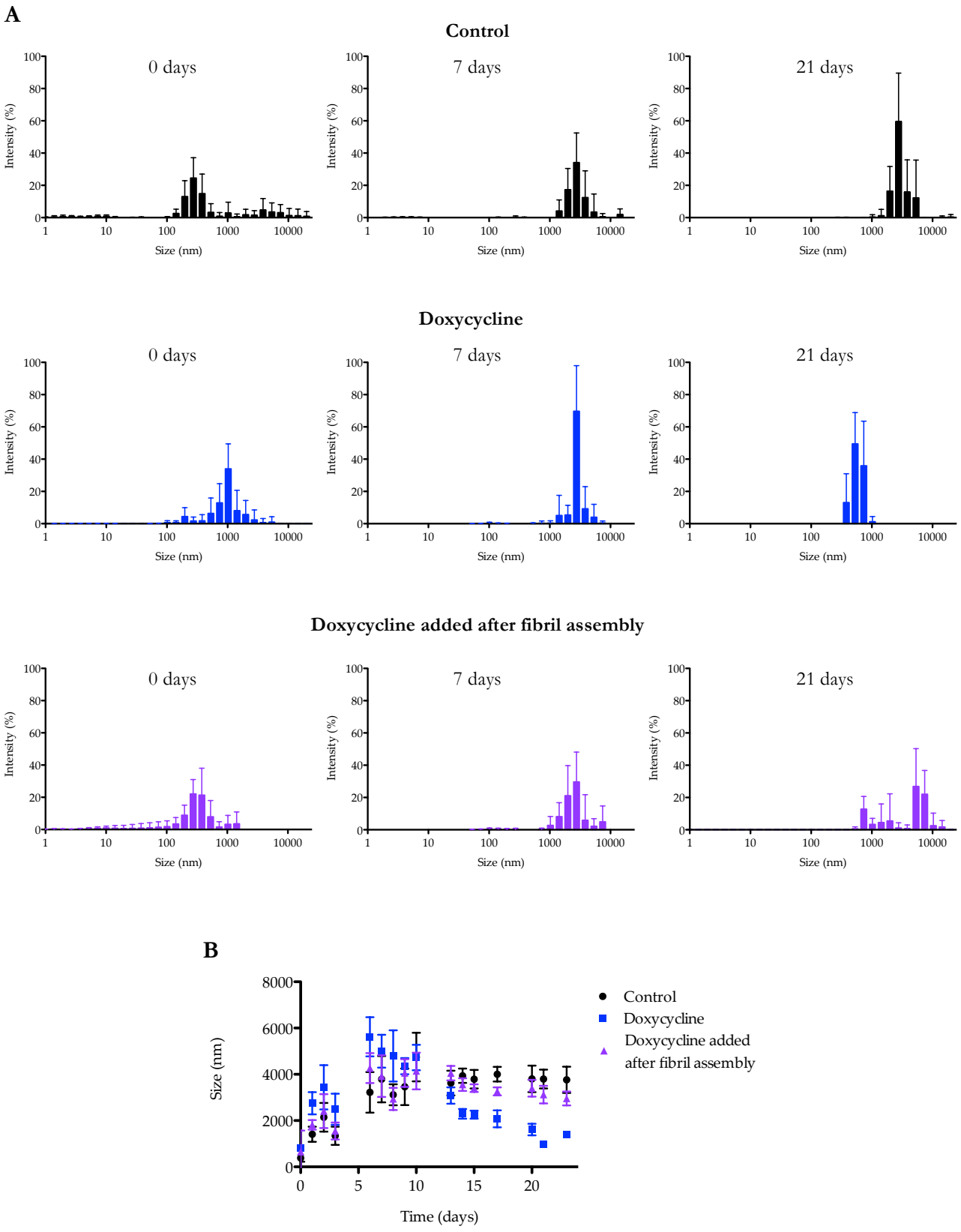

Figure 31: DLS analysis of the effect of doxycycline on WT-TTR fibrils assembled at pH 4.4. WT-TTR fibrils (3.6 μM) were incubated in the absence (Control), in the presence of a 50x molar excess of doxycycline (Doxycycline) or incubated with a 50x molar excess of doxycycline after fibril assembly (Doxycycline added after fibril assembly) for the indicated period of time at room temperature. (A) SDP analysis represented as size distribution; (B) Unimodal size analysis.

3.4 - WT-TTR fibrils assembled at pH 4.4 that undergo pH change to 7.4

3.4.1 - Effect of pH change to 7.4 in WT-TTR fibrils assembled at pH 4.4

A 1:5 dilution in Tris-HCl buffer at pH 8.7 of the fibrils assembled at pH 4.4 was performed to obtain fibrils at pH 7.4. The effect of pH change was studied by DLS, CD and TEM to observe if this alteration induces modifications in the size, structure and morphology of the WT-TTR fibrils. The far-UV CD spectra (Figure 32) demonstrates that there are no significant alterations in the fibrils secondary structure due to the pH change. The DLS results (Figure 33) show that the pH change induces an immediate but transitory increase in the size of the fibrils, seen by the increase of populations of bigger particle sizes (Figure 33A, 0 days). In the following days the particle populations of the fibrils that undergo pH change became similar to those that constitute the pre-formed fibrils assembled at pH 4.4 (Figure 33A and B, 3 and 6 days), although with a distribution comprising smaller particles.

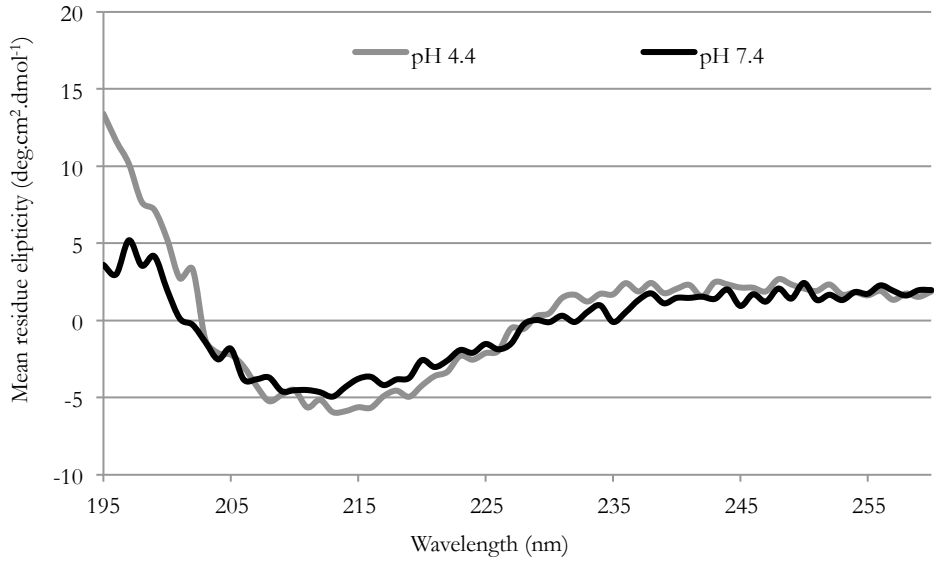

Figure 32: Far-UV CD spectra of WT-TTR fibrils assembled at pH 4.4 (grey) and of WT-TTR fibrils assembled at pH 4.4 that undergo pH change to 7.4 (black). Scans were collected between 195 and 260 nm at 1 nm intervals. Three spectral scans with an integration time of 5 seconds per nm were averaged. The protein concentration used was 3.6 μM and the cuvette pathlength was 0.2 mm. Baselines with buffer were also acquired and subtracted from the raw CD data.

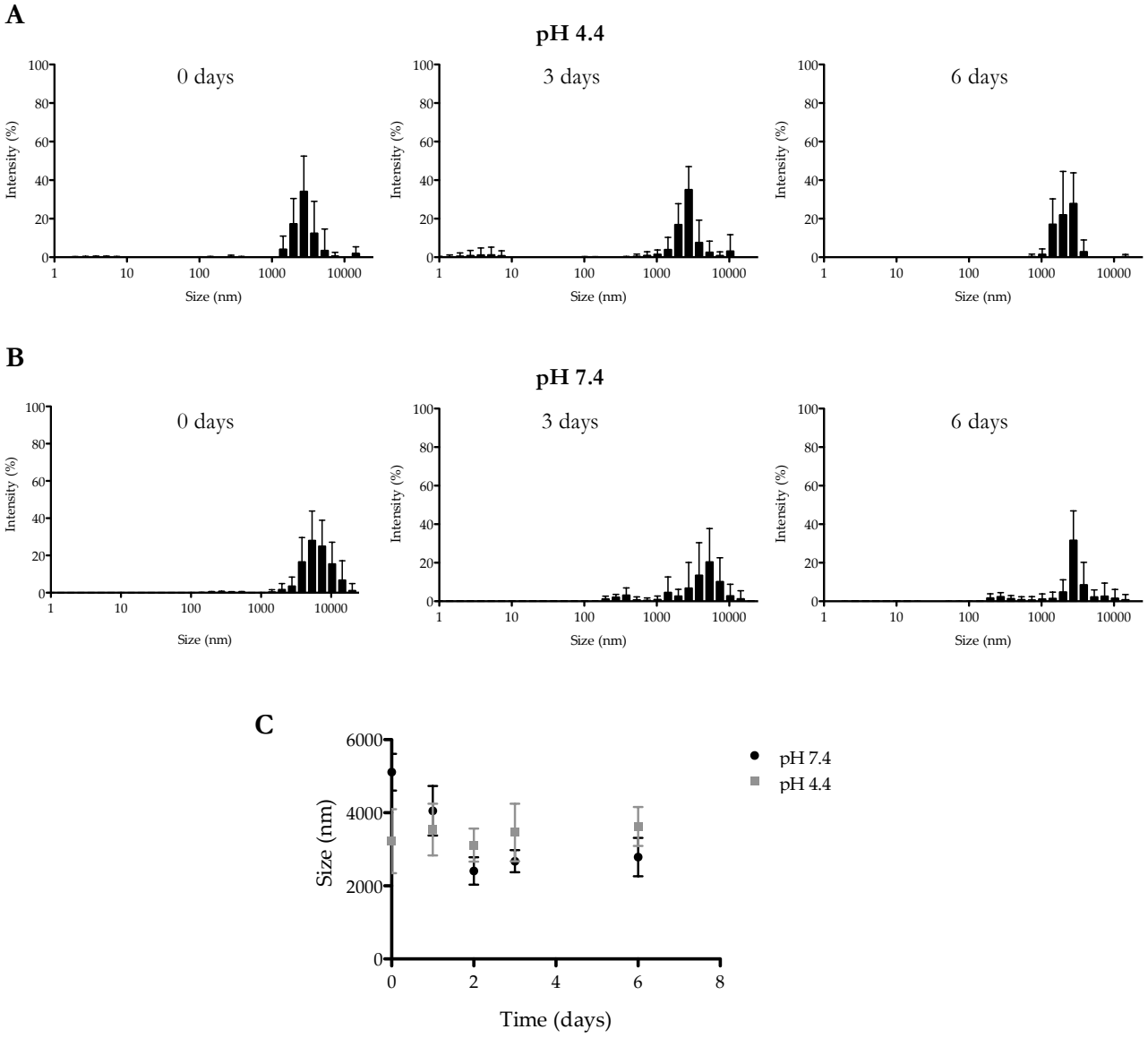

Figure 33: DLS analysis of the effect of pH change to 7.4 in pre-formed WT-TTR fibrils assembled at pH 4.4. (A) SDP analysis represented as size distribution of WT-TTR fibrils (3.6 μM) assembled at pH 4.4 (pH 4.4) (B) SDP analysis represented as size distribution of WT-TTR fibrils assembled at pH 4.4 that undergo pH change to 7.4 at 0, 3 and 6 days after pH change (pH 7.4) ; (C) Unimodal size analysis over time of WT-TTR fibrils assembled at pH 4.4 that undergo pH change to 7.4

In the micrographs it is visible that the WT-TTR fibrils assembled at pH 4.4 (Figure 34A) are not elongated structures like those assembled at pH 2 with 0.1 M NaCl (Figure 22A). They appear as more spheroid/globular structures. The pH change doesn't seem to alter their morphology (Figure 34B).

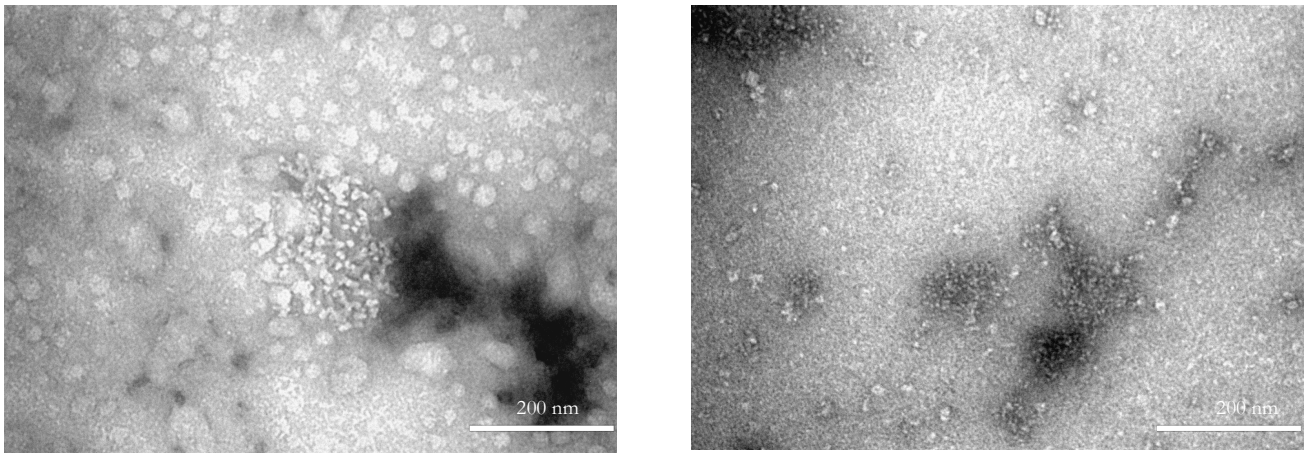

Figure 34: TEM images of WT-TTR fibrils assembled at pH 4.4 (A) and that undergo pH change to 7.4 (B).

3.4.2 - Effect of doxycycline on WT-TTR fibrils assembled at pH 4.4 that undergo pH change to 7.4 disruption

The effect of doxycycline on WT-TTR fibrils assembled at pH 4.4 that undergo pH change to 7.4 was studied by DLS (Figure 35). After size stabilization, also followed by DLS (Figure 33), WT-TTR fibrils at pH 7.4 were incubated either in the absence or presence of a 50x molar excess of doxycycline and DLS measurements were carried out everyday until apparent size stabilization. Doxycycline caused an immediate and persistent effect on the fibril sizes. The particle populations between 100 and 1000 nm increase and the particle populations between 1000 and 10000 decrease with the doxycycline treatment, when compared to the control (Figure 35A). This effect reached a maximum at seventeen days where almost the particle populations of doxycycline treated samples are comprised between 100 and 1000 nm which was not verified in the control samples where the majority of the particle populations are bigger than 1000 nm. Therefore it can be concluded that doxycycline disrupts WT-TTR fibrils assembled at pH 4.4 that undergo pH change to 7.4.

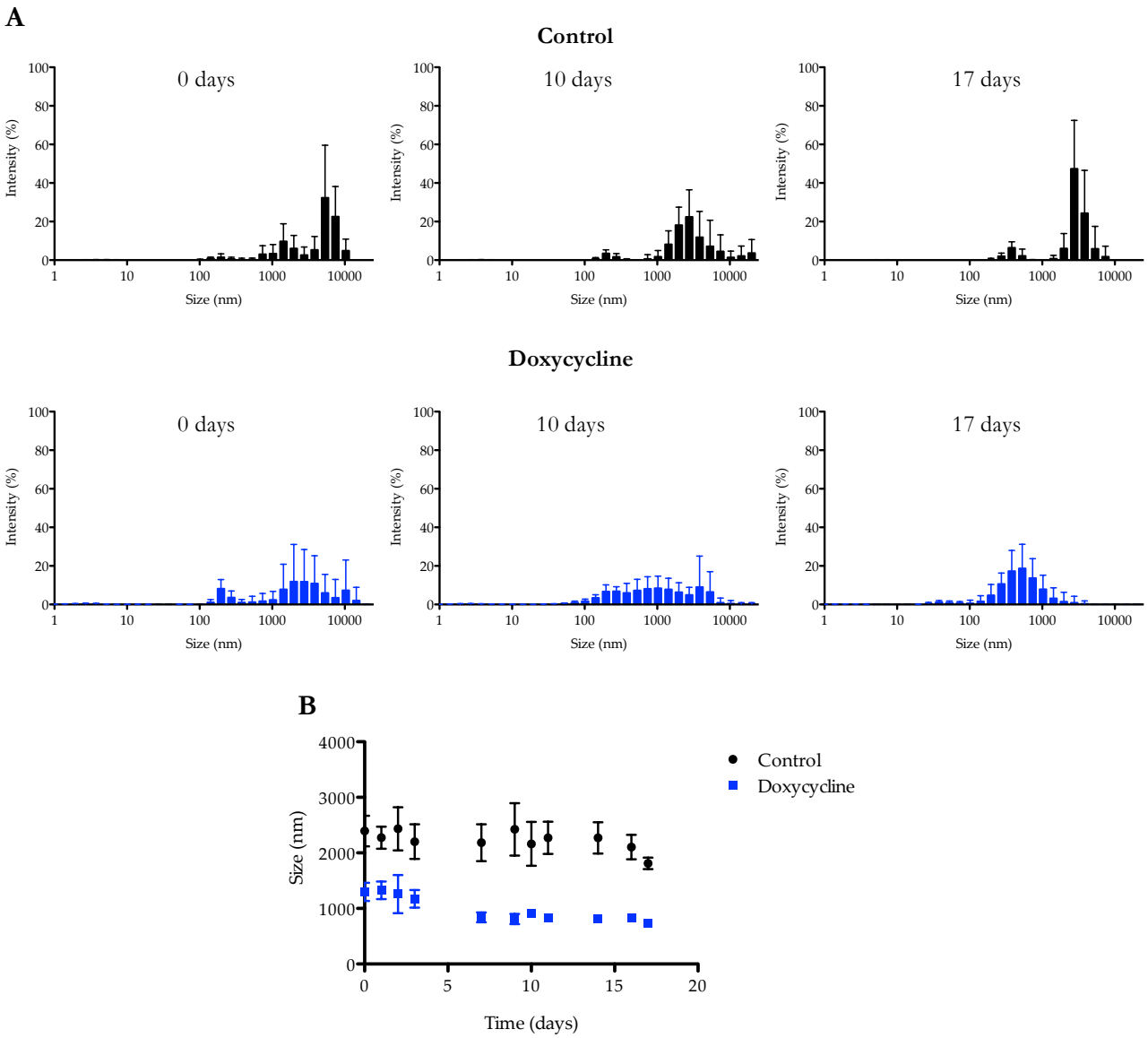

Figure 35: DLS analysis of the effect of doxycycline on WT-TTR fibril assembled at pH 4.4 that undergo pH change to 7.4. WT-TTR fibrils (3.6 μM) were incubated either in the absence (Control) or presence of a 50x molar excess of doxycycline (Doxycycline) for the indicated period of time at room temperature. (A) SDP analysis represented as size distribution; (B) Unimodal size analysis.

3.5 - WT-TTR fibrils induced by heating at pH 7.4

3.5.1 - WT-TTR fibril assembly induced by heating at pH 7.4

The protocol for WT-TTR fibril assembly induced by heating at pH 7.4 has not been widely used so far. Chung and colleagues used CD and calorimetry to demonstrate that heat-induced conformational rearrangements enable normal TTR to assemble into pre-fibrils at physiological pH[121] and Lundberg and colleagues characterised the morphology of heat-induced WT-TTR fibrils by atomic force microscopy[118].

To better characterize the process of fibril assembly turbidimetry, DLS and CD assays were performed. Measurements were taken everyday for the first three days, in the sixth day and after two days at 37°C (8th day).

An increase in the turbidimetry can bee seen in the six days of heating (Figure 36), which implies aggregation. The transition from 60°C to 37°C didn't induce a decrease in turbidimetry indicating that the decrease of temperature didn´t cause fibril breakdown (Figure 36, 8th day).

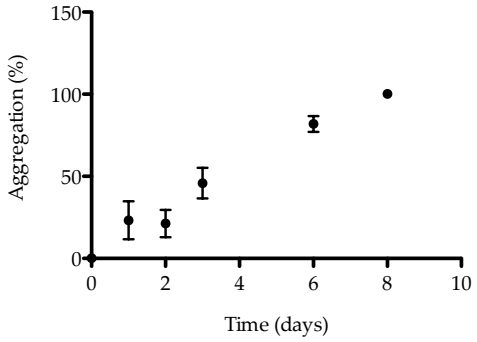

Figure 36: WT-TTR fibril assembly induced by heating at pH 7.4 monitored by turbidimetry. Samples were incubated at 60°C for the first six days and maintained at 37°C in the last two. Absorbance measurements were performed in a 96-well microplate at 450, 500, 550, 600 and 650 nm at 37°C. The percent aggregation was calculated for each wavelength using the following formula: Aggregation (%)= ((Absλ-Absmin)/(Absmax-Absmin)) x100. The percentages of aggregation for each wavelength were then averaged and represented with the corresponding standard deviation. Baselines without protein were also acquired and subtracted from the corresponding raw data before the calculation

The DLS assay confirms these observations. Both SDP and unimodal size analysis indicate fibril growth over time (Figure 37). In the SDP analysis an increase in particle populations between 1000 and 10000 nm and a decrease of particle populations of smaller sizes is visible over time (Figure 37A). The transition from 60°C to 37°C also didn't induce considerable fibril breakdown because the particle populations distribution in the 8th day is similar to that of the 6th day of heating.

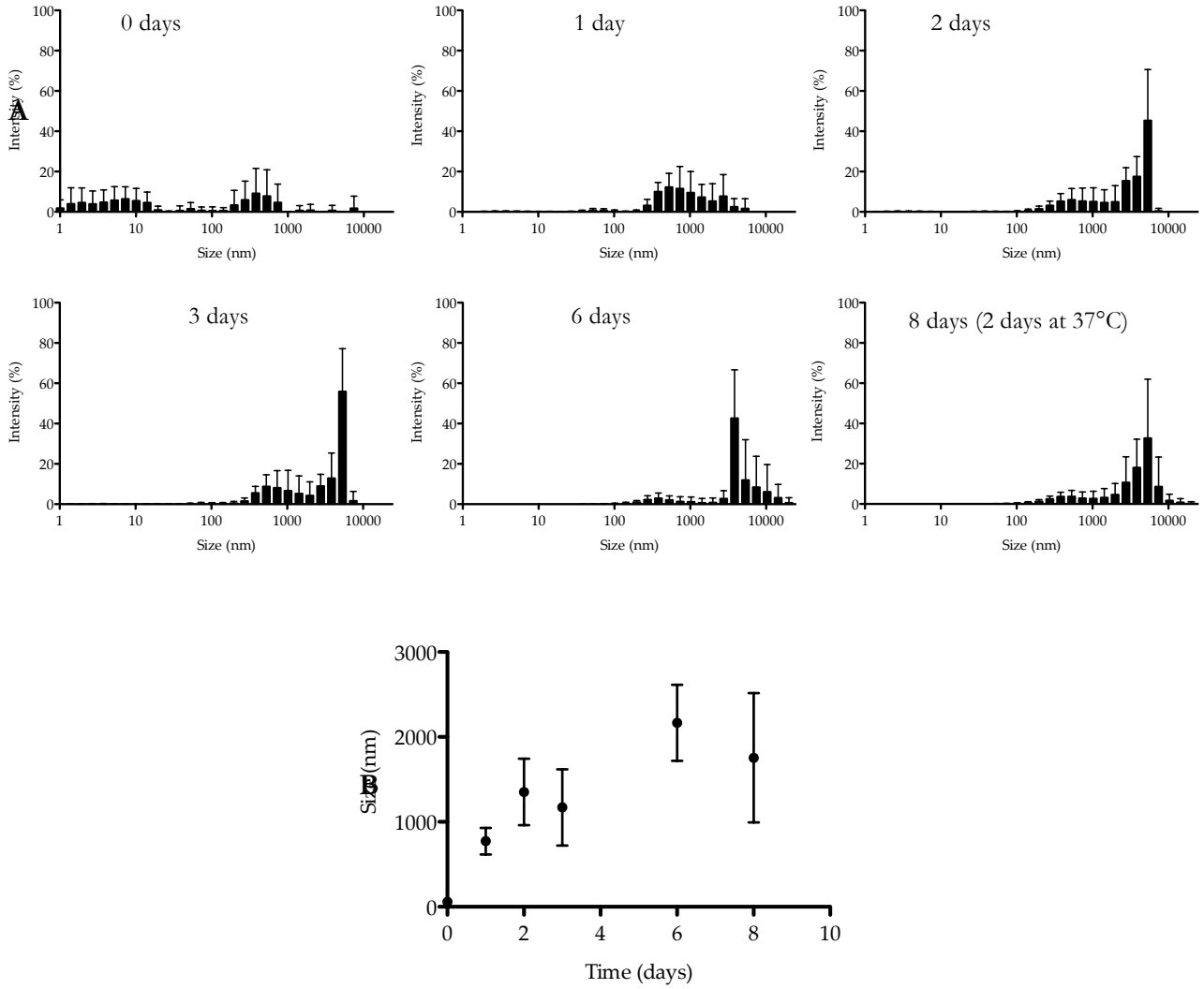

Figure 37: DLS analysis of WT-TTR fibril assembly induced by heating at pH 7.4. WT-TTR (3.6 μM) was incubated at 60°C for the first six days and maintained at 37°C in the last two, measurements were performed at 37°C. (A) SDP analysis represented as size distribution by intensity; (B) Unimodal size analysis.

The possible changes in secondary structure were analysed by far-UV CD. During the six days of incubation of WT-TTR at 60°C and after two days at 37°C there are no considerable alterations in the far-UV CD spectra (Figure 38). The characteristic WT-TTR far-UV CD is maintained indicating no significant change in the secondary structure due to fibril formation.

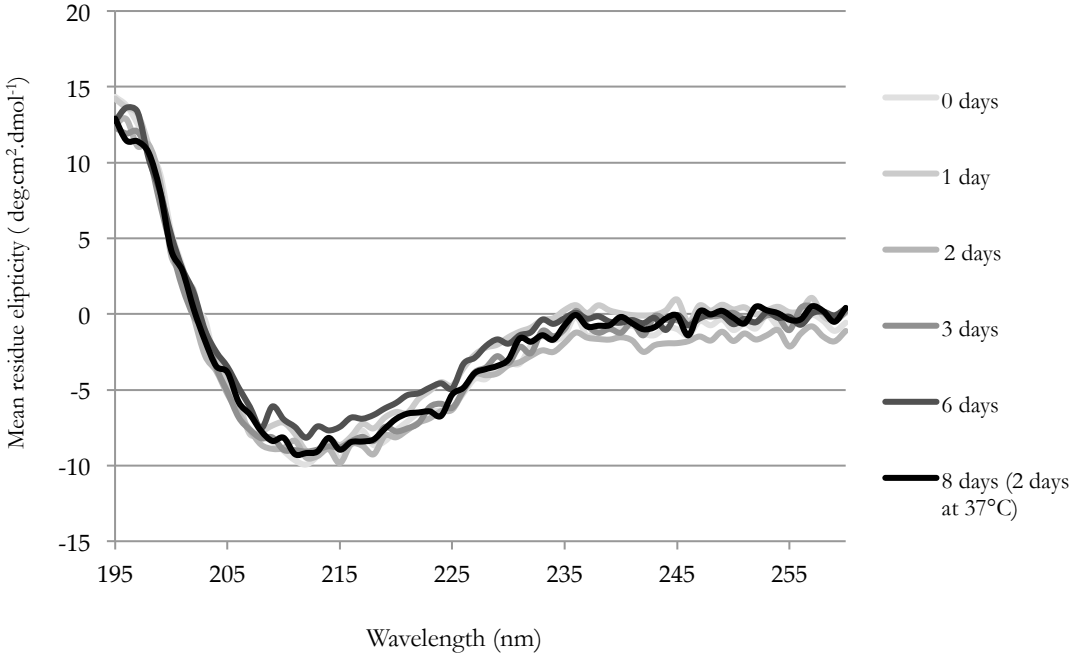

Figure 38: Far-UV CD spectra of WT-TTR fibril assembly induced by heating at pH 7.4. WT-TTR (3.6 μM) was incubated at 60° C for the first six days and maintained at 37°C in the last two, measurements were performed at 37°C. Scans were collected between 195 and 260 nm at 1 nm intervals. Three spectral scans with an integration time of 5 seconds per nm were averaged. The protein concentration used was 3.6 μM and the cuvette pathlength was 0.2 mm. Baselines with buffer were also acquired and subtracted from the raw CD data.

The ThT assay was also applied to the pre-formed WT-TTR fibrils induced by heating at pH 7.4 displaying positive results (Figure 39). In the fluorescence spectrum the emission maximum is around 482 nm, which results from the binding of ThT to amyloid fibrils.

Figure 39: Thioflavin-T assay of pre-formed WT-TTR fibrils induced by heating at pH 7.4. The spectrum of ThT fluorescence was collected between 460 and 560 nm with an excitation wavelength of 450 nm. The protein concentration used was 3.6 μM and the cuvette pathlength was 5 mm. Baseline with buffer and ThT was also acquired and subtracted from the raw fluorescence data.

3.5.2 - Study by ^{1}H STD NMR of the interaction of doxycycline with WT-TTR fibrils induced by heating at pH 7.4

The interaction between pre-formed WT-TTR fibrils induced by heating at pH 7.4 and doxycycline was studied by ^{1}H STD NMR. The ^{1}H NMR STD spectrum of doxycycline (2 mM) in the presence of TTR fibrils (20 µM) and the off-resonance spectrum are represented in figure 40.

The signals present in the ^{1}H STD NMR spectrum (Figure 40A) represent the doxycycline protons that are in direct contact with the fibrils and were identified by their chemical shifts. Signals from the aromatic protons H8, H7 and H9, the protons H5a and H6 and from the three methylic groups are observed. There are additional signals between 2,5 and 3 ppm that could not be unambiguously assigned due to the high density of resonances in this region.

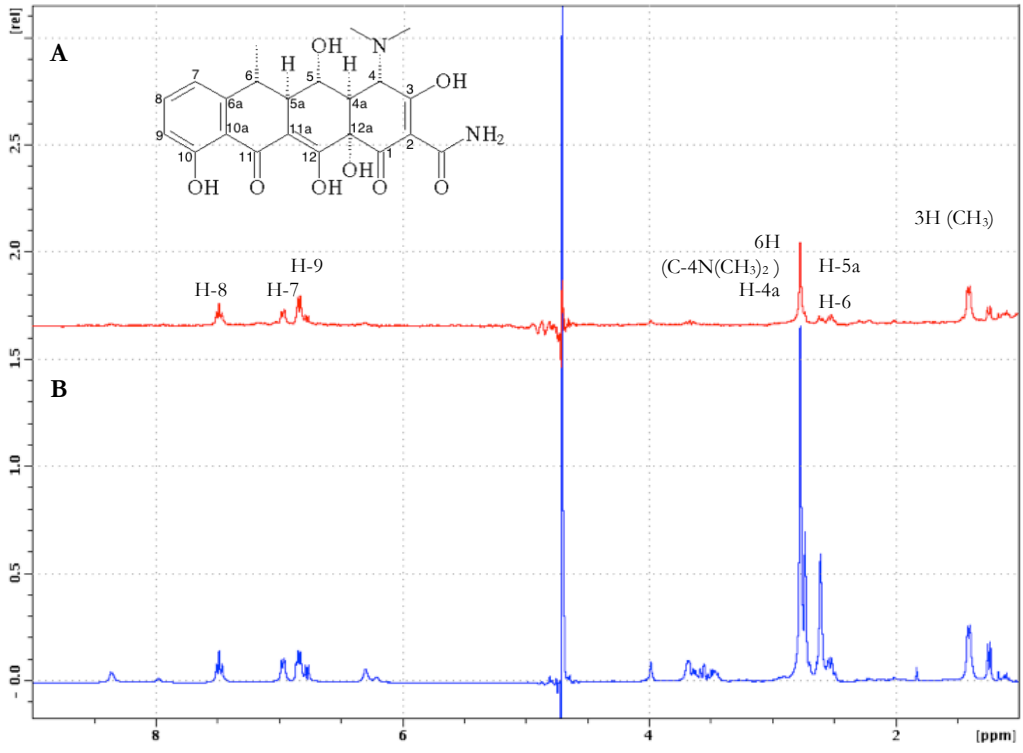

Figure 40: ^{1}H STD-NMR of doxycycline (2 mM) in the presence of WT-TTR fibrils (20 µM) induced by heating at pH 7.4. A- ^{1}H STD-NMR spectrum; B- Off resonance spectrum.

3.5.3 – Effect of Doxycycline on WT-TTR fibrils induced by heating at pH 7.4 disruption

The effect of doxycycline on pre-formed heat-induced WT-TTR fibrils was studied by DLS. The fibrils were incubated either in the absence or presence of a 50x molar excess of doxycycline and DLS measurements were carried out everyday until apparent size stabilization. Unimodal size analysis and SDP analysis were performed. Doxycycline didn´t have an immediate effect on fibril size, the particle populations present in the control sample are similar to the particle populations of the doxycycline treated sample (Figure 41A, 0 days). Over time the particle populations between 100 and 1000 nm increased in the doxycycline treated sample, a signal of fibril disruption. At seventeen days of incubation it is observed a decrease of particle populations bigger than 1000 nm in size and an increase of particle populations between 100 and 1000 nm in the doxycycline treated sample. In the control sample the major particle populations remain above 1000 nm (Figure 41A, 17 days). Thus, it can be concluded that doxycycline induces fibril disruption of heat-induced WT-TTR fibrils.

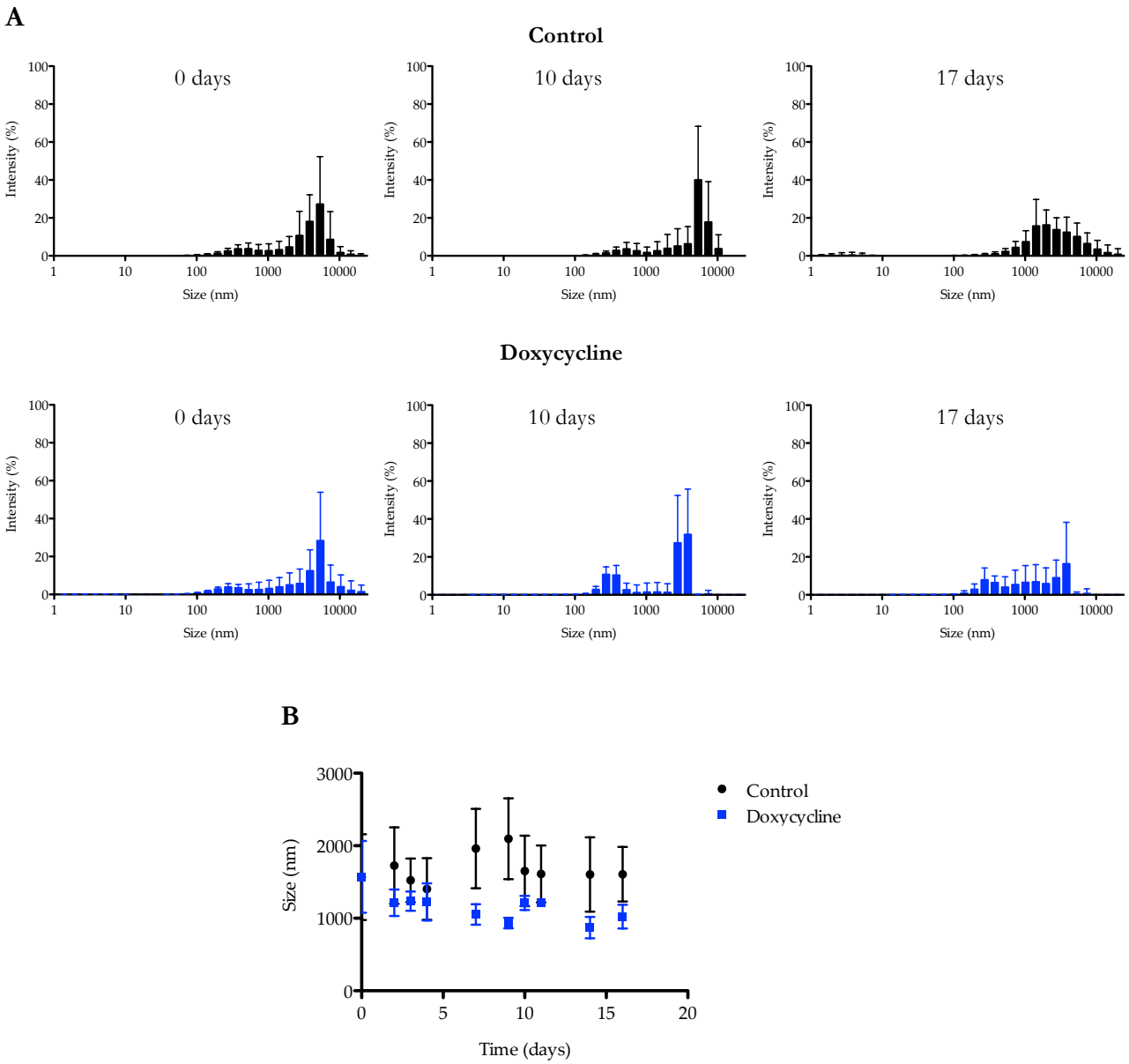

Figure 41: DLS analysis of the effect of doxycycline on WT-TTR pre-formed fibrils assembled by heating at pH 7.4. WT-TTR fibrils (3.6 μM) were incubated either in the absence (Control) or presence of a 50x molar excess of doxycycline (Doxycycline) for the indicated period of time at room temperature. (A) SDP analysis represented as size distribution (B) Unimodal size analysis.

Chapter 4: Discussion

The choice of an appropriate fibril formation protocol and amyloid fibril model is crucial to the identification and characterization of small molecule interactions with WT-TTR amyloid fibrils and consequently to the development of a protocol for screening of WT-TTR fibril disrupters.

Ideally the *in vitro* formed fibrils would have the same structure and morphology as *in vivo* fibrils and the fibril formation protocol would be as close as possible to the *in vivo* process of TTR amyloid formation, maintaining physiological conditions such as average protein concentration, pH and temperature. However the native tetrameric form of WT-TTR has a high conformational stability (ΔG_{unf} = 104 kJ/mol, at 37 ºC and pH 7.1)[122] and the amyloid formation process in these conditions is a very slow process, unsuitable to be used in screening protocols. Acidification is a commonly used method to initiate the assembly of TTR amyloid fibrils but the process of fibrillogenesis depends on various additional conditions such as temperature, protein concentration, ionic strength, agitation and pH. By lowering the pH the tetrameric structure of the protein is disrupted and is dissociated into a monomeric structure, different from the monomer at physiological pH. The altered monomers can associate and eventually form amyloid fibrils.

The pH-dependent effects in proteins are mainly electrostatic and originate from changes in the protonation states of acidic and basic residues[123]. Some of the titratable residues in a protein exhibit different behaviour compared with that of the isolated residues due to their interactions with other residues in the protein and the altered interactions with the solvent[124]. Of the 127 aminoacids that constitute the WT-TTR monomer 17 are acidic and 16 are basic.

The first fibril formation protocol used in this work was performed at pH 2 with 0.1 M NaCl. This process and his kinetics have already been studied and well characterized[58]. The acidification at pH 2 promotes tetramer dissociation and the addition of 0.1 M NaCl induces aggregation because the chloride ions shield the positive charges of the protein allowing for a conformational changes and assembly of the monomers into oligomers and eventually fibrils. This process is relatively time consuming and requires a high concentration of tetrameric WT-TTR to be effective in less time. The fibrils formed at this pH have already been studied by TEM and AFM, appearing as thin and long filamentous structures that bind ThT[118]. The TEM results (Figure 22A) confirm these observations concerning fibril morphology.

The pH change to pH 7.4 of pre-formed fibrils at pH 2, performed in this work, was an attempt to mimic the *in vivo* conditions of WT-TTR fibrils. WT-TTR amyloid deposits are extracellular[23] and in this location the pH is not acidic but around 7.4.

Herein the effect of pH modification on mature WT-TTR amyloid fibrils size, structure and morphology was studied by DLS, CD and TEM. In a previous study performed by Pires and colleagues alterations resulting from transient PBS incubation of WT-TTR protofibril bundles, a structure present in the early stages of aggregation induced by acidification, were reported[57,125]. In this case AFM was used to observe that after PBS incubation protofibril bundles disassembled halting the amyloid formation process[57,125]. However the effect of PBS incubation on mature WT-TTR amyloid fibrils assembled at pH2 with 0.1 M NaCl had not yet been studied. Our DLS results showed that pH alteration induces modifications in the size of the fibrils (Figure 20). After an immediate and transient increase in the size of the fibrils (0 days) the particle populations of higher sizes decreased and the particle populations between 100 and 1000 nm increased. After eleven days of incubation the most abundant particle populations at pH 2 and pH 7.4 are comprised between 1000 and 10000 nm however at pH 7.4 particle populations smaller than 1000 (between 100 and 1000 nm) are more frequent.

The CD results revealed an alteration in the secondary structure of the fibrils due to pH alteration (Figure 21). After 24 hours of PBS incubation the CD spectrum indicates a loss of β-sheet secondary structure.

TEM observations reinforce the DLS results. The very long unbranched structures existent at pH 2 appear to shorten after incubation in PBS for approximately one month (Figure 22B). However the overall filamentous morphology is preserved. At pH 7.4 WT-TTR fibrils remain ThT positive (Figure 23), a feasible indication of amyloid structures.

The second fibril formation protocol used was based on WT-TTR acidification at pH 4.4. This method is widely used for *in vitro* WT-TTR amyloid fibrillogenesis inhibitors screening, it is easily implemented in medium or high throughput screening formats in tubes or microwell plates[50,116]. This method is less time consuming than the previous method and does not require high concentrations of native WT-TTR. Fibrils can be formed at physiological concentrations (3.6 μM).

Atomic force microscopy studies showed that aggregates formed at the slightly higher pH of 4.0–5.5 have different morphology, displaying predominantly amorphous structures than the aggregates formed at a lower pH[118]. These aggregates are also different from the *in vivo* WT-TTR amyloid fibrils. The TEM images we obtained also endorse these observations. WT-TTR fibrils assembled at pH 4.4 (Figure 34A) are not elongated structures like those assembled at pH 2 with 0.1 M NaCl (Figure 22A) appearing as more spheroid/globular structures. Nevertheless these are ThT positive structures[118].

With this protocol turbidity assays are frequently used to monitor the degree of protein aggregation and fibril formation. At a pH between 4 and 5 the turbidity is higher, at more acidic pH aggregation does not induce a noticeable increase in turbidity[118].

Once again, to mimic the *in vivo* conditions of WT-TTR fibrils, the pH was modified to 7.4 by a 1:5 dilution in Tris-HCl buffer at pH 8.7 of the mature TTR fibrils assembled at pH 4.4. CD, DLS and TEM assays (Figure 32, 33 and 34) demonstrated that the pH change does not significantly alter fibril structure, size or morphology.

The third fibril formation protocol is the less well-studied process of the three. Lundberg and colleagues characterized temperature-induced fibrils at pH 7.4 by AFM. These fibrils were thicker than the *in vitro* fibrils seen at low pH, appearing to be more similar to fibrils seen *in vivo*[118]. Their observations could not be confirmed by TEM in this work because a representative micrograph could not be obtained.

To better characterize the aggregation process turbidimetry, DLS and CD assays were performed. The increase in turbidimetry verified over the six days of incubation at 60°C incubation (figure 36) and the increase in particle populations between 1000 and 10000 nm and decrease of particle populations of smaller sizes observed by DLS (Figure 37) imply aggregation. This process was not reverted by temperature change to 37°C because turbidimetry and particle populations remained unaltered. The far-UV CD spectra remained unaltered during the six days of incubation at 60°C and after temperature change to 37°C indicating no change in the characteristic β-sheet secondary structure due to fibril formation or temperature change (Figure 38). The temperature-induced fibrils are ThT positive (Figure 39), a feasible indication of amyloid structures.

Table 3 summarizes the main characteristics and requirements of the three fibril formation protocols. The pH 4.4 fibril formation protocol is the less time consuming, has low protein requirements and is suitable for pH change to 7.4 but the morphology of the fibrils isn't similar to the *in vivo* morphology, which is a major drawback. The pH2 with 0.1 M NaCl protocol is the more time consuming and requires higher concentrations of protein but it is extremely well characterized. The fibril morphology is similar to *in vivo* but pH change to 7.4 induces alteration on the size and secondary structure of the fibrils even thought they remain ThT positive. The heat-induced fibril formation protocol seems to be a very good candidate to be used on WT-TTR fibril disrupters screening. This protocol is not very time consuming, has low protein requirements, the fibrils are formed and remain at physiological pH and their morphology is similar to the in vivo morphology of WT-TTR fibrils.

Nevertheless the heat-induced amyloid formation by WT-TTR needs to be better characterized. Additional fluorescence studies with ThT or monitoring tryptophan emission over time could help to confirm and characterize the aggregation pathway. Further atomic force or transmission electron microscopy studies could also be important to characterize the morphology of the aggregates during the process. AFM could also characterize the height and periodic substructure of the heat-induced fibrils.

Table 3: Characteristics of WT-TTR fibril formation protocols.

	pH 2 with 0.1 M NaCl	pH 4.4	60°C heating
Protocol duration	At least 13 days	3 days	6 days
Protein requirements	High	Low	Low
Morphology of the fibrils	Long unbranched structures	Spheroid/globular structures Amorphous aggregates	AFM observations characterized this structures as more similar to *in vivo* WT-TTR fibrils[118]
Effect of pH change to physiological conditions	Alterations in the size and secondary structure of the fibrils. Fibrils remained ThT positive	No effect on size, secondary structure or morphology	Not needed, the reaction occurs at pH 7.4

In this work the effect of doxycycline on fibril assembly was also studied. The first and third fibril formation protocols could not be used. The first would imply a very high doxycycline final concentration (around 4 mM) to maintain the 1:50 protein/doxycycline ratio, which is not allowed by its relatively low solubility. In the third fibril formation protocol the doxycycline heating at 60°C induced an aberrant increase in the supposed size of the fibrils (data not shown) and the solution also became brown. The thermostability of doxycycline had already been studied in pharmaceutical formulations showing that doxycycline exhibits thermo-degradation after exposure to high temperatures (40-70°C)[126] consequently the assays did not proceed.

Using the pH 4.4 fibril formation protocol the effect of doxycycline on WT-TTR fibrils assembly was studied by turbidimetry, DLS and ThT fluorescence (Figures 26, 27 and 28). Taken together the results show that doxycycline does not arrest fibril formation.

In the development of any screening protocol saving time and resources without compromising the selection is crucial. When choosing small molecules that can directly disrupt WT-TTR fibrils the interaction of the molecules with the fibrils is essential to the process hence using an assay that can probe binding is very important and allow us to make a first selection of the compounds to test.

^{1}H STD NMR was chosen to probe the interaction between the WT-TTR fibrils and the compound being tested, doxycycline, due to its availability, relative ease of application, reduced protein requirements and applicability to large molecular weight proteins. However is important to note that this technique also has some drawbacks, only being suitable to probe low affinity interactions.

Doxycycline seems to be relatively stable at pH 2, 4.4 and 7.4. The ^{1}H NMR spectrum of doxycycline at pH 7.4, 4.4 and 2 (annex B) doesn't show alterations on the doxycycline proton signals, which could indicate degradation. The ^{1}H NMR spectrum of doxycycline in DMSO can be found in annex A for comparison.

Different concentrations of WT-TTR were tested in ^{1}H STD NMR preliminary experiments at pH2. 20 μM was the minimum concentration detectable and thus was used in the ^{1}H STD NMR assays.

Examining all the ^{1}H STD NMR spectra is noticiable that doxycycline interacts differently with fibrils assembled by the different fibril formation protocols or with fibrils that undergo pH change. The doxycycline protons involved in the binding to WT-TTR fibrils assembled at pH 2 with 0.1 M NaCl are the aromatic protons and the protons from the three methylic groups (Figure 18). When these fibrils undergo pH change to 7.4 the signals from the aromatic protons disappear from the spectrum (Figure 24) meaning that they are not involved in the interaction. As previously described the pH transition from pH 2 to pH 7.4 induces alterations in the structure of the fibrils and can cause changes in the protonation states of acidic and basic residues, which may modify the interactions between the fibrils and doxycycline. Additionally the protonation state of doxycycline is also changed by the pH transition. The pKa values for doxycycline are: pK_{a1}=3.02 ± 0.3, pK_{a2}=7.97 ± 0.15 and pK_{a3}=9.15 ± 0.3[127]. Therefore at pH 2 all the protonable groups are protonated and at pH 7.4 one of them is not. This may also alter the interactions between the fibrils and doxycycline.

In the ^{1}H NMR STD spectrum of doxycycline in the presence of WT-TTR fibrils assembled at pH 4.4 doxycycline proton signals are absent (Figure 29B). This result may be due to a very weak or very strong binding of doxycycline to the fibrils, to the absence of binding or to other technical aspect. In subsequent assays was observed that doxycycline disrupts WT-TTR fibrils assembled at pH 4.4 so the no binding hypothesis can be discarded. It is also necessary to take into account that the fibril sample at pH 4.4 is extremely cloudy and the fibrils seem to precipitate the RMN tube, which may affect the assay results.

The doxycycline protons involved in the binding to heat-induced fibrils (Figure 40) are the same as does involved in the binding with WT-TTR fibrils assembled at pH 2 with 0.1 M NaCl. The binding of doxycycline to these fibrils is not equal to the binding to WT-TTR fibrils assembled at pH 2 with 0.1 M NaCl that undergo pH change to 7.4 despite the pH being the same. The cause of this observation may be the different structure of the fibrils. The aminoacids available to interact with the doxycycline may not be the same in both causes ergo the binding is different.

^{1}H STD NMR or other NMR based techniques are not the only techniques that can be used to study the binding of small molecules to larger macromolecules. Isothermal titration calorimetry (ITC) is a quantitative technique that can determine the binding affinity, enthalpy changes and binding stoichiometry of the interaction between two molecules. This technique is broadly used as a secondary screening technique in high throughput screening. It has similar advantages to ^{1}H STD NMR and less drawbacks such as the narrow detection limits. ITC provides additional information, namely the thermodynamic characterization of the binding, and the determination of the binding affinity is more

straigthforward. Therefore, it would be interesting to incorporate ITC in the WT-TTR fibril disrupters screening and characterization protocol.

Herein the disruptive effect of doxycycline on WT-TTR fibrils was evaluated for the first time. In previous studies the effect of doxycycline as a fibril disrupter was tested on Leu55Pro or Val30Met fibrils[94,96]. DLS was the technique chosen to study the disruptive effect of doxycycline on the fibrils. This technique requires a small quantity of sample and allows a fast analysis being adequate for a screening protocol. The instrument used, the N5 Submicron Particle Size Analyser, provides two kinds of analysis: the unimodal size analysis and the SDP analysis. The unimodal size analysis that provides the mean size of the particles in the sample is not reliable due to the high PI of the fibril samples, but can help to have a quicker and easier assessment of size alteration over time. The SDP analysis provides more accurate information about the size and distribution of the particles populations in the sample but it is more time consuming and harder to perform. This technique was successfully applied in probing the disruptive effect of doxycycline on pre-formed WT-TTR fibrils prepared using the different fibril formation protocols. The molar excess of doxycycline used in this experiments was 50x, which was the concentration used in previous studies with doxycycline and Leu55Pro TTR fibrils[94].

Doxycycline does not have an immediate persistent effect on WT-TTR fibrils. It takes from eleven to twenty five days to reach a maximum effect. Doxycycline has a more pronounced disruptive effect on fibrils assembled at pH 4.4 and fibrils assembled at pH 4.4 that undergo pH change to 7.4 (Figure 31 and 35), but the effect is also evident in heat-induced fibrils (Figure 41) and visible in fibrils assembled at pH 2 with 0.1M NaCl (Figure 19) and fibrils that undergo pH change to 7.4 (Figure 25). As previously discussed this diverse effect of doxycycline on the WT-TTR fibrils prepared by the different protocols might be attributed to factors such as the pH of the sample or more likely to the different fibril structures.

Turbidimetry was another technique used to probe fibril disruption but it was only successfully applied to fibrils assembled at pH 4.4. The results obtained with this technique (Figure 30) were in accordance with the DLS results. Fibrils assembled at pH 2 and fibrils assembled at pH 2 that undergo pH change to 7.4 don't have detectable turbidities (data not shown). The heat-induced fibril growth could be detected by turbidimetry however when applying this assay in the following of fibril disruption the results were inconclusive and didn't correlate with the DLS assay results (data not shown). At pH 4.4 the WT-TTR fibrils are not elongated structures like those assembled at pH 2 with 0.1 M NaCl or induced by heating, appearing as more spheroid/globular structures classified as amorphous aggregates. This different morphology might be the cause of the turbidimetry observed at pH 4.4 and the lack of turbidimetry in the other sample conditions.

In this study only one concentration of doxycycline was tested, in the future is important to also test other concentrations to better characterize the effect of doxycycline. Furthermore the temperature used in the doxycycline incubation with the fibrils was room temperature, which is not ideal. It would be better to perform these procedures at 37ºC to mimic physiological conditions. This could not be accomplished due to technical difficulties. When the samples were incubated at 37ºC in capped quartz cuvettes the sample evaporated in a few days and the measurements could not be performed and other methods of sample isolation were tested but without success.

For the development of the fibril disrupters screening protocol would also be important to have additional techniques to better characterize the effect of the candidate compounds on the fibrils providing more insights about the morphology and specific size of the species resulting from fibril disruption. AFM and TEM are suitable candidates for that purpose.

Given the fact that small oligomeric species are the most cytotoxic species of the aggregation pathway, the evaluation of the toxicity of the generated species upon treatment is also very important and should be incorporated in the screening protocol. The caspase-3 activation assay on an Schawannoma cell line has been used for that purpose[128].

Other aspect concerning toxicity in a screening protocol is the evaluation of the effect of candidate compounds on cell viability. A good drug candidate must not compromise cell viability therefore assays such as MTT should be incorporated in the screening protocol. Doxycycline is an already approved antibiotic and is in clinical trial[98] to be approved for the treatment of TTR amyloidosis hence its effect on cell viability wasn´t tested in this work.

Chapter 5: Conclusion

The disaggregation of amyloid structures is one of the possible therapeutic strategies for the treatment of TTR amyloidosis. To date only a few compounds have been identified as possible fibril disruptors. The main goal of this work was to identify and characterize the interaction of small molecules with WT-TTR fibrils in order to develop a protocol for WT-TTR fibril disrupters screening.

The first step to achieve this goal was the selection of an appropriate fibril formation protocol and the characterization of the formed fibrils. Assembly at pH 2 with 0.1 M NaCl, assembly at pH 4.4 and heat-induced fibril assembly at pH 7.4 were the three methods tested for that purpose. Furthermore the possibility to mimic physiological conditions by altering the pH of the fibrils was also studied.

The heat-induced protocol seems to have some advantages over the other fibril formation protocols but requires further characterization. DLS, turbidimetry and CD were the techniques used to follow the aggregation process. The formed fibrils also require better characterization and TEM and AFM could be used to better describe their morphology and periodic properties.

Fibrils formed at pH 2 with 0.1 M NaCl that undergo pH change to 7.4 suffer alterations in their size and secondary structure but remain ThT positive. These alterations don´t occur with fibrils formed at pH 4.4 that undergo the same pH change. The pH 4.4 is not the ideal protocol mainly due to the morphology of the fibrils, observed by TEM, being very different from the *in vivo* morphology of the fibrils.

^{1}H STD NMR was the technique chosen to probe the interaction between the fibrils and the compounds being tested, s doxycycline, a known fibril disruptor, was used as reference compound. This is an important step in the screening protocol because it allows a first selection of the compounds to be tested. Fibril disruption might be a lengthy process and this first selection step based on fibril-compound interaction could prevent us to spent time and resources studding an ineffective candidate. ^{1}H STD NMR was successfully applied in probing the interaction of doxycycline with WT-TTR fibrils, with the results showing that doxycycline interacts diversely with WT-TTR amyloid formed in different sample conditions. Alternatively, ITC could be used to probe this interaction.

Herein the disruptive effect of doxycycline on WT-TTR fibrils was evaluated for the first time. DLS was the selected technique to characterize fibril disruption and the results show that doxycycline disassembles pre-formed WT-TTR fibrils in all the assembly conditions tested, however this effect is more pronounced in WT-TTR fibrils assembled at pH 4.4. Turbidimetry assays were also used but could only be applied to WT-TTR fibrils assembled at pH 4.4, with the results corroborating the DLS

assays. In the future, different concentrations of doxycycline should be used to better characterize its fibril disassembly effect.

For further development of the fibril disrupters screening protocol additional techniques to better characterize the effect of the candidate compounds on the fibrils should be used. AFM and TEM could provide more insights about the morphology and size distribution of the species resulting from fibril disruption. The cytotoxicity of the generated species and the toxicity of the compound should also be assessed.

Globally this work allowed us to choose a good fibril formation protocol candidate, the study of the interaction of doxycycline with WT-TTR fibrils and the characterization of its effect on fibril disruption and the selection of experimental techniques and conditions to use in the development of the screening protocol. Additionally, it was useful in the identification of aspects requiring further investigation.

Annexes

Annex A

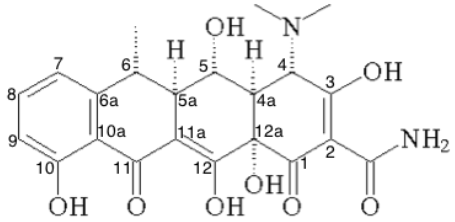

Doxycycline

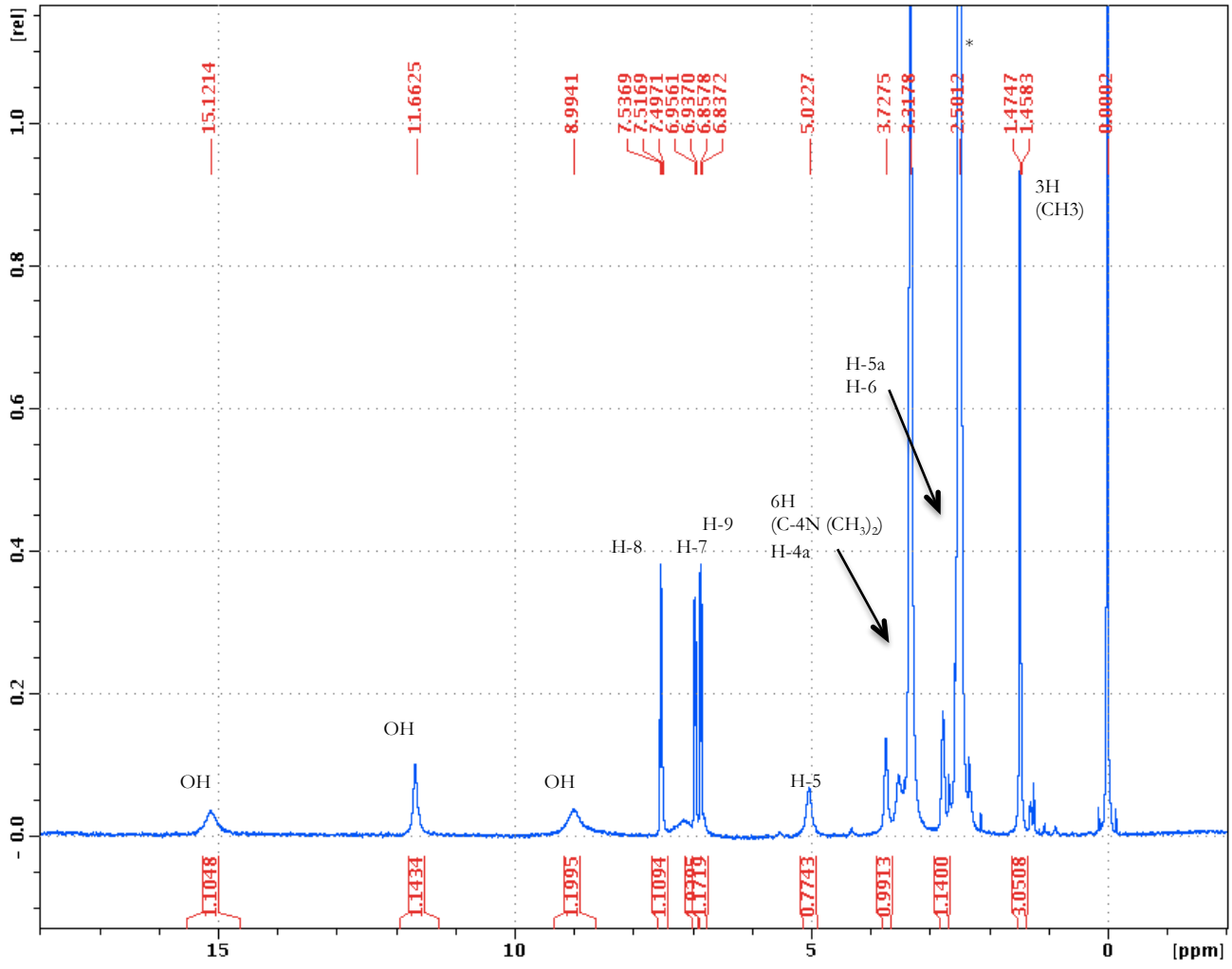

Figure A: ^{1}H NMR spectrum of doxycycline (6.9 mM) in DMSO. The asterisk corresponds to DMSO-d_6.

Annex B

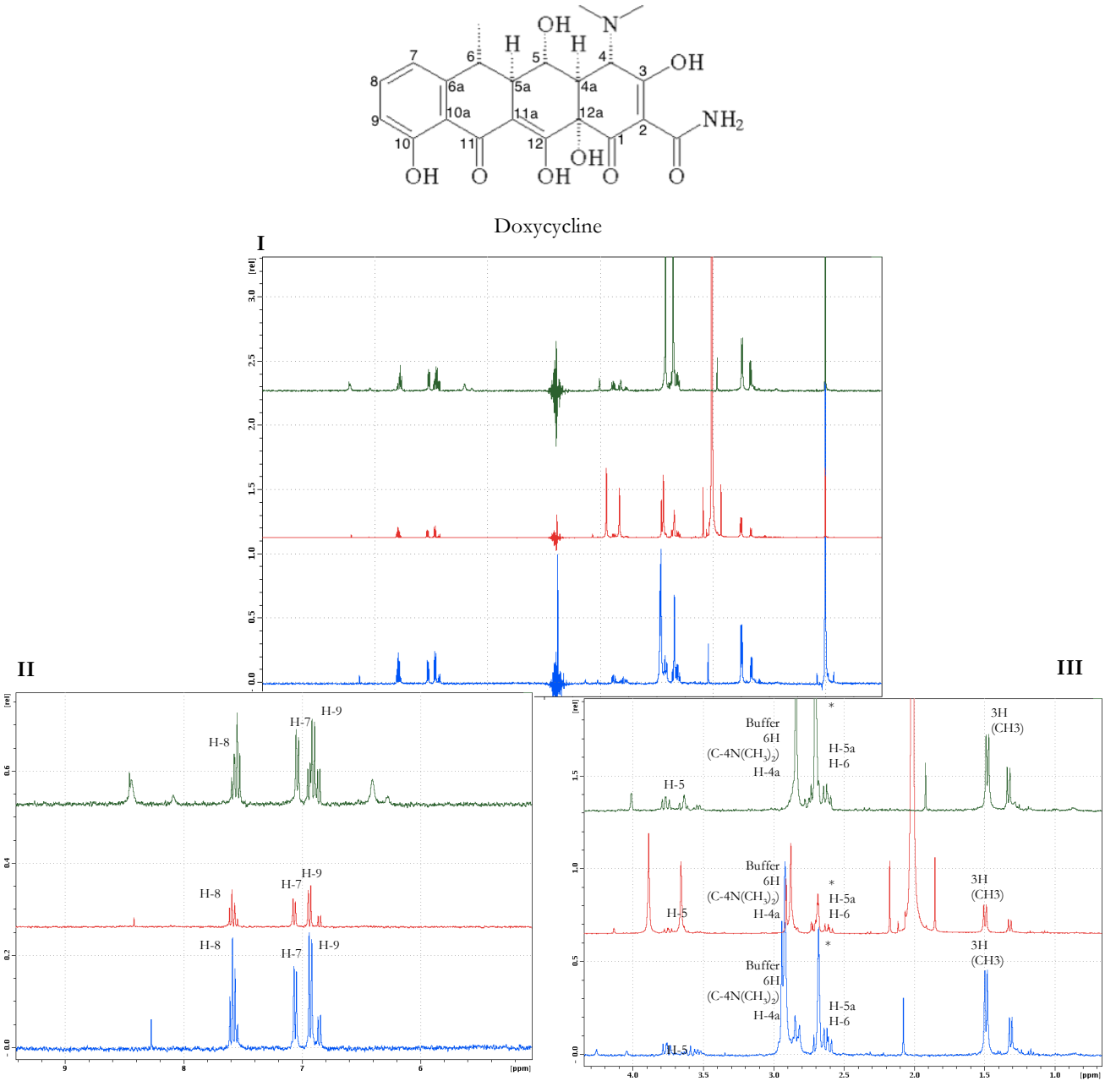

Figure B: ^{1}H NMR spectrum (I) and spectral expansions (II and III) of doxycycline (1 mM) in phosphate saline buffered (PBS) pH7.4 (green), acetate buffer pH 4.4 (red) and 10 mM HCl with 0.1 M NaCl pH 2 (blue). The signal at 0 ppm corresponds to the TSP reference and the asterisk to DMSO-d_6.

References

1. Knowles, T. P. J., Vendruscolo, M. & Dobson, C. M. The amyloid state and its association with protein misfolding diseases. *Nat. Rev. Mol. Cell Biol.* **15,** 384–96 (2014).

2. Bukau, B., Weissman, J. & Horwich, A. Molecular chaperones and protein quality control. *Cell* **125,** 443–51 (2006).

3. Stefani, M. & Dobson, C. M. Protein aggregation and aggregate toxicity: New insights into protein folding, misfolding diseases and biological evolution. *J. Mol. Med.* **81,** 678–699 (2003).

4. Greenwald, J. & Riek, R. Biology of amyloid: structure, function, and regulation. *Structure* **18,** 1244–60 (2010).

5. Sunde, M. *et al.* Common core structure of amyloid fibrils by synchrotron X-ray diffraction. *J. Mol. Biol.* **273,** 729–39 (1997).

6. Chiti, F. & Dobson, C. M. Protein misfolding, functional amyloid, and human disease. *Annu. Rev. Biochem.* **75,** 333–66 (2006).

7. Sunde, M. & Blake, C. The structure of amyloid fibrils by electron microscopy and X-ray diffraction. *Adv. Protein Chem.* **50,** 123–59 (1997).

8. Serpell, L. C. *et al.* The protofilament substructure of amyloid fibrils. *J. Mol. Biol.* **300,** 1033–9 (2000).

9. Sawaya, M. R. *et al.* Atomic structures of amyloid cross-beta spines reveal varied steric zippers. *Nature* **447,** 453–7 (2007).

10. Fitzpatrick, A. W. P. *et al.* Atomic structure and hierarchical assembly of a cross-β amyloid fibril. *Proc. Natl. Acad. Sci. U. S. A.* **110,** 5468–73 (2013).

11. Divry, D. & Florkin, M. Sur les proprietes optiques de l'amyloide. *Comptes Rendus la Soc. Biol.* **97,** 1808–1810 (1927).

12. Vassar, P. S. & Culling, C. F. Fluorescent stains, with special reference to amyloid and connective tissues. *Arch. Pathol.* **68,** 487–98 (1959).

13. Lue, L. F. *et al.* Soluble amyloid beta peptide concentration as a predictor of synaptic change in Alzheimer's disease. *Am. J. Pathol.* **155,** 853–62 (1999).

14. Andersson, K., Olofsson, A., Nielsen, E. H., Svehag, S.-E. & Lundgren, E. Only amyloidogenic intermediates of transthyretin induce apoptosis. *Biochem. Biophys. Res. Commun.* **294,** 309–14 (2002).

15. Seibert, F. B. & Nelson, J. W. Electrophoretic study of the blood protein response in tuberculosis. *J. Biol. Chem.* **143,** 29–38 (1942).

16. Kabat, E. a, Moore, D. H. & Landow, H. an Electrophoretic Study of the Protein Components in Cerebrospinal Fluid and Their Relationship To the Serum Proteins. *J. Clin. Invest.* **21,** 571–577 (1942).

17. Ingbar, S. H. Pre-albumin: a thyroxinebinding protein of human plasma. *Endocrinology* **63,** 256–9 (1958).

18. Kanai, M., Raz, A. & Goodman, D. S. Retinol-binding protein: the transport protein for vitamin A in human plasma. *J. Clin. Invest.* **47,** 2025–44 (1968).

19. Sparkes, R. S. *et al.* Assignment of the prealbumin (PALB) gene (familial amyloidotic polyneuropathy) to human chromosome region 18q11.2-q12.1. *Hum. Genet.* **75,** 151–4 (1987).

20. Connors, L. H., Lim, A., Prokaeva, T., Roskens, V. A. & Costello, C. E. Tabulation of human transthyretin (TTR) variants. *Amyloid* **10,** 160–184 (2009).

21. Saraiva, M. J. Transthyretin mutations in hyperthyroxinemia and amyloid diseases. *Hum. Mutat.* **17,** 493–503 (2001).

22. Blake, C. C. F., Geisow, M. J., Oatley, S. J., Rérat, B. & Rérat, C. Structure of prealbumin: Secondary, tertiary and quaternary interactions determined by Fourier refinement at 1.8 Å. *J. Mol. Biol.* **121,** 339–356 (1978).

23. Brito, R., Damas, A. & Saraiva, M. Amyloid Formation by Transthyretin: From Protein Stability to Protein Aggregation. *Curr. Med. Chem. Endocr. Metab. Agents* **3,** 349–360 (2003).

24. Blaner, W. S., Bonifácio, M. J., Feldman, H. D., Piantedosi, R. & Saraiva, M. J. M. Studies on the synthesis and secretion of transthyretin by the human hepatoma cell line Hep G2. *FEBS Lett.* **287,** 193–196 (1991).

25. Dickson, P. W. *et al.* High prealbumin and transferrin mRNA levels in the choroid plexus of rat brain. *Biochem. Biophys. Res. Commun.* **127,** 890–5 (1985).

26. Ong, D. E., Davis, J. T., O'Day, W. T. & Bok, D. Synthesis and secretion of retinol-binding protein and transthyretin by cultured retinal pigment epithelium. *Biochemistry* **33,** 1835–42 (1994).

27. Westermark, G. T. & Westermark, P. Transthyretin and amyloid in the islets of Langerhans in type-2 diabetes. *Exp. Diabetes Res.* **2008,** 429274 (2008).

28. Herbert, J. *et al.* Transthyretin: a choroid plexus-specific transport protein in human brain. The 1986 S. Weir Mitchell award. *Neurology* **36,** 900–11 (1986).

29. Oppenheimer, J., Surks, M., Bernstein, G. & Smith, J. Metabolism of iodine-131-labeled thyroxine-binding prealbumin in man. *Science* **149,** 748–50 (1965).

30. Feldt-Rasmussen, U. & Rasmussen, Å. K. Thyroid hormone transport and actions. *Pediatr. Adolesc. Med.* **11,** 80–103 (2007).

31. Wojtczak, A. Crystal structure of rat transthyretin at 2.5 A resolution: first report on a unique tetrameric structure. *Acta Biochim. Pol.* **44,** 505–17 (1997).

32. Goodman, D. S. & Raz, A. Extraction and recombination studies of the interaction of retinol with human plasma retinol-binding protein. *J. Lipid Res.* **13,** 338–47 (1972).

33. Naylor, H. M. & Newcomer, M. E. The structure of human retinol-binding protein (RBP) with its carrier protein transthyretin reveals an interaction with the carboxy terminus of RBP. *Biochemistry* **38,** 2647–53 (1999).

34. Oliveira, S. M., Cardoso, I. & Saraiva, M. J. Transthyretin: roles in the nervous system beyond thyroxine and retinol transport. *Expert Rev. Endocrinol. Metab.* **7,** 181–189 (2012).

35. Liz, M. A., Faro, C. J., Saraiva, M. J. & Sousa, M. M. Transthyretin, a new cryptic protease. *J. Biol. Chem.* **279,** 21431–8 (2004).

36. Tanskanen, M. *et al.* Senile systemic amyloidosis affects 25% of the very aged and associates with genetic variation in alpha2-macroglobulin and tau: a population-based autopsy study. *Ann. Med.* **40,** 232–9 (2008).

37. Westermark, P., Sletten, K., Johansson, B. & Cornwell, G. G. Fibril in senile systemic amyloidosis is derived from normal transthyretin. *Proc. Natl. Acad. Sci. U. S. A.* **87,** 2843–5 (1990).

38. Ueda, M. *et al.* Clinicopathological features of senile systemic amyloidosis: an ante- and post-mortem study. *Mod. Pathol.* **24,** 1533–44 (2011).

39. Nuvolone, M., Obici, L. & Merlini, G. Amyloid-related Disorders Transthyretin-associated Familial Amyloid Polyneuropathy — Current and Emerging Therapies. *Eur. Neurol. Rev.* **7,** 24–32 (2012).

40. Andrade, C. A peculiar form of peripheral neuropathy: familial atypical generalized amyloidosis with special involvement of the peripheral nerves. *Brain* **75,** 408–427 (1952).

41. Araki, S., Mawatari, S., Ohta, M., Nakajima, A. & Kuroiwa, Y. Polyneuritic Amyloidosis in a Japanese Family. *Arch. Neurol.* **18,** 593–602 (1968).

42. Andersson, R. Familial amyloidosis with polyneuropathy. A clinical study based on patients living in northern Sweden. *Acta Med. Scand. Suppl.* **590,** 1–64 (1976).

43. Costa, P. P., Figueira, A. S. & Bravo, F. R. Amyloid fibril protein related to prealbumin in familial amyloidotic polyneuropathy. *Proc. Natl. Acad. Sci. U. S. A.* **75,** 4499–503 (1978).

44. Tawara, S., Nakazato, M., Kangawa, K., Matsuo, H. & Araki, S. Identification of amyloid prealbumin variant in familial amyloidotic polyneuropathy (Japanese type). *Biochem. Biophys. Res. Commun.* **116,** 880–8 (1983).

45. Ando, Y. & Suhr, O. B. Autonomic dysfunction in familial amyloidotic polyneuropathy (FAP). *Amyloid* **5,** 288–300 (1998).

46. Holmgren, G., Wikström, L., Lundgren, H.-E. & Suhr, O. B. Discordant penetrance of the trait for familial amyloidotic polyneuropathy in two pairs of monozygotic twins. *J. Intern. Med.* **256,** 453–6 (2004).

47. Rapezzi, C. *et al.* Transthyretin-related amyloidoses and the heart: a clinical overview. *Nat. Rev. Cardiol.* **7,** 398–408 (2010).

48. Jacobson, D. R. *et al.* Variant-sequence transthyretin (isoleucine 122) in late-onset cardiac amyloidosis in black Americans. *N. Engl. J. Med.* **336,** 466–73 (1997).

49. Benson, M. D. Leptomeningeal amyloid and variant transthyretins. *Am. J. Pathol.* **148,** 351–4 (1996).

50. Arsequell, G. & Planas, a. Methods to evaluate the inhibition of TTR fibrillogenesis induced by small ligands. *Curr. Med. Chem.* **19,** 2343–55 (2012).

51. Morris, A. M., Watzky, M. A. & Finke, R. G. Protein aggregation kinetics, mechanism, and curve-fitting: a review of the literature. *Biochim. Biophys. Acta* **1794,** 375–97 (2009).

52. Johnson, S. M., Connelly, S., Fearns, C., Powers, E. T. & Kelly, J. W. The transthyretin amyloidoses: from delineating the molecular mechanism of aggregation linked to pathology to a regulatory-agency-approved drug. *J. Mol. Biol.* **421,** 185–203 (2012).

53. Lai, Z., Colón, W. & Kelly, J. W. The acid-mediated denaturation pathway of transthyretin yields a conformational intermediate that can self-assemble into amyloid. *Biochemistry* **35,** 6470–6482 (1996).

54. Quintas, A., Saraiva, M. J. & Brito, R. M. The tetrameric protein transthyretin dissociates to a non-native monomer in solution. A novel model for amyloidogenesis. *J. Biol. Chem.* **274,** 32943–9 (1999).

55. Quintas, a, Vaz, D. C., Cardoso, I., Saraiva, M. J. & Brito, R. M. Tetramer dissociation and monomer partial unfolding precedes protofibril formation in amyloidogenic transthyretin variants. *J. Biol. Chem.* **276,** 27207–13 (2001).

56. Johnson, S. M., Connelly, S., Fearns, C., Powers, E. & Kelly, J. W. The Transthyretin Amyloidoses: From Delineating the Molecular Mechanism of Aggregation Linked to Pathology to a Regulatory Agency Approved Drug. *J Mol Biol* **421,** 185–203 (2012).

57. Pires, R. H., Karsai, Á., Saraiva, M. J., Damas, A. M. & Kellermayer, M. S. Z. Distinct Annular Oligomers Captured along the Assembly and Disassembly Pathways of Transthyretin Amyloid Protofibrils. *PLoS One* **7,** (2012).

58. Faria, T. Q. *et al.* A look into amyloid formation by transthyretin: aggregation pathway and a novel kinetic model. *Phys. Chem. Chem. Phys.* **17,** 7255–7263 (2015).

59. Serpell, L. C. *et al.* Examination of the structure of the transthyretin amyloid fibril by image reconstruction from electron micrographs. *J. Mol. Biol.* **254,** 113–118 (1995).

60. Blake, C. & Serpell, L. Synchrotron X-ray studies suggest that the core of the transthyretin amyloid fibril is a continuous β-sheet helix. *Structure* **4,** 989–998 (1996).

61. Inouye, H. *et al.* Analysis of x-ray diffraction patterns from amyloid of biopsied vitreous humor and kidney of transthyretin (TTR) Met30 familial amyloidotic polyneuropathy (FAP) patients: axially arrayed TTR monomers constitute the protofilament. *Amyloid* **5,** 163–74 (1998).

62. Serag, A. a, Altenbach, C., Gingery, M., Hubbell, W. L. & Yeates, T. O. Arrangement of subunits and ordering of beta-strands in an amyloid sheet. *Nat. Struct. Biol.* **9,** 734–739 (2002).

63. Olofsson, A., Ippel, J. H., Wijmenga, S. S., Lundgren, E. & Öhman, A. Probing Solvent Accessibility of Transthyretin Amyloid by Solution NMR Spectroscopy. *J. Biol. Chem.* **279,** 5699–5707 (2004).

64. Correia, B. E., Loureiro-Ferreira, N. & Rodrigues, J. R. A structural model of an amyloid protofilament of Transthyretin. *Protein Sci.* **15,** 28–32 (2006).

65. Bateman, D. a, Tycko, R. & Wickner, R. B. Experimentally derived structural constraints for amyloid fibrils of wild-type transthyretin. *Biophys. J.* **101,** 2485–92 (2011).

66. Reixach, N., Deechongkit, S., Jiang, X., Kelly, J. W. & Buxbaum, J. N. Tissue damage in the amyloidoses: Transthyretin monomers and nonnative oligomers are the major cytotoxic species in tissue culture. *Proc. Natl. Acad. Sci. U. S. A.* **101,** 2817–2822 (2004).

67. Sörgjerd, K., Klingstedt, T., Lindgren, M., Kågedal, K. & Hammarström, P. Prefibrillar transthyretin oligomers and cold stored native tetrameric transthyretin are cytotoxic in cell culture. *Biochem. Biophys. Res. Commun.* **377,** 1072–1078 (2008).

68. Mendes Sousa, M., Cardoso, I., Fernandes, R., Guimarães, A. & Saraiva, M. J. Deposition of Transthyretin in Early Stages of Familial Amyloidotic Polyneuropathy. *Am. J. Pathol.* **159,** 1993–2000 (2001).

69. Misumi, Y. *et al.* Relationship between amyloid deposition and intracellular structural changes in familial amyloidotic polyneuropathy. *Hum. Pathol.* **43,** 96–104 (2012).

70. Damas, A. M. & Saraiva, M. J. Review: TTR amyloidosis-structural features leading to protein aggregation and their implications on therapeutic strategies. *J. Struct. Biol.* **130,** 290–9 (2000).

71. Ueda, M. & Ando, Y. Recent advances in transthyretin amyloidosis therapy. *Transl. Neurodegener.* **3,** 19 (2014).

72. Stangou, A. J. & Hawkins, P. N. Liver transplantation in transthyretin-related familial amyloid polyneuropathy. *Curr. Opin. Neurol.* **17,** 615–20 (2004).

73. Familial Amyloidotic Polyneuropathy World Transplant Registry. at <http://www.fapwtr.org/>

74. Wilczek, H. E., Larsson, M. & Ericzon, B.-G. Long-term data from the Familial Amyloidotic Polyneuropathy World Transplant Registry (FAPWTR). (2011). at <http://informahealthcare.com/doi/abs/10.3109/13506129.2011.574354072>

75. Kurosawa, T., Igarashi, S., Nishizawa, M. & Onodera, O. Selective silencing of a mutant transthyretin allele by small interfering RNAs. *Biochem. Biophys. Res. Commun.* **337,** 1012–8 (2005).

76. Ackermann, E. J. *et al.* Clinical development of an antisense therapy for the treatment of transthyretin-associated polyneuropathy. *Amyloid* **19 Suppl 1,** 43–4 (2012).

77. ISIS-TTRrx Clinical Trials. at <http://ttrstudy.com/isis-ttrrx-clinical-trials/>

78. Haraoka, K. *et al.* Presence of variant transthyretin in aqueous humor of a patient with familial amyloidotic polyneuropathy after liver transplantation. *Amyloid* **9,** 247–51 (2002).

79. Kawaji, T., Ando, Y., Hara, R. & Tanihara, H. Novel therapy for transthyretin-related ocular amyloidosis: a pilot study of retinal laser photocoagulation. *Ophthalmology* **117,** 552–5 (2010).

80. Coelho, T. *et al.* Tafamidis for transthyretin familial amyloid polyneuropathy: A randomized, controlled trial. *Neurology* **79,** 785–792 (2012).

81. Coelho, T. *et al.* Long-term effects of tafamidis for the treatment of transthyretin familial amyloid polyneuropathy. *J. Neurol.* **260,** 2802–14 (2013).

82. Berk, J. L. *et al.* Repurposing diflunisal for familial amyloid polyneuropathy: a randomized clinical trial. *JAMA* **310,** 2658–67 (2013).

83. Gustavsson, A., Engström, U. & Westermark, P. Mechanisms of transthyretin amyloidogenesis. Antigenic mapping of transthyretin purified from plasma and amyloid fibrils and within in situ tissue localizations. *Am. J. Pathol.* **144,** 1301–11 (1994).

84. Redondo, C., Damas, A. M., Olofsson, A., Lundgren, E. & Saraiva, M. J. Search for intermediate structures in transthyretin fibrillogenesis: soluble tetrameric Tyr78Phe TTR expresses a specific epitope present only in amyloid fibrils. *J. Mol. Biol.* **304,** 461–70 (2000).

85. Terazaki, H. *et al.* Immunization in familial amyloidotic polyneuropathy: counteracting deposition by immunization with a Y78F TTR mutant. *Lab. Invest.* **86,** 23–31 (2006).

86. Ferreira, N. *et al.* Binding of epigallocatechin-3-gallate to transthyretin modulates its amyloidogenicity. *FEBS Lett.* **583,** 3569–76 (2009).

87. Ferreira, N., Saraiva, M. J. & Almeida, M. R. Natural polyphenols inhibit different steps of the process of transthyretin (TTR) amyloid fibril formation. *FEBS Lett.* **585,** 2424–30 (2011).

88. Ferreira, N., Saraiva, M. J. & Almeida, M. R. Epigallocatechin-3-gallate as a potential therapeutic drug for TTR-related amyloidosis: 'in vivo' evidence from FAP mice models. *PLoS One* **7,** e29933 (2012).

89. Kristen, A. V *et al.* Green tea halts progression of cardiac transthyretin amyloidosis: an observational report. *Clin. Res. Cardiol.* **101,** 805–13 (2012).

90. Merlini, G. *et al.* Interaction of the anthracycline 4 ' -iodo-4 ' -deoxydoxorubicin with amyloid fibrils : Inhibition of amyloidogenesis. *Proc.Natl.Acad.Sci.USA* **92,** 2959–2963 (1995).

91. Cardoso, I., Merlini, G., Joa, M., Leu, T. & Leu, T. T. R. 4'-iodo-4'-Deoxydoxorubicin and tetracyclines disrupt transthyretin amyloid fibrils in vitro producing noncytotoxic species: screening for TTR fibril disrupters. *FASEB J.* **17,** 803–809 (2003).

92. Keene, C. D. *et al.* Tauroursodeoxycholic acid, a bile acid, is neuroprotective in a transgenic animal model of Huntington's disease. *Proc. Natl. Acad. Sci.* **99,** 10671–10676 (2002).

93. Macedo, B., Batista, A. R., Ferreira, N., Almeida, M. R. & Saraiva, M. J. Anti-apoptotic treatment reduces transthyretin deposition in a transgenic mouse model of Familial Amyloidotic Polyneuropathy. *Biochim. Biophys. Acta* **1782,** 517–22 (2008).

94. Forloni, G., Colombo, L., Girola, L., Tagliavini, F. & Salmona, M. Anti-amyloidogenic activity of tetracyclines: studies in vitro. *FEBS Lett.* **487,** 404–407 (2001).

95. Cardoso, I., Brito, M. & Saraiva, M. J. Extracellular matrix markers for disease progression and follow-up of therapies in familial amyloid polyneuropathy V30M TTR-related. *Dis. Markers* **25,** 37–47 (2008).

96. Cardoso, I. & Saraiva, M. J. Doxycycline disrupts transthyretin amyloid: evidence from studies in a FAP transgenic mice model. *FASEB J.* **20,** 234–9 (2006).

97. Cardoso, I., Martins, D., Ribeiro, T., Merlini, G. & Saraiva, M. J. Synergy of combined doxycycline/TUDCA treatment in lowering Transthyretin deposition and associated biomarkers: studies in FAP mouse models. *J. Transl. Med.* **8,** 74 (2010).

98. Obici, L. *et al.* Doxycycline plus tauroursodeoxycholic acid for transthyretin amyloidosis: a phase II study. *Amyloid* **19 Suppl 1,** 34–6 (2012).

99. Tscharnuter, W. in *Encyclopedia of Analytical Chemistry* 5469–5485 (John Wiley& Sons Ltd, 2000). doi:10.1002/9780470027318

100. *N5 Submicron Particle Size Analyzer-PCS Software Help Manual.* (Beckman Coulter, Inc., 2003).

101. Meyer, B. & Peters, T. NMR spectroscopy techniques for screening and identifying ligand binding to protein receptors. *Angew. Chemie - Int. Ed.* **42,** 864–890 (2003).

102. Bhunia, A., Bhattacharjya, S. & Chatterjee, S. Applications of saturation transfer difference NMR in biological systems. *Drug Discov. Today* **17,** 505–513 (2012).

103. Krishnan, V. V. Ligand Screening by Saturation-Transfer Difference (STD) NMR Spectroscopy. *Curr. Anal. Chem.* **1,** 307–320 (2005).

104. Viegas, A., Manso, J., Nobrega, F. L. & Cabrita, E. J. Saturation-transfer difference (STD) NMR: A simple and fast method for ligand screening and characterization of protein binding. *J. Chem. Educ.* **88,** 990–994 (2011).

105. Mayer, M. & Meyer, B. Characterization of ligand binding by saturation transfer difference NMR spectroscopy. *Angew. Chemie - Int. Ed.* **38,** 1784–1788 (1999).

106. Kelly, S. M., Jess, T. J. & Price, N. C. How to study proteins by circular dichroism. *Biochim. Biophys. Acta - Proteins Proteomics* **1751,** 119–139 (2005).

107. Greenfield, N. Using circular dichroism spectra to estimate protein secondary structure. *Nat Protoc.* **1,** 2876–2890 (2007).

108. Sauer, M., Hofkens, J. & Enderlein, J. Basic Principles of Fluorescence Spectroscopy. *Handb. Fluoresc. Spectrosc. Imaging From Single Mol. to Ensembles* 1–30 (2011). doi:10.1002/9783527633500.ch1

109. So, P. T. C. & Dong, C. Y. Fluorescence Spectrophotometry. *Encycl. Life Sci.* 1–4 (2002). doi:10.1038/npg.els.0002978

110. Ladokhin, A. S. Fluorescence Spectroscopy in Peptide and Protein Analysis. *Encyclopedia of Analytical Chemistry* 5762–5779 (2000).

111. Munishkina, L. a & Fink, A. L. Fluorescence as a method to reveal structures and membrane-interactions of amyloidogenic proteins. *Biochim. Biophys. Acta* **1768,** 1862–85 (2007).

112. Hawe, A., Sutter, M. & Jiskoot, W. Extrinsic fluorescent dyes as tools for protein characterization. *Pharm. Res.* **25,** 1487–99 (2008).

113. Naiki, H., Higuchi, K., Hosokawa, M. & Takeda, T. Fluorometric determination of amyloid fibrils in vitro using the fluorescent dye, thioflavin T1. *Anal. Biochem.* **177,** 244–9 (1989).

114. Biancalana, M. & Koide, S. Molecular mechanism of Thioflavin-T binding to amyloid fibrils. *Biochim. Biophys. Acta* **1804,** 1405–12 (2010).

115. Lindgren, M., Sörgjerd, K. & Hammarström, P. Detection and characterization of aggregates, prefibrillar amyloidogenic oligomers, and protofibrils using fluorescence spectroscopy. *Biophys. J.* **88,** 4200–12 (2005).

116. Dolado, I. *et al.* Kinetic assay for high-throughput screening of in vitro transthyretin amyloid fibrillogenesis inhibitors. *J. Comb. Chem.* **7,** 246–252 (2005).

117. Gras, S. L., Waddington, L. J. & Goldie, K. N. Transmission electron microscopy of amyloid fibrils. *Methods Mol. Biol.* **752,** 197–214 (2011).

118. Lundberg, E., Olofsson, A., Westermark, G. T. & Sauer-Eriksson, a E. Stability and fibril formation properties of human and fish transthyretin, and of the Escherichia coli transthyretin-related protein. *FEBS J.* **276,** 1999–2011 (2009).

119. Lai, Z., Colón, W. & Kelly, J. W. The acid-mediated denaturation pathway of transthyretin yields a conformational intermediate that can self-assemble into amyloid. *Biochemistry* **35,** 6470–82 (1996).

120. Colon, W. & Kelly, J. W. Partial denaturation of transthyretin is sufficient for amyloid fibril formation in vitro. *Biochemistry* **31,** 8654–60 (1992).

121. Chung, C. M., Connors, L. H., Benson, M. D. & Walsh, M. T. Biophysical analysis of normal transthyretin: implications for fibril formation in senile systemic amyloidosis. *Amyloid* **8,** 75–83 (2001).

122. Skoulakis, S. & Goodfellow, J. M. The pH-dependent stability of wild-type and mutant transthyretin oligomers. *Biophys. J.* **84,** 2795–804 (2003).

123. Yang, A. S. & Honig, B. On the pH dependence of protein stability. *J. Mol. Biol.* **231,** 459–74 (1993).

124. Honig, B. & Nicholls, A. Classical electrostatics in biology and chemistry. *Science (80-.).* **268,** 1144–1149 (1995).

125. Pires, R. H., Saraiva, M. J., Damas, A. M. & Kellermayer, M. S. Z. Structure and assembly-disassembly properties of wild-type transthyretin amyloid protofibrils observed with atomic force microscopy. *J. Mol. Recognit.* **24,** 467–476 (2011).

126. Injac, R., Djordjevic-Milic, V. & Srdjenovic, B. Thermostability testing and degradation profiles of doxycycline in bulk, tablets, and capsules by HPLC. *J. Chromatogr. Sci.* **45,** 623–628 (2007).

127. Kogawa, A. & Salgado, H. Doxycycline Hyclate: a Review of Properties, Applications and Analytical Methods. *Ijlpr.Com* **2,** (2012).

128. Palha, J. A. *et al.* 4'-Iodo-4'-Deoxydoxorubicin Disrupts the Fibrillar Structure of Transthyretin Amyloid. *Am. J. Pathol.* **156,** 1919–1925 (2000).